University of Cincinnati

Date: 6/8/2020

I, Robert T Kleven, hereby submit this original work as part of the requirements for the degree of Doctor of Philosophy in Biomedical Engineering.

It is entitled:

Transcranial Ultrasound for the Treatment of Stroke

Student's name: **Robert T Kleven**

This work and its defense approved by:

Committee chair: Christy Holland, Ph.D.

Committee member: Kevin Haworth, Ph.D.

Committee member: T. Douglas Mast, Ph.D.

Committee member: Marepalli Rao, Ph.D.

Committee member: Mario Zuccarello, MD

36753

Transcranial Ultrasound

for the Treatment of Stroke

A dissertation submitted to
the Graduate School of the University of Cincinnati
in partial fulfillment of the requirements for the degree of

Doctor of Philosophy

In Biomedical Engineering
Department of Biomedical Engineering
College of Engineering and Applied Science

June 8th, 2020
Robert Kleven
B.A. Central College, 2013

Dissertation Committee:
Christy K. Holland, Ph.D. (Committee Chair)
Kevin J. Haworth, Ph.D.
T. Douglas Mast, Ph.D.
Marepalli Rao, Ph.D.
Mario Zuccarello, M.D.

ABSTRACT

Recent advances in point of care clinical diagnostic ultrasound scanners and image-guided procedures have been accompanied by an exponential expansion of therapeutic ultrasound technologies. Treatment strategies for stroke, a leading cause of morbidity and mortality worldwide, have been limited using lytic agents and interventional approaches with poor clinical outcomes. Sonothrombolysis, the adjuvant use of ultrasound exposure to enhance and accelerate thrombus break down with a thrombolytic agent, has been successful *in vitro* but has lacked demonstration of clinical success in large randomized controlled stroke treatment trials to date. This dissertation describes the development of unfocused low frequency (≤ 220 kHz) therapeutic ultrasound to enhance lysis through mechanically agitation and improved lytic diffusion.

A porcine cerebral thromboembolism model is described in Chapter II. This model employs a xenographic human retracted clot to approximate recombinant tissue plasminogen activator (rt-PA) lytic susceptibility in humans. To reveal the relationship between clot mass loss and flow restoration, an *in vitro* study was designed to model porcine neurovascular anatomy and physiology. Therapeutic agents were administered directly into clots via two different microcatheter designs (end hole and multiple-side-hole). Sonothrombolysis increased clot mass loss relative to either sham or rt-PA only *in vitro* with the multiple-side-hole microcatheter. Controlled *in vivo* studies were conducted in a porcine thromboembolism model with highly retracted human clots. Sonothrombolysis increased the rate of successful reperfusion (mTICI 2b or 3) at earlier time points compared to clots treated with rt-PA only or sham.

A juvenile porcine intracerebral hemorrhage model is described in Chapter III. Three thrombolytic metrics were compared *in vitro* and *ex vivo* to determine which metric best measures thrombolysis due to rt-PA: residual thrombus mass, volume, and density. The thrombus density

was the most effective of the three metrics at differentiating between sham and rt-PA treated thrombi. *In vivo*, thrombolytic efficacy was observed between sham and both rt-PA only and sonothrombolysis treatment arms based on the thrombus density,

The goal of Chapter IV was to design a pulsed ultrasound (US) exposure scheme that reduced intracranial constructive interference and tissue heating and maintained thrombolytic efficacy relative to intermittent continuous wave (CW) insonation. Three 220-kHz US schemes were evaluated, two pulsed insonation schemes and an intermittent CW insonation scheme. *In vitro* measurements with flow were performed to assess thrombolysis using time-lapse microscopy. All insonation schemes promoted sustained stable cavitation *in vitro* and augmented thrombolysis compared to rt-PA alone. An *in silico* study using a finite-difference model of transcranial US propagation was performed to estimate the intracranial acoustic field and temperature rise in human stroke patients for each insonation scheme. Intracranial constructive interference was not reduced with pulsed US using a pulse length of 15 cycles compared to intermittent CW US. The 33.3% duty cycle pulsed US scheme reduced heating in the temporal bone as much as 60% relative to the intermittent CW scheme. These findings demonstrate that a 33.3% duty cycle pulsed US scheme with a 15-cycle burst can reduce bone heating and achieve equivalent thrombolytic efficacy as an intermittent CW scheme.

ACKNOWLEDGEMENTS

Committee

I would like to acknowledge and thank my graduate advisor, Dr. Christy K. Holland, who has mentored me over the past five years. Dr. Holland has guided me through the vicissitudes of research and set a wonderful example to me on how to contribute to academic inquiry, industrial development, and clinical practice. She has been invaluable in molding my curiosity into a coherent, driven, and focused search for answers in scientific discovery. She has taught me to use each mistake to learn, grow, and improve to yield better work through intellectual discourse. It has been a privilege to study under her.

In addition to my advisor, I would also like to thank each of my dissertation committee members. Dr. Haworth has provided a constant source of encouragement, rigor, and accountability within our laboratories and outside. Dr. Mast has intellectually challenged me both in the classroom and the lab and developed my theoretical knowledge of ultrasound. Dr. Zuccarello has grounded my research in clinical knowledge and questions, always pushing me to what is possible and what is reasonable. Dr. Rao has helped me to evaluate my research critically and guided my statistical analysis and experimental design. This dissertation would not have been possible without the guidance and feedback of my committee.

IgUTL

I would like to extend heartfelt thanks to the Image-guided Ultrasound Therapeutic Laboratories (IgUTL). In particular, I would like to thank Dr. Bader who first took me under his wing and showed me the ropes of ultrasound research. Dr. Shekhar and Dr. Mercado-Shekhar, both shared the ups and downs of medical and scientific research and helped me through my early growing pains, especially during my first manuscript. Dr. Karani was a wonderful

colleague who always was up for a stimulating intellectual conversation as we worked alongside each other discussing philosophy, politics, music, sports, and his love of rap music which got me through many late nights in lab. Dr. Huang kindly showed me how to manage my lab data in an organized and efficient manner and could always share a lab victory or defeat. Dr. Lafond has always been willing to help on an experiment, even with short notice, and critically vetted my work as well as tolerated my many musings in the image processing room. I would like to thank Dr. Salido for her encouragement and assistance, especially with the computational aspects of this project, and her enthusiasm for all things Spanish. Also, I thank Dr. Zemzemi who has provided invaluable help during our many conversations on animal models and *in vitro* studies. Additional thanks to the students I have worked with and trained, including Zach Watkins, Sam Ford, Karthik Sakthivel, Ian Walling, and Robert Sabilia. I would like to thank the veterinary staff at CCHMC and UC/LAMS, especially Jasmine Hales and Carissa Lester, Casie Furby, Holly Stallkamp, Dr. Tetens-Woodring, and Dr. Jonalagadda, as well as Nicole Hilvert with the CCHMC Department of Radiology.

UC MSTP

The Medical Scientist Training Program (MSTP) has also provided invaluable resources and support under the NIH grant T32 GM063483. In particular, I would like to thank Dr. Herr, Dr. Hershey, Dr. Abruzzo, and Dr. Cowley. I would also like to acknowledge the many students in the program who have assisted me through my studies: Calvin Chan and Seth Reighard for their advice and friendship, Ben Kay and Eric Smith who have given me invaluable guidance over my studies, and Pablo Alarcon for his spirited friendship.

Family

I would like to extend my thanks to my father Terence Kleven. He has set a brilliant example and encouraged all his children to pursue higher education, to shoot for the stars, and to be excellent citizens of the world. Graduate school has opened my eyes to the amount of constant hard work he has done staying active in the academic community while teaching full time. My mother, Kathryn Kleven, has taught me everything I know and has demonstrates a love of learning every day. I would also like to thank my brothers and sisters, who have tolerated my enthusiastic love of telling others what to do, and how to do it. And finally, I would like to acknowledge my fiancé Sarah Cunningham, who has been a rock through the many trials and tribulations of graduate school and has loved and supported me through all of them.

Funding

All three specific aims covered in this dissertation were funded primarily by the National Institute of Neurological Diseases and Disorders (NINDS) through the grant number R01 NS047603 and by the National Institute of General Medical Sciences (NIGMS) through grant number T32 GM063483. I would like to extend my sincere thanks to the National Institutes of Health and the NINDS for their support of stroke research. Specific grant funding for individual projects is covered below, as well as the assistance of various groups and departments at the University of Cincinnati and Cincinnati Children's Hospital Medical Center (CCHMC).

Specific Chapters

Chapter II.

In addition to the NINDS R01 grant above, this study was also supported by the Radiological Society of North America Medical Student Grant. We thank Betsy A. DiPasquale and Kelley Stanley from Cincinnati Children's Hospital Medical Center Anatomical Pathology

Core for help with histological analysis. We also thank Jasmine Hale who provided surgical anesthesia support throughout these studies. I would also like to thank Kunal Karani for his help on this section of the project, without which, it could not have succeeded. I would also like to thank Professor Xiasheng Guo (Nanjing University), for providing the 220 kHz ultrasound transducer used in the *in vitro* studies.

Chapter III

I would like to thank Guillaume Bouchoux, Azzdine Ammi, and Shenwen Huang, who set the groundwork for this project and were always willing to answer my questions as I revitalized the porcine ICH model. In addition, the veterinary staff at LAMS who adapted so quickly to our needs and modifications as we developed the model. I would like to thank Bruce Giffin and Martin Malony for their help on this project. I would also like to acknowledge Seth Thomas, Karthik Sakthivel, and Samantha Ford for their help throughout this project which has been above and beyond all expectations.

Chapter IV

I would like to thank Guillaume Bouchoux, PhD, who developed the finite difference model that was used in this work. This work was also supported by the National Institutes of Health (grant number K25 HL133452) I would also like to thank Professor Xiasheng Guo (Nanjing University) for providing the 220 kHz ultrasound transducer used in the *in vitro* studies.

Table of Contents

ABSTRACT ..... **II**

ACKNOWLEDGEMENTS ..... **V**

Committee ..... *v*
IgUTL ..... *v*
UC MSTP ..... *vi*
Family ..... *vii*
Funding ..... *vii*
SPECIFIC CHAPTERS VII
Chapter II. ..... *vii*
Chapter III ..... *viii*
Chapter IV. ..... *viii*

PUBLICATIONS ..... **XII**

MANUSCRIPTS CURRENTLY BEING WRITTEN FOR PUBLICATION ..... **XII**

PRESENTATIONS ..... **XII**

LIST OF FIGURES ..... **XIII**

CHAPTER II XIII
CHAPTER III XV
CHAPTER IV XVII

LIST OF TABLES ..... **XX**

CHAPTER III XX
CHAPTER IV XX

CHAPTER I: INTRODUCTION **1**

I.1 BACKGROUND 1
I.1.1 Pathophysiology of stroke *1*
I.1.2 Pharmacologic and Surgical Therapies for Stroke *2*
I.2 SONOTHROMBOLYSIS 6
I.2.1 Overview *6*
I.2.2 Mechanisms, Agents, and Approaches *7*
I.2.3 Cavitation monitoring *9*
I.2.5 Clinical studies of Sonothrombolysis *10*
I.3 MODELS OF THROMBOLYSIS *IN VITRO* 12
I.3.1 Clot composition *12*
I.3.2 Thrombus Retraction *13*
I.3.3 Presence of Flow *13*
I.3.4 Thrombolytic Metrics *14*
I.4 ANIMAL MODELS OF STROKE 15
I.5 SPECIFIC AIMS 16
I.5.1 Specific Aim 1: (Chapter II) *17*
I.5.2 Specific Aim 2: (Chapter III) *18*
I.5.3 Specific Aim 3: (Chapter IV) *18*
I.6 DISSERTATION OVERVIEW 19

CHAPTER II: ULTRASOUND ACCELERATED THROMBOLYSIS IN A PORCINE THROMBOEMBOLISM MODEL **21**

II.1 INTRODUCTION: 21
II.2 METHODS: 22

II.2.1 Characterization of Definity® infused through two microcatheter designs 22
II.2.2 Retracted human whole blood clot synthesis 23
II.2.3 Human whole blood clot lytic susceptibility 24
II.2.4 Effects of X-ray Contrast on Lytic Susceptibility 24
II.3.5 In Vitro Flow Phantom Thromboembolism Protocol 25
II.2.6 Porcine thromboembolism model 28
II.2.7 Statistics 36
II.3 RESULTS: 36
II.3.1 Infusion of Definity® microbubbles through microcatheters 36
II.3.2 Effects of X-ray Contrast on Lytic Susceptibility results 37
II.3.2 In vitro flow phantom thromboembolism results 38
II.3.3 In vivo porcine thromboembolism results 40
II.3.4 Vasospasm 44
II.4 DISCUSSION: 44
II.4.1 Catheter effects on ultrasound contrast agents 44
II.4.2 Clot mass loss and flow in vitro 45
II.4.3 Porcine thromboembolism model development 46
II.4.4 Restoration of Perfusion in vivo 47
II.4.5 Limitations 49
II.5 CONCLUSIONS: 50

CHAPTER III: THROMBOLYTIC EFFICACY OF TRANSCRANIAL ULTRASOUND IN A PORCINE INTRACEREBRAL HEMORRHAGE MODEL 52

III.1 INTRODUCTION: 52
III.2 METHODS: 54
III.2.1 In vitro thrombolytic assay 54
III.2.2 Comparison of clots incubated with plasma or artificial cerebrospinal fluid 56
III.2.3 Ex vivo thrombolysis protocol 57
III.2.4 In vivo thrombolysis protocol 60
III.2.7 Ultrasound field measurements and simulations 63
III.3 RESULTS: 64
III.3.1 Development of a thrombolytic assay in vitro 64
III.3.2 Comparison of clots incubated with plasma or artificial cerebrospinal fluid 71
III.3.3 Validation of thrombolytic assay ex vivo 72
III.3.4 In vivo thrombolysis 73
III.3.5 Ultrasound field measurements and simulations 75
III.4 DISCUSSION: 76
III.4.1 Development of thrombolytic assay in vitro 76
III.4.2 Comparison of clots incubated with plasma or artificial cerebrospinal fluid 79
III.4.3 Validation of thrombolytic assay ex vivo 80
III.4.4 In vivo thrombolysis 81
III.4.6 Ultrasound field measurements and simulations 82
III.5 CONCLUSIONS: 82

CHAPTER IV: THE EFFECT OF INSONATION SCHEME ON LYTIC EFFICACY AND PREDICTED INTRACRANIAL PRESSURE AND TEMPERATURE 84

IV.1 INTRODUCTION: 84
IV.2 METHODS: 85
IV.3 RESULTS: 85
IV.4 DISCUSSION 89

CHAPTER V: CONCLUSIONS AND FUTURE DIRECTIONS 91

V.1 GOALS OF STUDY 91

V.2 SUMMARY OF FINDINGS IN CHAPTER II....91
V.2.1 In vitro findings....*91*
V.2.2 In vivo findings....*92*
V.3 SUMMARY OF FINDINGS IN CHAPTER III....93
V.3.1 Metrics of Thrombolysis....*93*
V.4 SUMMARY OF FINDINGS IN CHAPTER IV....94
V.5 IMPACT ON FIELD....94
V.6 RECOMMENDATIONS FOR FUTURE STUDIES....96
BIBLIOGRAPHY....100

PUBLICATIONS

Kleven, R.T., Karani, K.B., Salido, N.G., Shekhar, H., Haworth, K.J., Mast, T.D., Tadesse, D.G., Holland, C.K. (2019). The effect of 220 kHz insonation scheme on rt-PA thrombolytic efficacy in vitro. *Physics on Medicine and Biology, 64*(16).

Mercado-Shekhar, K.P., **Kleven, R. T.**, Aponte Rivera, H., Lewis, R., Karani, K.B., Vos, H.J., Abruzzo, T., Haworth, K.J., Holland, C.K. (2018). Effect of clot stiffness on recombinant tissue plasminogen activator lytic susceptibility in vitro. *Ultrasound in Medicine and Biology, 44*(12), 2710-2727.

Shekhar, H., **Kleven, R. T.**, Peng, T., Palaniappan, A., Karani, K. B., Huang, S., McPherson D. D., Holland, C. K. (2019). In vitro characterization of sonothrombolysis and echocontrast agents to treat ischemic stroke. *Scientific Reports, 9*(9902)

Kooiman, K., Roovers, S., Langeveld, S.A.G., **Kleven, R.T.**, Dewitte, H., O'Reilly, M.A., Escoffre, J., Bouakaz, A., Verweij, M.D., Hynynen, K., Lentacker, I., Stride, E., Holland, C.K., Ultrasound-Responsive Cavitation Nuclei for Therapy and Drug Delivery, Ultrasound in Medicine and Biology, 2020, 26(6): 1296-1325

MANUSCRIPTS CURRENTLY BEING WRITTEN FOR PUBLICATION

Kleven, R.T., Karani, K.B., Hilvert, N., Ford, S.M. Mercado-Shekhar, K.P., Abruzzo, T., Racadio, J.M., Holland, C.K. Thrombolytic efficacy of 220 kHz ultrasound in a porcine thromboembolism model. *(In preparation for submission to Scientific Reports)*

Kleven, R.T., Huang, S., Thomas, S., Ford, S.M, Sakthivel, K., Holland, C.K. Thrombolytic efficacy of transcranial ultrasound at 120 kHz in a porcine intracerebral hemorrhage model. *(In preparation for submission to Translational Stroke Research)*

PRESENTATIONS

Kleven, R.T., Shekhar, H., Karani, K. B., Haworth, K.J., Holland, C.K. (May, 2018). Effect of duty cycle on the efficacy of 220 kHz ultrasound-enhanced rt-PA thrombolysis *in vitro*. Presented by **Robert Kleven** at the International Society of Therapeutic Ultrasound, Nashville, TN.

Shekhar, H., **Kleven, R.T.**, Palaniappan, A., Peng, T., Karani, Kunal, K.B., Huang, S., McPherson, D., Holland, C. K. (May, 2018). Lytic efficacy of 220 kHz sonothrombolysis with rt-PA and echocontrast agents. Presented by Himanshu Shekhar at the International Society of Therapeutic Ultrasound, Nashville, TN.

Kleven, R. T., Karani, K. B., Salido, N. G., Shekhar, H., Haworth, K. J., Holland, C. K. (September, 2019). Sonothrombolysis: Effect of 220 kHz insonation scheme. Presented by Christy Holland at the meeting of the World Federation of Ultrasound in Medicine and Biology, Melbourne, Australia.

LIST OF FIGURES

Chapter II

Figure II.1. Percent clot mass loss as a function of varying concentrations of recombinant tissue plasminogen activator in a static clot model. 1.5 cm clots were incubated in 30 mL porcine plasma with varying concentration so of rt-PA and the clot mass measured before and after treatment. The degree of thrombolysis increased significantly with concentration up to 6.20 μg/mL ($p < 0.05$), at which point it did not change significantly ($p > 0.18$). Significance is shown using compact letter display to categorize statistically equivalent groups based on a one-way ANOVA.

Figure II.2. *In vitro* vascular occlusion model. A human whole blood clot was deployed in a 2.4 mm inner diameter latex tube mimicking the ascending pharyngeal artery (APA) via an 8 F guide catheter and held in place by a mesh of fine needles crossing the lumen. A collateral tube simulated flow in the external carotid artery (ECA). A flow probe monitored flow through the occluded APA mimic. The afterload was set to a height at which the hydrodynamic pressure in both tubes was 90 mmHg. A passive cavitation detector (PCD) was aligned with the clot and field of the 220 kHz sonothrombolysis transducer.

Figure II.3. B-mode Ultrasound images of the *in vitro* flow phantom with an end port microcatheter positioned within 2 mm of the face of the clot (A) or a multiple side port microcatheter traversing the clot (B).

Figure II.4. Representative digital subtraction angiographic images showing porcine cranial vascular anatomy during the interventional procedure. Standard anatomy can be observed in (A). The common carotid artery (CCA) can be seen branching into the ascending pharyngeal artery (APA), occipital artery (OA), and external carotid artery (ECA). The APA ends in the *rete mirabile* (rete), a collection of capillaries which reform into the internal carotid artery which feeds the porcine Circle of Willis. Note the presence of collateral vessels extending from the ECA to the rete and Circle of Willis. The ECA is occluded using bare platinum and hydrogel coils (B) which diverts flow preferentially to the APA and reduces collateral circulation to the brain.

Figure II.5. Computational simulation of the ultrasound field using a validated finite difference code on (A) an axial CT with the ultrasound field overlaid in shades of blue and (B) 3D-rendered display. The transducer (green) is coupled to the skin over the porcine jowls. The clot (outlined in red) is located at the base of the skull, between the two porcine mastoid processes. An unobstructed path for the ultrasound beam was observed medial to the mandible on the ipsilateral side of the clot.

Figure II.6. Examples of digital subtraction angiograms (DSAs) before embolization (A, D, G), after embolization of the ascending pharyngeal artery (B, E, H), and after 2 hours of treatment (C,F,I). Treatments at each time point include saline alone (A-C), rt-PA alone (D-F), and rt-PA, Definity®, and ultrasound (G-I). The deployed clot lodged in the APA near the rete mirabile which occluded flow. Some collateral vessels were observed once the APA was occluded. Evidence of lysis was observed in the saline treated clot as an advancement of contrast across the clot at the end of the 2-hour treatment period (B-C). However, restoration of flow to the rete mirabile was more common in vessels occluded by clots treated lytic or sonothrombolysis (F, I). Flow defects were still present in perfused vessels indicating residual clot burden (F, I). Perfusion of the Circle of Willis was observed before treatment due to the extensive collateral vessels present in swine.

Figure II.7. Dissected left ascending pharyngeal artery (A) with residual clot and (B) the corresponding 120-minute angiogram. The coils in the external carotid artery were visible on the DSA image distal to the APA which ends in the *rete mirabile* embedded in the porcine skull.

Figure II.8. Measured attenuation coefficients (± 1 standard deviation) as a function of frequency at 25 °C for Definity® measured directly with no infusion through a catheter (black), or after being infused through a multiple side port microcatheter (green), or an end port microcatheter (blue). $N = 6$ for the no catheter and multiple side port microcatheter measurements, and $n = 3$ for the end port microcatheter measurements.

Figure II.9. Change in enzymatic activity of rt-PA (ΔAbs/time) as a function of the percent Optiray by volume. For Optiray volumes 10% or less, the activity of rt-PA to hydrolyze substrate was unaffected ($p > 0.87$). However, as the volume of Optiray increased, the activity of rt-PA significantly decreased. Overall a fourfold reduction in rt-PA activity was observed between the lowest and highest volume of Optiray measured (0-85%) ($p < 0.0001$). A one-way ANOVA was performed and significance was shown using compact letter display to identify statistically equivalent groups.

Figure II.10. *In vitro* percent clot mass loss results for human whole blood clots with $n = 10$ for each group. The end port microcatheter was positioned at the proximal face of the clot, and the multiple side port microcatheter crossed the clot axially. Clots treated with rt-PA had increased clot mass loss compared to saline, but no improvement was observed with the addition of the Definity®, and 220 kHz intermittent continuous wave ultrasound exposure for clots treated with the end port microcatheter. Both lytic and sonothrombolysis treatments resulted in significantly greater mass loss compared to clots treated with saline alone ($p < 0.01$ for both). Significance is marked with an Asterix, (*: $p < 0.05$, **: $p < 0.01$). A one-way ANOVA was performed and significance was shown using compact letter display to identify statistically equivalent groups.

Figure II.11. *In vitro* flow through APA flow model with $n = 10$ for each group. Human whole blood clots were treated with either saline, rt-PA at 1 mg/mL, or rt-PA (1 mg/mL) along with Definity® (2 μL/mL) and 220 kHz intermittent continuous wave ultrasound. Saline, rt-PA, or rt-PA mixed with Definity®, delivered either through an end port microcatheter positioned within 5 mm of the clot or a multiple side port microcatheter which was positioned across the clot. Flow measurements spanned -0.2 mL/min for a fully occluded APA mimic to 0.75 mL for a fully recanalized APA mimic. No increase in flow was observed for clots treated with the end port microcatheter. Flow was observed in clots treated with rt-PA or rt-PA, Definity®, and 220 kHz ultrasound using a multiple side port microcatheter.

Figure II.12. Total ultraharmonic cavitation emissions between 330-2000 kHz over the 30 minutes treatment period. Cavitation was highly variable for each trial for both the end port microcatheter (blue) and the multiple side port microcatheter (green). No difference in total ultraharmonic emissions was found between the two microcatheters on a Student's t-test ($p > 0.77$).

Figure II.13. mTICI scores for (A) clots treated using the end port microcatheter or (B) the multiple side port microcatheter. For plot (A), $n = 12$ for saline alone, $n = 7$ for rt-PA alone, and $n = 5$ for rt-PA, Definity®, and 220 kHz intermittent continuous wave ultrasound. In plot (B), $n = 5$ for all three treatments. No recanalization up to or greater than mTICI = 2b was observed for any clots treated with the end port microcatheter. Clots treated with the multiple side port catheter infused with saline alone showed some improvement in the degree of contrast penetration into the clot and had some mild improvement in downstream perfusion for some cases. The introduction of rt-PA to the clot showed improvement with 2/5 clots showing distal perfusion by 75-105 minutes. Improvement was accelerated with rt-PA, Definity®, and ultrasound, in which 2/5 clots achieved a mTICI score of 2b or greater between 0-60 minutes.

Figure II.14. Representative longitudinal histology images of residual clot burden in APAs with Verhoeff-Van Giessen (VVG) stain, which highlights elastic fibers. Residual clot volume (yellow) is pronounced in clots treated with (A) saline compared to (B) rt-PA, or (C) rt-PA, Definity®, and ultrasound. The percent patent area within each histology specimen is quantified and compared across the three treatments and two microcatheters (D). A one-way ANOVA was performed and significance was shown using compact letter display to identify statistically equivalent groups.

Figure II.15. Percent reduction in vessel diameter monitored during clot delivery and treatment with (A) the end port microcatheter and (B) the multiple side port catheter. All vessel diameters were compared to the diameter before embolization. Vasospasm was highly variable. For occlusions created by directly injecting the clot into the APA and instrumenting the vessel, vasospasm was significantly higher and did not resolve over time (A). For occlusions created by deploying the clot into the common carotid artery, vasospasm and was highest during the first 30 minutes after treatment started (B).

Chapter III

Figure III.1. Diagram of *ex vivo* porcine intracerebral hemorrhage model with infusion apparatus. Pressure is monitored during infusion using the pressure transducer before the catheter.

Figure III.2. Thrombus volume estimation based on optical imaging. Thrombus area on both the anterior and posterior sections of each slice were measured and the volume determined using equation (1).

Figure III.3. *In vivo* protocol of porcine ICH. ICH was infused through a catheter placed in the frontal white matter of an anesthetized crossbred pig (~20 kg). The catheter was positioned 11 mm anterior and 11 mm right of the coronal and sagittal sutures, respectively. After a 3-hour incubation period, rt-PA was injected into the thrombus (for treatment arms only) and then the catheter removed. The burr hole was sealed with bone wax and for ultrasound treated pigs, and ultrasound transducer was then positioned above the thrombus and coupled to the skull using ultrasound gel.

Figure III.4. Initial clot mass of 3 mL *in vitro* fresh porcine clots. Each clot was blotted and weighed prior to treatment. No significant difference was noted with a one-way ANOVA.

Figure III.5. Clot mass loss for 3 mL *in vitro* fresh porcine clots measured using blotting (A), spinning (B), or lyophilization (C). All clots were incubated in 30 mL thawed fresh-frozen porcine plasma gassed for 30 minutes. A one-way ANOVA was used to compare treatments and compact letter display used to identify statistically equivalent groups.

Figure III.6. Residual clot mass for 3 mL fresh porcine clots measured using blotting (A), spinning (B), or lyophilization (C). All clots were incubated in 30 mL thawed fresh-frozen porcine plasma gassed for 30 minutes. A one-way ANOVA was used to compare treatments and compact letter display used to identify statistically equivalent groups.

Figure III.7. Clot volumes for 3 mL *in vitro* fresh porcine clots measured before treatment using optical imaging (A), or after treatment using displacement (B) or optical imaging (C). All clots were incubated in 30 mL thawed fresh-frozen porcine plasma gassed for 30 minutes. Sham clots received no treatment, and were compared to rt-PA only (0.3 mg rt-PA), sonothrombolysis without Definity® (120 kHz, 0.5 MPa_{p-p}, 0.3 mg rt-PA), sonothrombolysis with Definity® (120 kHz, 0.5 MPa_{p-p}, 0.3 mg rt-PA, 0.15 mL Definity®). A one-way ANOVA was used to compare treatments and compact letter display used to identify statistically equivalent groups.

Figure III.8. Fresh 3 mL porcine clots normalized by the final clot volume calculated using optical imaging (A) or displacement (B). All clots were incubated in 30 mL thawed fresh-frozen porcine plasma gassed for 30 minutes. Sham clots received no treatment, and were compared to rt-PA only (0.3 mg rt-PA), sonothrombolysis without Definity® (120 kHz, 0.5 MPa_{p-p}, 0.3 mg rt-PA), sonothrombolysis with Definity® (120 kHz, 0.5 MPa_{p-p}, 0.3 mg rt-PA, 0.15 mL Definity®). A one-way ANOVA was used to compare treatments and compact letter display used to identify statistically equivalent groups.

Figure III.9. Clot mass loss for clots incubated in porcine plasma and artificial CSF. Clots were treated either with a direct inject of 0.3 mg rt-PA into the center of the clot (both rt-PA groups), or received no treatment (plasma, a-CSF). Artificial CSF did not result in a significant change in clot mass loss for clots receiving no treatment or clots receiving treatment with rt-PA. For both plasma and a-CSF, clots treated with rt-PA had significantly greater clot mass loss ($p < 0.0001$). A one-way ANOVA was used to compare treatments and compact letter display used to identify statistically equivalent groups.

Figure III.10. Residual thrombus mass (A), thrombus volume (B), and residual thrombus density (C) for frozen porcine thrombi formed in an *ex vivo* porcine model of ICH. Saline treated thrombi exhibited higher residual thrombus mass and density after extraction than rt-PA treated thrombi with a significance of $p = 0.012$, and $p < 0.0083$ respectively and a power of 80% with an n of 3. A Student's t-test was used to compare treatments and statistical significance is shown with Asterix *: $p < 0.05$, **: $p < 0.01$.

Figure III.11. Images of coronal sections for sham (A), rt-PA only (B), and sonothrombolysis without Definity® (C) *in vivo* porcine studies. Note the presence of intracerebral hemorrhage (ICH) in the right frontal white matter of the porcine brain as well as the presence of subarachnoid hemorrhage (SAH).

Figure III.12. Comparison between the residual thrombus density data acquired from porcine studies performed by Ammi et al. and for this dissertation. Data analyzed from the studies performed by Ammi et al. is shown in triangles and new data is shown in circles. On two-way ANOVA, only the ratio of the residual mass to volume was significantly different with respect to both treatment arm and study time period ($p < 0.05$, $p < 0.01$, respectively).

Figure III.13. Combined *in vivo* residual thrombus density. A one-way ANOVA was used to compare treatments and statistically equivalent groups are shown by compact letter display.

Figure III.14. Computational model of acoustic propagation through porcine skull using 3D rendered (A) model (A), and sagittal (B) and coronal (C) views. The ultrasound transducer was positioned parallel to the bone, using a plastic holder and an acoustic gel pad for transmission (not shown on the diagram). The position of the catheter used for blood injection and treatment

administration is indicated by the green line (the catheter was removed during ultrasound exposure). The average thrombus size is represented by the red spheroid. (B) The map of the acoustic pressure obtained in the cranial cavity was obtained by simulation and is shown relatively to the pig skull (yellow contours).

Chapter IV

Figure IV.1. Insonation schemes for (A) the intermittent continuous wave (CW) ultrasound with 50 seconds active and 30 quiescent, (B) the 62.5% and (C) the 33.3% duty cycle pulsed ultrasound with 15-cycle pulses. A limited time period is shown for all three insonation schemes for clarity. The hash marks indicate that the pulse continues with the same pulse duration and quiescent time as seen before the hash marks.

Figure IV.2. Time-lapse microscopy system used to monitor clot lysis during treatment. An acrylic tank was lined with an acoustic absorber to attenuate tank reflections. Clots were loaded in a glass micropipette confocal with both the therapy transducer (220 kHz single-element transducer) and the passive cavitation detector (2.25 MHz single-element transducer). The clot width was monitored using a CCD camera. The clot was exposed to a flow rate of 0.65 mL/min with the human plasma, recombinant tissue plasminogen activator, and Definity® included as appropriate.

Figure IV.3. Energy Spectra for (A) continuous wave (CW), (B) 62.5% duty cycle pulsed ultrasound (US), and (C) 33.3% duty cycle pulsed ultrasound. The frequency bandwidth for the harmonic (blue) and ultraharmonic (green) in the CW US scheme is 4 kHz, and the inharmonic band (red) is two frequency bands of 25-kHz bandwidths surrounding each ultraharmonic. The frequency bandwidth for harmonic and ultraharmonic frequency bands in the pulsed US schemes are all 50-kHz.

Figure IV.4. Ultraharmonic energy measurements as a function of the peak-to-peak pressure for 33.3% duty cycle 15 cycle pulsed ultrasound (US), 62.5% duty cycle 15 cycle pulsed US, and intermittent continuous wave (CW) US at 220 kHz. Each point is the summation of the cavitation signal over 80 seconds. The point of change in the slope defined by the piecewise linear fit is defined as the cavitation threshold.

Figure IV.5. Simulated peak-to-peak pressure maximums in four tissues in 20 CT scans for 220 kHz continuous wave (CW) ultrasound (US), and 220 kHz pulsed US with 15-cycle pulses at 62.5% duty cycle and 33.3% duty cycle. The pressure was reported in four regions: (A) extracranial soft tissue (ST), (B) bone, (C) brain, and (D) clot. The pressure maximum in the clot was fixed at 0.44 MPa for all 20 patients. No statistically significant difference in the pressure was found within each region examined.

Figure IV.6. Simulated acoustic and acoustic pressure fields in a representative subject for (A) continuous wave (CW) ultrasound, (B) pulsed ultrasound with 62.5% duty cycle, and (C) pulsed ultrasound with 33.3% duty cycle. The absolute peak-to-peak pressure maximum for the simulations is displayed in gray scale. Temperature is displayed using a heat map with a minimum color priority write threshold of 1 °C. CT features such as the bone (cyan) and the skin and internal epithelium (beige), and the clot (green), are plotted using contour lines. The transducer is outlined in magenta. Constructive interference is prominent in the soft tissue between the temporal bone and the transducer. Some constructive interference is also present in the brain tissue close to the contralateral temporal bone, however, the pressure in this region did not exceed the pressure in the M1 section of the middle cerebral artery. Temperature rise was prominent in the ipsilateral bone along the transducer axis.

Figure IV.7. Simulated temperatures in 20 patients for 220 kHz continuous wave (CW) or pulsed ultrasound (US) with 15-cycle pulses at either 62.5% duty cycle or 33.3% duty cycle. Temperature was calculated using the bioheat transfer equation. A heating source was determined from the time-averaged intensity derived from the acoustic pressure (eq.4). The maximum temperature after 400 s was reported in four regions: (A) extracranial soft tissue (ST), (B) bone, (C) brain, and (D) clot. A one-way ANOVA was used to compare treatments and statistically equivalent groups are shown by compact letter display.

Figure IV.8. Comparison of various patient specific parameters including bone thickness (A-C), bone density (D-F), and incident angle between transducer and bone (G-I) and the maximum pressure in the external soft tissue (A,D,G), bone (B,E,H), and brain (C,F,I) for 20 simulations. A linear fit was applied to each relationship. Table IV.I contains the R^2 values for each correlation.

Figure IV.9. Maximum peak-to-peak pressure in the soft tissue (A), bone (B), and brain (C) as a function of the free field maximum peak-to-peak pressure. A linear fit was applied to each relationship. Table IV.I contains the R^2 values for each correlation.

Figure IV.10. The maximum temperature for 20 simulations as a function of four variables: bone thickness (A), bone density (B), incident angle (C), and the acoustic pressure at the transducer surface (D). All temperature maximums occurred in the bone. A linear fit was applied to each relationship. Table IV.I contains the R^2 values for each correlation.

Figure IV.11. Normalized clot width as a function of time for each treatment. All clots were treated in human fresh frozen plasma. A clot fraction over 100% indicates clot swelling and consequent increase in diameter. Clot swelling was observed early during treatment for clots treated with recombinant tissue plasminogen activator (rt-PA) alone. Clots treated with rt-PA, Definity®, and the 33.3% pulsed scheme showed minor clot swelling in the first few minutes. Each line is the mean of 16 measurements with the standard deviation given by the error bars.

Figure IV.12. (A) Fractional clot loss (FCL) and (B) average lytic rate (ALR) achieved with each treatment group. The recombinant tissue plasminogen activator (rt-PA) concentration was 3.15 μg/mL. All ultrasound (US) groups included plasma and rt-PA (3.15 μg/mL) and Definity® (2 μL/mL) in the presence of flow (0.65 mL/min). A one-way ANOVA was used to compare treatments and statistically equivalent groups are shown by compact letter display. $N = 16$ for each group. The median value is given by the center line in each box. A Tukey boxplot is used where the boxes span the interquartile range and the bars span the data from maximum to minimum excluding any outliers.

Figure IV.13. (A) Ultraharmonic (UH) energy and (B) harmonic energy for the ultrasound (US) insonation schemes used in this study. Energy was summed over a frequency bandwidth of

4-kHz around the center frequency for the continuous wave (CW) US scheme and 50-kHz for the pulsed US. Ultraharmonics and harmonics were chosen based on frequencies below 2-MHz with a signal-to-noise ratio greater than 10 dB. Note the higher magnitude of energy in the harmonic frequencies. Statistical significance using a Kruskal-Wallis test is shown by compact letter display. A Tukey boxplot is used where the boxes span the interquartile range and the bars span the data from maximum to minimum excluding any outliers. One outlier is present in the UH energy for 33.3% duty cycle pulsed US.

Figure IV.A1. Normalized error between exact and approximate solutions for intensity as a function of the aperture radius normalized by the wavelength (ka). For $0.3 < ka < 30.9$, the assumption that the acoustic propagation resembles a plane wave at the natural focus is invalid. Outside of this *ka* range, the intensity is proportional to the square of the pressure.

LIST OF TABLES

Chapter III

Table III.1. Intracranial field measurements in 3 porcine skulls. The free field was first measured, then the porcine skull positioned relative to the transducer as described in the *in vivo* thrombolysis methods.

Chapter IV

Table IV.I. Correlation of patient and ultrasound parameters on the maximum pressure measured in silico. The bone thickness, mean bone density, incident angle between transducer and bone, and the free field maximum peak-to-peak pressure required to achieve 0.44 MPa peak-to-peak pressure at the clot were all compared to the peak-to-peak pressure maximum in each tissue type (external soft tissue, bone, and brain). P_{ff} is the pressure in the free field.

Table IV.II. Correlation of patient and ultrasound parameters on the maximum temperature measured in silico. The bone thickness, mean bone density, incident angle between transducer and bone, and the free field maximum peak-to-peak pressure required to achieve 0.44 MPa peak-to-peak pressure at the clot were all compared to maximum temperature in the bone. P_{ff} is the pressure in the free field.

CHAPTER I: INTRODUCTION

I.1 Background

I.1.1 Pathophysiology of stroke

Stroke is the fifth leading cause of mortality and a leading cause of morbidity in the United States [1]. Stroke can be subdivided into two major, yet contrasting classes, ischemic and hemorrhagic. Ischemic stroke is characterized by a reduction in blood flow within vessels feeding the brain, and hemorrhagic stroke is characterized by bleeding which diverts blood flow into the intraparenchymal, intraventricular, or subarachnoid space and forms a thrombus. Despite these different etiologies, the pathophysiologies of both stroke subtypes converge with the formation of a blood clot.

For ischemic stroke, vascular occlusion can occur either by the formation of a thrombus locally (thrombotic stroke), or by the translocation of an occlusive material (air, clotted blood, fat) from a distal site to the vessel (embolic stroke). The interruption of blood flow deprives the brain tissue of essential nutrients including oxygen and glucose [2]. The brain is one of the most metabolically active organs in the body receiving about 20% of the cardiac output despite being only 2% of the total body weight [2]. Infarcted tissue distal to the occlusion, which may receive collateral circulation, forms a penumbra of hypoxic tissue with the ability to recover if blood flow is reestablished within a few hours [3]. Both the ischemic core, and the surrounding penumbra, contain neurons that die after as little as 3 minutes of anoxic conditions [3]. Therefore, time is a critical factor to preserve brain tissue in the penumbra of an occlusion.

Ischemic stroke is characterized by the absence of flow, and hemorrhagic stroke is characterized by uncontrolled flow. Spontaneous hemorrhagic stroke occurs due to aneurysm rupture, hypertension, or vascular malformations [4]–[6]. Additionally, hemorrhagic stroke can

occur secondary to an ischemic stroke as the damaged blood vessels break down [1], [7]–[9]. As blood enters the intraparenchymal space, pressure builds up which can cause brain herniation, which in turn can lead to death via compression of the cardiac and respiratory centers of the brain [10]. The diversion of flow can cause hypoperfusion to the distal regions of the affected blood vessel causing hypoxia and cell death similar to ischemic stroke [7]. The diverted blood of a hemorrhagic stroke eventually clots and this thrombus prevents further bleeding into the parenchyma and restores blood flow to hypoperfused tissue in the vessel path, preserving downstream brain tissue. However, the new thrombus can cause problems to the adjacent brain tissue.

Hemorrhage size has also been linked to outcomes, where small volume hemorrhages are associated with better prognosis [11], [12]. Extravascular blood is toxic to brain tissue and can lead to local apoptosis, programmed cell death [13]. The generation of reactive oxygen species (ROS) from hemoglobin, heme, and complement factors in the extravascular blood trigger local apoptosis [13]. Therefore, the increasing volume of hemorrhage results in an increasing concentration of local ROS and greater toxic effects. The immune system responds by removing pro-oxidative blood products through phagocytosis by microglial cells, however this response alone is insufficient to protect brain tissue in many hemorrhagic strokes [14].

I.1.2 Pharmacologic and Surgical Therapies for Stroke

Several clinical studies have examined effective strategies to treat large volume 30-80 mL hemorrhages by lysing (liquefying) and removing as much of the thrombus as possible with the goal of reducing the intracranial pressure and the exposure of the brain parenchyma to blood, either through surgery or thrombolytic-aided hematoma drainage [15], [16]. These studies have shown that minimally invasive surgery to evacuate supratentorial hemorrhage improves both

morbidity and mortality [15], [16]. More recently the MISTIE III trial, a large randomized controlled trial, was published demonstrating no significant improvement between medical management and minimally invasive surgery used to reduce hematoma size in acute intracerebral hemorrhage [17]. The MISTIE III investigators noted, however, that the surgical end point of reducing the hematoma to 15 mL or less was only achieved in 58% of patients treated with minimally invasive surgery. For the subset of patients treated with minimally invasive surgery whose hematoma volume was reduced below 15ml, there was significant improvement in clinical outcomes compared to medical treatment [17]. Therefore, technical improvements to liquefy and remove the thrombus from the brain may contribute to better outcomes. In this way, both ischemic and hemorrhagic strokes can benefit from the development of improved thrombolytic therapies, both surgical, and pharmaceutical.

Initial thrombolytic therapy protocols focused on intravenous (IV) delivery of a thrombolytic drug to break down clots in the arterial system [18]–[20]. Early development of exogenous thrombolytics started with the use of a bacterial derived fibrinolysin, streptokinase, which was observed to break down human plasma clots composed of fibrin [21]. An endogenous serine protease used to break down thrombi *in vivo*, recombinant tissue plasminogen activator (rt-PA), was shown to be more efficacious than previously isolated fibrinolysins [22]–[24]. The IV administration of rt-PA became the standard of care in stroke following a 1995 landmark NINDS study [25] which showed efficacy if administered within 3 hours of symptom onset. Subsequent clinical studies, such as ECASS I and II, showed no efficacy beyond 3 hours along with an increase in intracerebral hemorrhage (ICH) for patients who received rt-PA compared to placebo, which delayed its use internationally [26], [27]. Later studies showed efficacy when administered up to

4.5 hours after symptom onset [28], [29]. IV rt-PA therapy is currently the gold standard of stroke therapy in both clinical and research settings.

Despite its promise, rt-PA has shown only modest lytic efficacy. Due to drug complications, the exclusion criteria for rt-PA are so stringent that in 2015 the American Heart Association identified that only 3.4-5.2% of presenting ischemic stroke patients ultimately receive rt-PA [30]. Of patients who receive rt-PA, only 33% achieve a modified Rankin Scale score of 0-1 (no disability after 6 months) compared to 20% in corresponding controls [31]. Thus despite this therapeutic improvement, stroke continues to be a leading cause of morbidity worldwide [32].

Intravenously administered thrombolytics were shown to be effective for smaller occlusions in distal sites (M2 or M3 branch of middle cerebral artery, MCA), but had limited efficacy for large occlusions such as the M1 portion of the MCA or the internal carotid artery (ICA) [33]–[38]. With the advent of improved intravascular techniques, it became possible to locally deliver thrombolytics intra-arterially (IA) at these more resistant, large vessel thrombi. In both the PROACT I and II trials, significant improvement in vessel recanalization was observed with IA thrombolytics delivered into the thrombus over IV heparin alone [39], [40]. These improvements in IA embolectomy techniques fueled further research into arterial approaches to thrombolysis, which eventually replaced IA thrombolytic delivery.

Mechanical thrombectomy using minimally invasive techniques has become first line treatment for large vessel occlusions due to improved efficacy and expansion of the treatment window from 4.5 hours to 16 hours, and even more recently, to 24 hours [41], [42]. The MERCI (Mechanical Embolus Removal in Cerebral Ischemia) retriever, the first endovascular device for IA thrombus removal, was associated with the recanalization of occluded vessels in 48-68% of the intention-to-treat group in early trials compared to the 18-30% spontaneous recanalization rate

seen in the PROACT II trial [39], [43], [44]. However, Broderick et al. (IMS trial) compared medical treatment with thrombolytics to endovascular intervention and found no improvement in long term outcomes or survival for endovascular intervention despite the improvement in recanalization [45]. These findings were followed by two more trials, SYNTHESIS and MR-RESCUE which also demonstrated no improvement in long term outcomes despite improved recanalization rates [46], [47]. Both studies concluded that baseline imaging and selection of patients with large vessel occlusions could address limitations in their protocols as well as improvements in embolectomy devices and more experience in their use clinically. Manufacturers borrowed concepts from stent-based coronary procedures to improve next generation embolectomy devices [48]–[51]. Five trials were conducted to compare pharmacologic and supportive treatments (including IV rt-PA) to next generation endovascular treatment [52]–[56]. MR CLEAN was the first clinical trial demonstrating an improvement in the functional independence of individuals treated with endovascular techniques compared to thrombolytics alone [52]. Four remaining studies were prematurely concluded based on the superiority of endovascular treatment over medical management [52]–[56]. More recently, the DAWN and DEFUSE 3 trials have demonstrated efficacy for embolectomy therapy for patients within 6-24 hours after stroke onset [41], [57].

Despite a clear improvement in efficacy, mechanical thrombectomy remains difficult to implement. Fewer than 10% of patients with acute ischemic stroke qualify for mechanical thrombectomy within the allotted 24 hour period because of limitations due to thrombus location [42], [58], [59]. Patients who qualify for mechanical thrombectomy are still delayed by limited identification and transport delays, as patients often must be taken to a stroke center with trained interventionalists who can provide this complex critical care. There has been increasing pressure

to develop treatments that may be available at earlier time points to provide effective and time-sensitive therapy for patients.

Improvements in stroke therapy using IV thrombolytics and mechanical thrombectomy have been instrumental in reducing stroke mortality with faster recanalization and expanded treatment windows. However, thrombolytic therapy still has limited efficacy in intravascular applications due to diffusion-dependent action, which is a function of flow. Endovascular techniques have worked very well for a catastrophic class of large vessel strokes in which patients can reach a tertiary center with endovascular capabilities. However, this is relegated to a small subset of patients. Improvements in the efficacy and availability of thrombolytic treatment would address major limitations in current therapy and expand stroke therapy.

I.2 Sonothrombolysis[1]

I.2.1 Overview

Due to limitations in thrombolytic efficacy and speed, ultrasound in combination with thrombolytic drugs with or without cavitation nuclei (sonothrombolysis), has been under extensive investigation in the last two decades [60]. Following the advent of lithotripsy to treat kidney stones, ultrasound was applied to break up blood clots by Sobbe et al. and later tested in a canine model using 26.5 kHz ultrasound [61], [62]. These studies sparked a new field of ultrasound mediated thrombolysis. Treatment of a clot with ultrasound alone has been effective with both high intensity focused ultrasound (HIFU) including histotripsy [63]–[68], as well as intravascular

[1] *Adapted from Ultrasound in Medicine and Biology, 46(6), Kooiman, K., Roovers, S., Langeveld, S., **Kleven, R.**, DeWitte, H., O'Reilly, M., Escoffre, J., Bouakaz, A., Verweij, M., Hynynen, K., Lentacker, I., Stride, E., Holland, C., Ultrasound-responsive Cavitation Nuclei For Therapy And Drug Delivery, 1311-1313, Copyright (2020). Quoted text is identified by a vertical line in the left margin. Reproduced with permission. All rights reserved.*

low frequency (20 kHz) ultrasound probes [69]–[71]. However, these methods also cause detrimental off-target effects, including vessel damage, necrosis, and hemorrhage [72], [73]. To avoid negative bioeffects on surrounding tissue, low intensity ultrasound has been studied as an adjuvant to thrombolytic therapy [60], [74], [75]. The use of ultrasound to improve pharmaceutically induced thrombolysis was first explored by Hong et al., Tachibana, and Francis et al. who independently investigated ultrasound-enhanced lysis in the presence of streptokinase, urokinase, and rt-PA respectively [76]–[78]. Recent findings suggest that acoustic cavitation is responsible for acceleration of thrombolysis by ultrasound (US) energy [79]–[83]. Since then, ultrasound has been studied to assist in the treatment of stroke [84]–[87], myocardial infarction [88]–[90], acute peripheral arterial occlusion [91], deep vein thrombosis [92], and pulmonary embolism [93]–[95].

I.2.2 Mechanisms, Agents, and Approaches

A main limitation of IV thrombolytic therapy is the poor penetration of thrombolytics into thrombi [96], [97]. Ultrasound improves recombinant tissue plasminogen activator (rt-PA) diffusion into thrombi and augments lysis primarily via acoustic radiation force and streaming [77], [81], [98]–[103]. Additionally, ultrasound enhances the removal of fibrin degradation products via ultrasonic bubble activity, or acoustic cavitation, that induces microstreaming [81]–[83], [98], [99], [104]–[107]. Two types of cavitation are correlated with enhanced thrombolysis, stable cavitation, with nonlinear bubble motion resulting in acoustic emissions at the subharmonic and ultraharmonics of the fundamental frequency [108]–[110], and inertial cavitation, with substantial radial bubble growth and rapid collapse generating broadband acoustic emissions [111], [112].

Specialized contrast agents and tailored ultrasound schemes have been investigated with the aim of optimizing sonothrombolysis. Ultrasound contrast agents (UCA) provide bubble nuclei for cavitation and reduce the pressure required to nucleate and sustain cavitation [113], [114]. Petit et al. observed a greater degree of rt-PA lysis with BR38 microbubbles exposed to 1 MHz pulsed ultrasound at an amplitude causing inertial cavitation (1.3 MPa peak rarefactional pressure) than at a lower amplitude causing stable cavitation (0.35 MPa peak rarefactional pressure) [99]. Goyal et al. also measured a higher degree of thrombolysis with 1 MHz pulsed ultrasound at 1.0 MPa peak rarefactional pressure with inertial cavitation than at 0.23 MPa peak rarefactional pressure with stable cavitation in an *in vitro* model of microvascular obstruction using perfluorobutane-filled, lipid shelled microbubbles as a nucleation agent [115], [116]. Additionally, Kleven et al. (Chapter IV) observed more than 60% fractional clot width loss for highly retracted human whole blood clots exposed to rt-PA, Definity® and 220 kHz pulsed or continuous wave (CW) ultrasound at an acoustic output with sustained stable cavitation throughout the insonification periods (0.22 MPa peak rarefactional pressure), with similar results in other studies [83], [117], [118].

Echogenic liposomes loaded with rt-PA enhanced lysis compared to rt-PA alone at concentrations of 1.58 and 3.15 mg/mL, suggesting that encapsulation of rt-PA could reduce the rt-PA dose by a factor of two with equivalent lytic activity [119]. Subsequently it has been demonstrated that these liposomes protect rt-PA against degradation by plasminogen activator inhibitor-1 (PAI-1), while achieving equivalent thrombolytic efficacy relative to rt-PA, Definity®, and intermittent 220 kHz CW ultrasound [118]. Promising agents, including a nanoscale (< 100 nm) contrast agent [120] and magnetically targeted microbubbles [121], have also demonstrated enhanced rt-PA thrombolysis *in vitro*. All these investigators noted that in the

absence of a thrombolytic, the stable and inertial cavitation due to ultrasound did not degrade the fibrin network.

Several minimally invasive techniques have also been explored, with or without the inclusion of rt-PA or exogenous cavitation nuclei. In the clinical management of stroke, rapid treatments are needed because of the neurologist's adage "time is brain". Thus, treatment options that promote fast thrombus removal, reduce edema and intracerebral bleeding, and improve patient outcomes are of immense value. Magnetic resonance image-guided high intensity focused ultrasound has been investigated for the treatment of both ischemic [68] and hemorrhagic [122] stroke, and Zafar et al. have provided an excellent review of the literature for this approach [123]. Histotripsy, a form of high intensity focused ultrasound that relies on the mechanical action of microbubble clouds to ablate thrombi with and without rt-PA [63], [64], [124], [125] is under development to treat deep vein thrombosis. Additionally, ultrasound-accelerated catheter-directed thrombolysis using the EKOS system (EKOS/BTG, Bothell, WA, USA) combines 2 MHz low-intensity pulsed ultrasound and rt-PA without cavitation nuclei to improve lytic efficiency to treat deep vein thrombosis [92] and pulmonary embolism [126].

I.2.3 Cavitation monitoring

Acoustic cavitation has been shown to mediate direct fibrinolysis [127] and accelerated rt-PA lysis [81], [98], [105], [128]. Passive and active cavitation detection techniques have been developed to monitor acoustic cavitation [83], [129], [130]. Passive cavitation imaging, or passive acoustic mapping, employs a transducer array that listens passively (i.e., no transmit) to emissions from acoustically activated microbubbles [131]–[133]. Vignon et al. developed a prototype active array enabling spectral analysis of bubble activity for sonothrombolysis applications [134]. Superharmonic Doppler effects have also been utilized to monitor bubble activity from 500 kHz

pulsed therapeutic ultrasound [135]. Both a linear array [136]–[138] and a sparse hemispherical array [139] have been integrated into a clinical magnetic resonance image-guided high intensity focused ultrasound system to assess microbubble dynamics during sonothrombolysis in the brain.

I.2.4 Preclinical studies of Sonothrombolysis

Information gathered from animal studies can help inform human clinical trials, despite a strong species dependence of clot rt-PA lytic susceptibility [140], [141]. A comprehensive systematic evaluation of 16 *in vivo* preclinical sonothrombolysis studies was carried out by Auboire et al. summarizing treatment efficacy and safety outcomes in models of ischemic stroke [142]. Since that review was published, the efficacy of sonothrombolysis using nitrogen microbubbles stabilized with a non-crosslinked shell delivered intra-arterially through a catheter and rt-PA delivered intravenously has been demonstrated in a rat model of ischemic stroke [143].

I.2.5 Clinical studies of Sonothrombolysis

A rich literature exists of clinical trials exploring the safety and efficacy of sonothrombolysis. Several clinical trials have demonstrated an improvement in IV thrombolytic efficacy when combined with ultrasound (1-2 MHz) and ultrasound contrast agents [84]–[86], [144], [145]. Two recent meta-analyses of seven randomized controlled trials [87], [123] attempt to determine whether the administration of rt-PA and ultrasound improve outcomes in acute ischemic stroke. Both analyses conclude that sonothrombolysis significantly enhances complete or partial recanalization, with improved neurologic function (assessed via the National Institutes of Health Stroke Scale, NIHSS). Included in these meta-analyses is the NOR-SASS trial which was canceled prematurely due to funding with no improvement observed in treatment with ultrasound over thrombolytics alone [146]. Despite this observation, the authors point out that this population was unselected, meaning patients were not treated based on the presence of a thrombus

in the major vessels, while most other studies select treatment and controls from patients presenting with confirmed large vessel occlusions on angiogram. Indeed, 7 patients were identified to have been treated using the wrong acoustic window and patients were treated using a fanning technique when a thrombus could not be defined on computed tomography angiography (CTA). These patients which may have received incomplete treatment were included in the analysis despite suboptimal treatment which may have biased the results [146]. An ongoing clinical trial (TRUST; NCT03519737) will determine whether large vessel occlusions can be recanalized with sonothrombolysis (Cerevast Medical, Inc., Bothell, WA, USA) and either tenecteplase or alteplase [147], while patients are transferred to a stroke center for mechanical thrombectomy [148].

In addition to stroke, ultrasound has been shown to augment thrombolysis in other pathologies. Several clinical trials have shown that high mechanical index (MI) pulsed diagnostic ultrasound exposure of Definity® before and after percutaneous coronary intervention for ST elevation myocardial infarction can prevent microvascular obstruction and improve cardiac functional outcomes [88]–[90]. A systematic review of 16 catheter-directed sonothrombolysis clinical trials comprised mostly of retrospective case series using the EKOS system without microbubble infusions determined that this treatment modality is safe and promising for the treatment of deep vein thrombosis (DVT). However, a large-sample randomized prospective clinical trial is needed to improve the clinical evidence for use as a front-line therapy for DVT [92]. In retrospective studies in patients with pulmonary embolism Lee et al. [95] conclude that catheter directed sonothrombolysis is safe and decreases right-sided heart strain, but Schissler et al. [149] conclude that this therapy is not associated with a reduction in mortality nor increased resolution of right ventricular dysfunction. And finally, an ongoing trial in a small cohort of 20 patients with acute peripheral arterial occlusions [91] will determine whether Luminity® (marketed

in the US as Definity®) and 1.8 MHz transdermal diagnostic ultrasound with intermittent high MI (1.08) and low MI (0.11) for visualization of the microbubbles and flow will improve recanalization. In summary, sonothrombolysis has demonstrated clinical benefit in the treatment of acute and chronic thrombotic disease. Ultrasound-assisted thrombolysis has a potential role as an emerging viable and therapeutic option for future management of stroke and cardiovascular disease.

I.3 Models of Thrombolysis *in vitro*

I.3.1 Clot composition

Modeling stroke *in vitro* faces several challenges: thrombus composition and structure, the presence of flow, methods of treatment delivery, and lytic metrics. Enzymatic thrombolysis due to thrombolytics (plasminogen, rt-PA) designed for humans is highly species dependent as these drugs have variable sensitivity to clots composed of non-human fibrin proteins [141], [150]. Therefore, the use of a human clot is key in predicting clinical outcomes. Additionally, thrombi extracted from living subjects vary in composition, mechanical properties, and susceptibility to rt-PA. Liebeskind et al. noted three main categories of thrombi from histologically processed specimens from patients: those composed primarily of fibrin (44%), those composed primarily of red blood cells (RBC, 26%), and those with a mixed composition (30%) [151]. Similar thrombus compositions were observed by Simons et al. [152]. Sporns et al. noted that thrombi which embolized from the heart and lodged in cranial vasculature had a significantly higher proportion of fibrin and platelets and a significantly lower presence of RBCs than thrombi formed natively in the cranial vasculature [153]. All of these studies examined thrombi retrieved with endovascular devices and therefore may have biased the analysis towards thrombi that could survive the removal process and those portions resistant to lysis with rt-PA. Using imaging analysis, Molina et al.

[154] and Cho et al. [155] concluded that cardioembolic thrombi are richer in RBCs than thrombi formed in other locations and are more susceptible to lysis with rt-PA than fibrin-rich thrombi. The high proportion of RBCs in thrombi makes them easier to break up, and high fibrin content thrombi tend to be more resistant to rt-PA lysis.

I.3.2 Thrombus Retraction

Thrombus retraction, which occurs within a few hours of formation, has also been shown to affect lysis and is related to thrombus age [82], [106], [156]. The degree of thrombus retraction can be affected by the thrombus environment when the platelets are activated, with different activating agents inducing different degrees of retraction [82], [157]. For example, a clot (a thrombus formed outside the body) formed within a borosilicate glass tube undergoes significant retraction, purging serum from the clot volume, modifying the fibrin diameter, and decreasing permeability to thrombolytics [82], [157]. Such highly retracted clot models are more resistant to lysis than unretracted clots and are useful to study improvements in thrombolytic therapy as they model thrombi commonly seen in stroke [151], [153], [158].

I.3.3 Presence of Flow

In addition to clot composition, flow can be highly variable in stroke and *in vitro* studies have varied widely in their inclusion of flow [159]. Often, a symptomatic stroke is fully occlusive, creating a flow defect that can be simulated by a simple static fluid system [159]. Many thrombolysis models used in sonothrombolysis studies employ a static volume of plasma or blood to expose the clot to a target therapy [81], [103], [106], [160]–[166]. The use of uninterrupted or partially occluded flow systems has also been used extensively to account for the potential recanalization, partial occlusions, or to mimic intraarterial delivery of therapeutics [80], [82], [83], [105], [118], [120], [121], [167], [168]. The inclusion of collateral circulation more closely

resembles *in vivo* conditions, where a vessel can be partially or fully occluded and flow is able to divert to another vessel based on the local flow dynamics [169], [170]. This also opens up the opportunity to use clinical metrics assessing downstream perfusion *in vitro* [171].

I.3.4 Thrombolytic Metrics

The method to assess thrombolytic efficacy is critical to predicting the clinical potential of a therapy. Many studies in the field of sonothrombolysis have used clot mass loss to assess thrombolytic efficacy [77], [79], [81], [98], [100], [106], [120], [160]–[163], [169], [170], [172]. Clot width or size has also been used to provide real-time analysis to lytic efficacy [83], [118], [121], [141], [167], [168]. In other studies, investigators have looked directly at clot degradation products, such as iodine intercalated into the clot during thrombosis [128], d-dimer [172]–[174], hemoglobin [175], or radiolabeled fibrin/fibrinogen [99], [103], [166], [176]. These techniques provide a direct quantitative comparison assessing the lysis of the fibrin superstructure or its bound components. For microvascular applications, Leeman et al. [80] developed a metric based on the vascular pressure in a partially occluded vessel which provided physiologically relevant information. All of these methods can help elucidate the thrombolytic efficacy of a treatment. However, some of these quantitative metrics cannot be implemented in animal studies.

In vivo thrombolytic metrics rely on physiological and imaging-based metrics or clinical scoring. Physiologic parameters such as flow, as detected by Doppler [85], [159], the ratio of the right and left ventricle dimensions (RV/LV ratio) [93], [177], or perfusion based on CTA, including Thrombolysis in Myocardial infarction (TIMI), modified Treatment in Cerebral Ischemia (mTICI), or arterial occlusive lesion (AOL) scores [85], [93], [178], [179]. Additionally, D-dimer has been used in an *in vivo* model of stroke in rats using human clots [180]. Clinical scores such as the modified Rankin Scale (mRS) [41], [52], [144], or the National Institute of

Health Stroke Scale (NIHSS) [85], [159] have been used extensively in clinical trials. However, these scores assess clinical outcomes that can be difficult to translate to animal studies.

I.4 Animal models of stroke

Preclinical animal models can be divided into rodent and large animal models. Rodent models have small brain sizes, which can allow comprehensive brain analysis without excess cost or labor. Additionally, rodent models tend to be more consistent and reliable due to the strictly controlled genetic lines and the prevalence of protocols and metrics designed for these species [181], [182]. Rats in particular have been used effectively in stroke due to the similarities in their cerebrovascular architecture with humans [183] and homogeneity between strains [184]. However rodent models lack a developed white matter and gyrencephallic brain structure making it hard to translate results observed in these models to clinical outcomes. Additionally, rodent animal models are small, which result in animal models with thrombi which are very different sizes and dimensions than those seen clinically. As lysis is diffusion dependent, these models may not be appropriate for modeling thrombolysis in humans.

Large animal models have been used extensively in stroke research, including swine, rabbits, dogs, sheep, and non-human primates [142], [185], [186]. The great expense and difficulty using non-human primates and dogs has limited their use in research. Other animals, like swine, rabbits, and sheep have found particular advantages based on vessel size, blood flow, cardiovascular similarities, and compatibility with clinical imaging modalities (MRI, CT) [187]. Sheep, and to a lesser extent cows, have similar susceptibilities to thrombolysis when exposed to human plasmin and rt-PA, while swine show much less activation of plasmin from rt-PA and less reactivity to human plasmin [140], [150]. This decrease in sensitivity to rt-PA is most likely due to the poor activation of porcine plasminogen by human cell-derived rt-PA [140].

Given this thrombolytic resistance of porcine clots to human thrombolytic treatment, it is pertinent to explore a xenographic (human) clot in a porcine animal model [141], [188]. Pigs have been traditionally used for vascular and interventional studies due to their large size, which makes them amenable to interventional techniques. An additional advantage of pigs in ultrasound studies is that juvenile pigs have a similar skull thickness to the adult temporal bone window which has been used in human studies for ultrasound enhanced thrombolysis [86], [159], [189].

Animal models also need to mimic the conditions under which ultrasound would propagate through the skull. High frequency ultrasound (> 1 MHz) is attenuated by the skull and prevents its use in a cohort of patients [189]. Frequencies above 1 MHz undergo significant attenuation through the skull causing an insufficient temporal bone window for transcranial doppler (TCD) in 29 % of patients [162], [189], [190]. Ultrasound frequencies between 120-500 kHz can be implemented to avoid this temporal bone acoustic insufficiency [191], [192]. However, in the TRUMBI trial at a lower frequency (300 kHz), Daffertshoefer et al. observed a significant increase in intracerebral hemorrhage for patients treated with ultrasound compared to those receiving rt-PA alone [193]. Retrospective computational analysis of the TRUMBI trial identified standing waves within the brain parenchyma which would cause higher intracranial acoustic pressure amplitudes than originally predicted [194]. Further adverse reactions could be prevented with more investigations into the biosafety of sonothrombolysis to prevent off-target bioeffects [194]–[196].

I.5 Specific Aims

Low frequency (120-220 kHz) unfocused ultrasound therapy has been used successfully *in vitro* to accelerate thrombolysis. This effect has not been explored in a large animal model which is a necessary step to developing clinical applications. The central hypothesis of this dissertation is that microbubbles exposed to ultrasound nucleate stable cavitation, which promotes

thrombolysis in the brain. The goal of this project is to use microbubbles exposed to pulsed or intermittent CW ultrasound at 120 and 220 kHz to improve thrombolysis *in vivo*. To explore this central hypothesis, the following hypotheses and specific aims will be examined in each chapter.

Chapter II: Ultrasound Accelerated Thrombolysis in a Porcine Thromboembolism Model

Hypothesis 1: Intermittent continuous wave 220 kHz ultrasound and Definity® enhances rt-PA lysis of human retracted clots and improves recanalization of occluded vessels.

This hypothesis was tested in an *in vitro* system based on the porcine cranial circulation as well as in the porcine cranial circulation *in vivo* according to the following specific aims.

I.5.1 Specific Aim 1: (Chapter II) **Evaluate** the thrombolytic efficacy of rt-PA, Definity®, and 220 kHz ultrasound in a porcine artery thromboembolism model

Aim 1a. Establish an occlusion in a porcine thromboembolism model with a retracted human whole blood clot and evaluate thrombolytic efficacy of rt-PA with and without ultrasound and Definity® *in vivo.*

Aim 1b. Determine the relationship between reperfusion (flow) and mass loss in an occlusive model of stroke *in vitro*.

Chapter III: Thrombolytic Efficacy of Transcranial Ultrasound in a Porcine Intracerebral Hemorrhage Model

Hypothesis 2: Transcranial 120 kHz pulsed ultrasound exposure without Definity® enhances rt-PA lysis of intracranial thrombi in juvenile pigs.

To test this hypothesis, several metrics of thrombolytic efficacy were evaluated *in vitro* and *ex vivo.* Once a metric of thrombolysis was chosen, hypothesis 2 was examined according to the following specific aims.

I.5.2 Specific Aim 2: (Chapter III) Evaluate the efficacy of transcranial 120 kHz ultrasound to enhance thrombolysis in an *in vivo* porcine intracerebral hemorrhage model.

Aim 2a. Develop a protocol to assess thrombolytic efficacy for porcine thrombi formed in the porcine brain parenchyma *in vitro and ex vivo*.

Aim 2b. Evaluate thrombolytic efficacy of 120 kHz transcranial ultrasound for porcine thrombi formed in an *in vivo* intracerebral hemorrhage model.

Chapter IV: The Effect of Insonation Scheme on Lytic Efficacy and Predicted Intracranial Pressure and Temperature

Hypothesis 3: Pulsed 220 kHz ultrasound exposure of cranial tissues produces less constructive interference and causes lower thermal deposition compared to intermittent continuous wave ultrasound.

This hypothesis was explored *in silico* using a finite difference method to predict the acoustic field and temperature deposition in 20 ischemic stroke patients based on CT scans. Furthermore, the lytic efficacy of each insonation scheme was compared *in vitro*. The following specific aims were employed to test hypothesis 3.

I.5.3 Specific Aim 3: (Chapter IV) Evaluate the predicted cranial acoustic pressure amplitude and temperature in simulations based on human skulls and the *in vitro* measured thrombolytic efficacy for pulsed and intermittent continuous wave ultrasound.

Aim 3a. Design a pulsing scheme at 220 kHz based on patient skull dimensions and evaluate the predicted acoustic pressure amplitude and temperature for the pulsed ultrasound scheme compared to an intermittent continuous wave scheme.

Aim 3b. Compare the thrombolytic efficacy of the pulsed ultrasound scheme in Aim 3a to an intermittent continuous wave scheme *in vitro*.

I.6 Dissertation overview

The focus of this dissertation was to determine whether unfocused low frequency (120-220 kHz) ultrasound enhanced thrombolysis in clinically relevant animal thromboembolism and intracerebral hemorrhage models, with the goal of translating this technology to clinical studies in the future. In particular, this dissertation has explored three themes pertaining to sonothrombolysis: the design of *in vivo* models used to test novel stroke therapeutics, the determination of lytic metrics to evaluate thrombolysis, and the effects of pulsed ultrasound driving parameters employed to enhance thrombolysis at 220 kHz. To accomplish this, studies were conducted *in silico* in both human and porcine models, *in vitro*, *ex vivo*, and *in vivo* with porcine models of stroke.

In Chapter II, a porcine thromboembolism model was used to test thrombolytic efficacy of 220 kHz pulsed ultrasound in conjunction with rt-PA and Definity® microbubbles. The work in Chapter II established a variation of the porcine model adapted from Culp et al. with the introduction of a human xenographic clot in the cerebral circulation. The experiment was first conducted in an *in vitro* model of the porcine cranial circulation and then translated into the *in vivo* model. Using the *in vitro* model of the porcine cranial circulation, the lytic metrics of clot mass loss and restoration of flow were compared. Perfusion based on clinical scores from angiography were used to assess the same treatments in a living model and the clot burden was assessed by measuring the percent patent area on histological examination of the APA vessels postmortem.

In Chapter III we assessed a model of intracerebral hemorrhage in a juvenile pig. Three thrombolytic metrics (residual thrombus mass, volume, and density) were tested *in vitro* and *ex vivo* to determine their sensitivity to thrombolysis based on sham and rt-PA treated clots. A

thrombolytic metric was then selected to analyze porcine thrombus specimens from studies performed by Ammi et al. Further studies were performed to supplement this data.

In Chapter IV, design constraints of a low frequency ultrasound therapy were explored and a new pulsing scheme was compared to a previously published intermittent insonation scheme. Three insonation schemes were explored, including two pulsed insonation schemes, and an intermittent insonation scheme. Using computed tomography scans of 20 patients with middle cerebral artery occlusions as input, computational simulations with a validated finite difference method were used to predict the intracranial pressure and temperature elevations due to each insonation scheme in the intervening soft tissue, bone, brain, and clot. Each insonation scheme was then compared using a time-lapse microscopy system to evaluate the effect of each insonation scheme of the thrombolysis of the clot in flow.

Finally, these studies were summarized in Chapter V. The key findings were highlighted and suggestions for future work detailed.

CHAPTER II: ULTRASOUND ACCELERATED THROMBOLYSIS IN A PORCINE THROMBOEMBOLISM MODEL[2]

II.1 Introduction:

Sonothrombolysis has been explored as an adjuvant therapy for the treatment of ischemic stroke [74], [197]. Although technical efficacy of sonothrombolysis has been demonstrated in the laboratory, this approach has not improved clinical outcomes in acute stroke trials [144]. *In vitro* [60] laboratory studies of sonothrombolysis do not predict outcomes *in vivo* [144], [198]. In particular, the correlation between clot mass loss (CML), a quantitative metric for *in vitro* [142] thrombolysis, and tissue reperfusion measured *in vivo* is unknown, and the relationship is poorly understood [199].

Culp et al. [200] described a swine arterial occlusion model based on embolization of a fresh autologous porcine clot into the ascending pharyngeal artery (APA). The effect of 1 MHz pulsed ultrasound and microbubble infusions on rt-PA thrombolysis has been investigated in that model [178], [199]–[201]. Recent studies have shown that human clots exhibit greater lysis than porcine clots when exposed to rt-PA (a recombinant human enzyme) and human plasmin [141], [150]. One objective of this study, therefore, was to develop a modified porcine sonothrombolysis model based on human clots. We chose to study highly retracted human clots, in order to mimic the fibrinolytic susceptibility of the thrombi responsible for clinical strokes in humans [151], [153], [202]. Our model also employed clots with physical dimensions that render them recalcitrant to

[2] *Adapted from, "Accelerated Sonothrombolysis with an Ultrasound Contrast Agent in a Xenographic Porcine Cerebral Thromboembolism Model," a manuscript in preparation for submission to an academic journal. Its use in this dissertation will be declared to the journal upon submission. Quoted text is identified by a vertical line in the left margin.*

treatment with thrombolytic drugs which accentuates improvements in reperfusion afforded by adjuvant therapies [202].

This porcine xenographic embolism model is used to assess sonothrombolysis at 220 kHz as a treatment for vascular occlusion such as those seen in stroke. Intermittent continuous wave 220 kHz ultrasound (50 seconds on, 30 seconds off) has been used successfully *in vitro* to enhance rt-PA thrombolysis [117], [118]. Hitchcock et al. have demonstrated that intermittent continuous wave ultrasound improves ultraharmonic signal during treatment, increasing stable cavitation by allowing time for bubbles to reperfuse the treatment region during the quiescent period [105]. It was hypothesized that intermittent continuous wave 220 kHz ultrasound and Definity® enhances rt-PA lysis of human retracted clots and improves recanalization of occluded vessels. To test this hypothesis, a porcine thromboembolism was adapted to use a human clot. The study was performed in two phases. The first phase deployed the retracted human clot directly into the APA and delivered treatment using an end-hole microcatheter at the face of the clot. The second phase deployed the clot into the common carotid where it lodged in the APA due to occlusion of the major collateral vessel using coils. Treatment in phase 2 was delivered through a multi-side-hole microcatheter traversing the clot axially to ensure delivery of rt-PA. Thrombolysis was assessed for both microcatheters *in vitro*. To determine if microbubbles were successfully delivered intact to the thrombus, attenuation spectroscopy was performed on Definity® samples infused through both the end-hole and multi-side-hole microcatheters.

II.2 Methods:

II.2.1 Characterization of Definity® infused through two microcatheter designs

To deliver microbubbles to the occlusion *in vitro* and *in vivo*, it was necessary to ensure some bubbles survived passage through the microcatheter used to deliver treatment. To assess the

effects of infusing microbubbles through 150 cm microcatheters, attenuation spectroscopy was performed following a protocol established by Raymond et al. [203] Definity® microbubbles (Lantheus Medical Imaging, North Billerica, MA, USA) were activated according to the manufacturer instructions using a Vial-Mix (Lantheus Medical Imaging) and withdrawn from the vial using a 19 g needle. The vial was vented to a gas-impermeable bag (Tedlar, Zefon International, Ocala, FL, USA) of octafluoropropane (OFP) during withdrawal, to prevent air from contaminating the vial. Definity® (2 μL/mL) was infused at the *in vivo* flow rate (10 mL/hr) through two different types of microcatheters, one with a single end port (2.8 F Rapidtransit, Codman Neurovascular, Raynham, MA, USA), and the other with multiple side ports positioned 5 cm along the distal end (2.9 F Micromewi, 5 cm infusion length, Medtronics, Minneapolis, MN, USA). Following the infusion, Definity® was further diluted in phosphate buffered saline (PBS) to a final ratio of 1:2000 and placed in a sample holder between two polyvinylidene fluoride (PVDF) broadband transducers and the attenuation of a transmitted pulse was measured between 2-25 MHz. The attenuation of diluted Definity® without infusion through a microcatheter was also measured directly as a control. Each experiment was repeated three times for the end port microcatheter and six times for the multiple side port microcatheter and no catheter measurements.

II.2.2 Retracted human whole blood clot synthesis

Human whole blood was obtained from donors under an approved IRB protocol (# 2012-2575) and with informed consent. One milliliter aliquots of fresh human whole blood were pipetted into borosilicate glass Pasteur pipettes (inner diameter, ID, 4 mm, 4 inches long, Chang Bioscience, Fremont, CA, USA) and the bottom was sealed with beeswax. The aliquots were first incubated at 37 °C for 3 hours, and then refrigerated at 4 °C for 3-17 days to promote the formation of highly retracted clots [82]. Lytic susceptibility of whole blood clots formed in this way do not

change significantly within this time period [106]. Prior to use, clots were removed from the glass pipettes, trimmed to 1.5 cm lengths, and the width of each clot was recorded using a dissection microscope (BX51, Olympus, Melville, NY). A 1.5 cm length was chosen to evaluate the type of highly retracted thrombi that do not respond well to conventional lytic therapy [202]. Each clot was also blotted and weighed following a previously established protocol [81]. Clots were loaded into 1 mL syringes of 50% Optiray (Liebel-Flarshiem LLC, Raleigh, NC, USA): 50% phosphate buffered saline for delivery through a guide catheter (Vista Brite Tip, Cordis, Santa Clara, CA, USA) used in both *in vitro* and *in vivo* studies.

II.2.3 Human whole blood clot lytic susceptibility

Lytic susceptibility of human whole blood clots was tested using a protocol established by Datta et al. [81], [106], [204]. Prior to loading the clots in syringes, a subset of clots was set aside and their lytic susceptibility was assessed using a static porcine plasma protocol. Clots were incubated in 30 mL of thawed fresh frozen porcine plasma for 30 minutes at 37 °C. Various volumes of rt-PA were added to the plasma to achieve a concentration range between 0-100 μg/mL to determine an rt-PA concentration at which clot mass loss no longer increased (Figure II.1). 15.75 μg/mL rt-PA was chosen as the rt-PA concentration to conduct quality control on all subsequent clots. For every blood draw, four clots were tested (2 no treatment, 2 treated with 15.75 μg/mL rt-PA) to ensure clot mass loss did not differ significantly between each donor's clots. This concentration of rt-PA was selected to ensure that small errors in measurement would not affect the outcome of the experiment.

II.2.4 Effects of X-ray Contrast on Lytic Susceptibility

To ensure that digital subtraction angiography performed *in vivo* would not affect results, the effect of Optiray, an X-ray contrast agent, on recombinant tissue plasminogen activator activity

was assessed using a spectrophotometric method [205], [206]. In brief, rt-PA was diluted into a solution of 0.01% Triton-X (Sigma-Aldrich, St Louis, MO, USA) in PBS, and Optiray (between 0-85% by volume) to a concentration of 1 μg/mL and final volume of 1.9 mL. The concentration of PBS was modified to fix the pH in the final solution at 7.4. The solution was warmed to 37 °C and 100 μL of a chromogenic substrate (S02288, Chormogenix, DiaPharma Group, Inc., West Chester, OH, USA) was added to the diluted rt-PA. The chromogenic substrate was hydrolyzed by the rt-PA to form a chromophore which was measured continuously using a spectrophotometer (UV-1700, Shimadzu, Japan) and kept at 37 °C using a temperature controller (TCC-240A, Shimadzu, Japan). The absorbance of the solution was measured at 405 nm for 5 minutes and the change in the absorbance over time (ΔAbs/min) was measured for each sample (Optiray between 0-85%) to determine the enzymatic activity (fibrinolytic efficacy) at each Optiray concentration.

II.3.5 In Vitro Flow Phantom Thromboembolism Protocol

A porcine carotid artery flow phantom was created in a 37 °C water tank to direct flow to two branching tubes, one mimicking the APA, another the external carotid artery (ECA) (Figure II.2). Latex tubing (2.4 mm inner diameter) primed with sodium-citrate anticoagulated porcine plasma (Lampire Biological Laboratories, Pipersville, PA, USA) was pumped through the flow phantom with a syringe pump (Pump 11 Elite, Harvard Apparatus, Holliston, MA) at a rate of 1.5 mL/min. This flow rate was selected to be within the range of flow rates observed by Alexandrov et al. [159] in partially occluded cerebral vessels. A Luer connector with a metal mesh mimicked the *rete mirabile* [207], [208]. An 8 F guide catheter was passed through a hemostasis valve (AccessPLUS, Merit Medical, South Jordan, UT, USA) to deliver clots into the APA mimic and provide microcatheter access to the flow phantom (Figure II.2). A flow probe (ME1PXN,

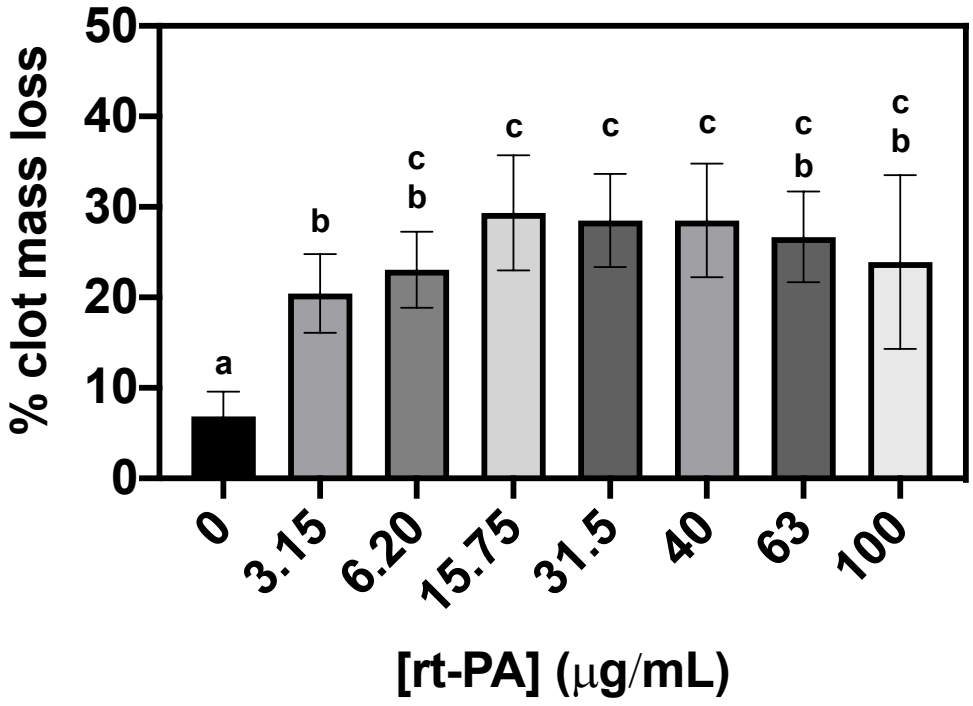

Figure II.1. Percent clot mass loss as a function of varying concentrations of recombinant tissue plasminogen activator in a static clot model. 1.5 cm clots were incubated in 30 mL porcine plasma with varying concentration so of rt-PA and the clot mass measured before and after treatment. The degree of thrombolysis increased significantly with concentration up to 6.20 μg/mL ($p < 0.05$), at which point it did not change significantly ($p > 0.18$). Significance is shown using compact letter display to categorize statistically equivalent groups based on a one-way ANOVA.

Transonic, Ithaca, NY, USA) was placed 12 cm proximal to the simulated *rete mirabile*. A preformed clot was embolized into the APA phantom at the location of the *rete* mimic using the guide catheter.

A custom-designed unfocused transducer (220 kHz center frequency, 38 mm aperture) was positioned so that the clot in the vessel phantom was in the natural focus (5.2 cm). The transducer was driven with a function generator (33250A, Agilent Technologies, Inc., Santa Clara, CA) and power amplifier (Model 75A250, Amplifier Research, Souderton, PA). The total cavitation energy

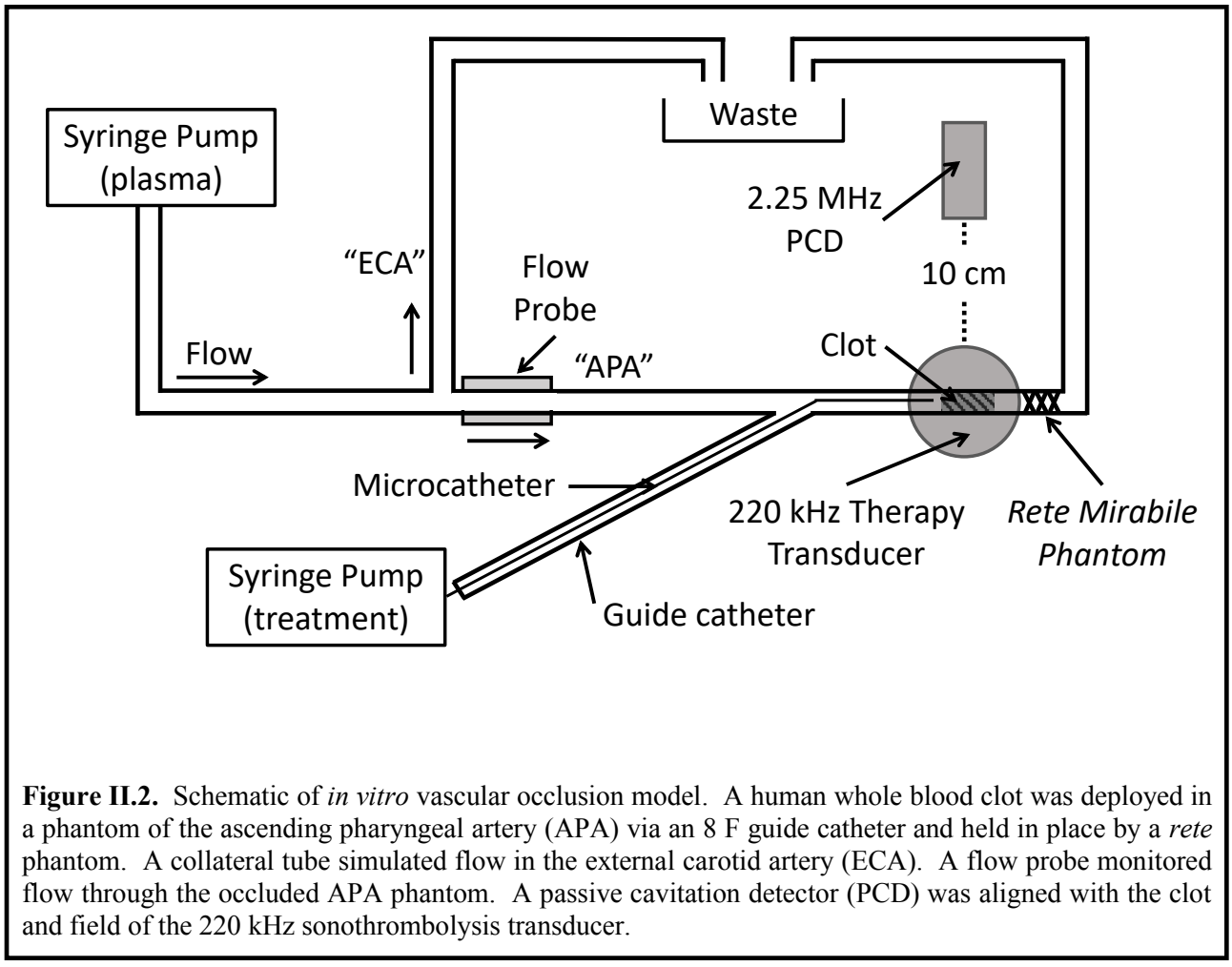

Figure II.2. Schematic of *in vitro* vascular occlusion model. A human whole blood clot was deployed in a phantom of the ascending pharyngeal artery (APA) via an 8 F guide catheter and held in place by a *rete* phantom. A collateral tube simulated flow in the external carotid artery (ECA). A flow probe monitored flow through the occluded APA phantom. A passive cavitation detector (PCD) was aligned with the clot and field of the 220 kHz sonothrombolysis transducer.

was quantified using a passive cavitation detector (19 mm aperture, 2.25 MHz center frequency, 595516C, Picker International, Cleveland, OH) as described by Bader et al. [83].

Two types of microcatheters were deployed through the guide catheter and either positioned at the face of the clot (end hole), or advanced across the clot (multi-side hole) based on the *in vivo* protocols in phase 1 and 2 respectively (Figure II.3). Saline, 1 mg/mL rt-PA only, or 1 mg/mL rt-PA and 2 μL/mL Definity® was infused through the microcatheters for 30 minutes [117] at a rate of 10 mL/hr (n = 10 per treatment arm) for the sham, lytic, and sonothrombolysis treatment arms, respectively. An intermittent continuous wave ultrasound insonation scheme (50 s on, 30 s off) was employed (220 kHz, 0.44 MPa peak-to-peak) for clots treated with rt-PA and

Definity® [83], [117]. The difference between the initial and final clot mass (CML) was calculated as a percentage of the initial mass.

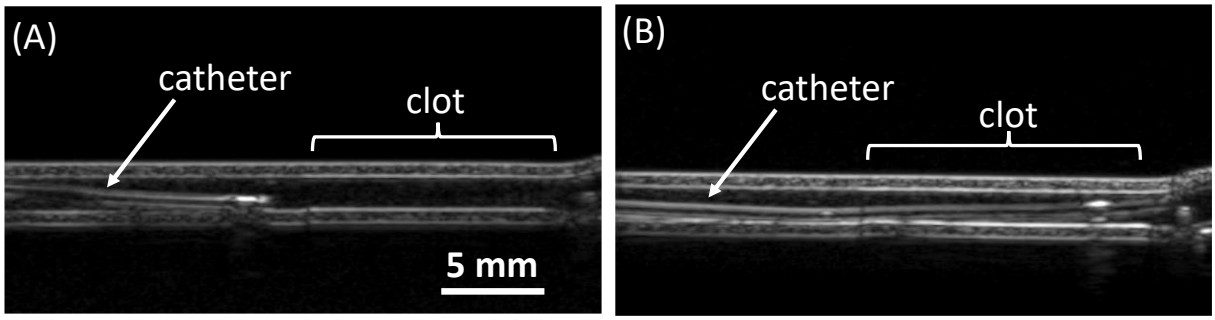

Figure II.3. B-mode Ultrasound images of the *in vitro* flow phantom with an end port microcatheter positioned within 2 mm of the face of the clot (A) or a multiple side port microcatheter traversing the clot (B).

Cavitation signals were monitored using a passive cavitation detector (19 mm aperture, 2.25 MHz center frequency, 595516C, Picker International, Cleveland, Ohio, USA) aligned following the protocol described by Bader et al. [83]. The received RF signal was filtered with a 10 MHz low-pass filter (J73E, TTE Inc, Los Angeles, CA, USA) and amplified using a wideband low-noise amplifier (CLC100, Cadeka Microcircuits LLC, Colorado, USA). The signal was digitized (12-bit resolution, 10 ms duration, 31.25 MHz sampling frequency) using a digital oscilloscope (Picoscope 4227, PicoTech, St. Neots, Cambridgeshire, UK). Total cavitation energy was quantified from the power spectrum calculated over 10 ms windows captured every 13 ms and summed over the full 30 minute treatment, following the method described by Bader et al. [83].

II.2.6 Porcine thromboembolism model

The porcine thromboembolism research protocol was approved by our local Institutional Animal Care and Use Committee. Two clot deployment methods were employed in different

phases of the study. In phase 1, an occlusion was established by embolizing retracted human clots directly into the APA through an 8 F guide catheter stationed in the APA. Treatment was administered through end-hole microcatheters stationed at the face of the occlusion. Phase 2 experiments mitigated APA vasospasm noted in the former approach by avoiding placement of the embolizing guide catheter into the APA. For this method, the primary collateral, the ECA, was first occluded by coil embolization, and the embolizing guide catheter was stationed in the common carotid artery (CCA). Occlusion of the ECA in this way ensured that human clots embolized from a guide catheter stationed in the CCA would enter the target APA, rather than the larger and higher flow ECA. After embolizing a retracted human clot into the APA, a multi-side-hole microcatheter was advanced across the clot and used to administer treatment directly into the clot. A total of 12 female swine (Yorkshire, mean weight 49.1 ± 4.6 kg) and 8 female swine (Yorkshire, mean weight of 52.6 + 3.2 kg) were used in phase 1 and phase 2, respectively. Inclusion of each pig was based on successful establishment of a clot in the APA during embolization. Treatment was randomized by coin flip after establishing an occlusion in the APA but was not blinded as the interventionalist also set up, aligned, and monitored the ultrasound therapy. Each pig was treated bilaterally for a total of 24 occluded vessels in phase 1: 12 sham, 7 rt-PA only, and 5 sonothrombolysis. A total of 15 APA vessels were occluded in phase 2: 5 in each treatment arm. One vessel was not occluded successfully in phase 2 and was not included in the analysis.

Anesthetic care

Swine were sedated using IM acepromazine (1.1 mg/kg) and ketamine (33 mg/kg) and put on assisted ventilation with continuous isoflurane (2-3%). To avoid adverse reactions to Definity®, pigs were pre-treated with 40 mg of IV methylprednisolone and 2 mg/kg carprofen [200], [209].

Intravenous nicardipine (0.1 mg/kg/hr) was also given to prevent vasospasm during and after embolization [210].

Angiographic technique and measurements

10 F introducer sheaths were placed in both femoral arteries using the Seldinger technique [211]. The CCAs were catheterized bilaterally using 8 F guide catheters (Vista Brite Tip). Digital subtraction angiography (DSA) was performed with a FD20-Allura-Clarity angiographic system (Philips, Best, The Netherlands). The luminal diameter of each APA and ECA was measured on DSA images using the digital image processing software of the angiographic system (Figure II.4A). Percent lumen reduction of the APA was calculated as $\frac{D(t_i)-D(t)}{D(t_i)} \times 100\%$, where $D(t_i)$ is the initial diameter prior to embolization and $D(t)$ is the diameter at each time point, *t*.

Coil embolization of ECA

To enable embolization of retracted human clots directly into the porcine APA, the embolizing guide catheter was advanced into the proximal APA in phase 1. In phase 2, the embolizing guide catheter was stationed in the CCA, approximately 4 cm proximal to the CCA bifurcation, and the ECA was occluded by fluoroscopically guided embolization using a combination of bare platinum pushable coils, detachable Hydrocoils® (Microvention Inc, Aliso Viejo, CA, USA) and Azur 35D® coils (Terumo, Somerset, NJ, USA). Coil embolization of the ECA was performed bilaterally through 5 F Berenstein catheters (Merit Medical), coaxially advanced from the 8 F embolizing guide catheters. Twenty minutes after coil embolization of the ECA, DSA was performed through the 8 F guide catheter stationed in the CCA (Figure II.4B).

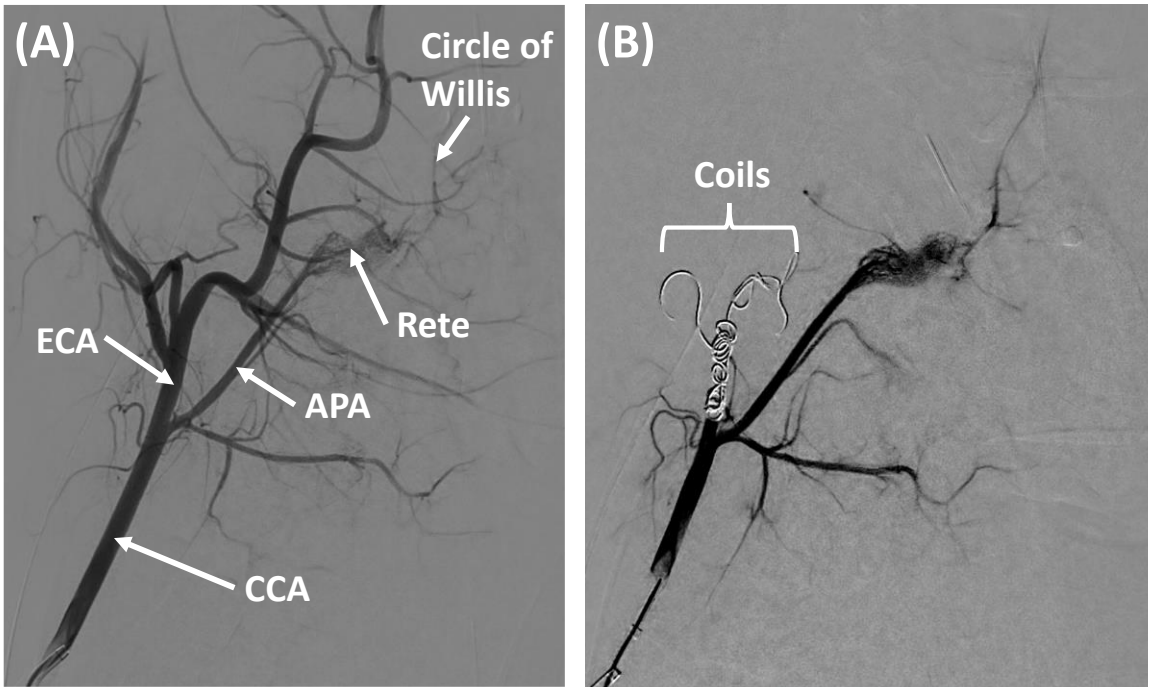

Figure II.4. Representative digital subtraction angiographic images showing porcine cranial vascular anatomy during the interventional procedure. Standard anatomy can be observed in (A). The common carotid artery (CCA) can be seen branching into the ascending pharyngeal artery (APA), occipital artery (OA), and external carotid artery (ECA). The APA ends in the *rete mirabile* (*rete*), a collection of capillaries which reform into the internal carotid artery which feeds the porcine Circle of Willis. Note the presence of collateral vessels extending from the ECA to the rete and Circle of Willis. The ECA is occluded using bare platinum and hydrogel coils (B) which diverts flow preferentially to the APA and reduces collateral circulation to the brain.

Embolization of porcine APA with retracted human clots

To perform APA embolization, a clot was transferred to the 8 F embolizing guide catheter. Transfer was facilitated using a large bore one-way stopcock (G00164, Cook Medical, Bloomington, IN, USA). Fluoroscopically guided embolization of the clot into the APA was performed by slow and steady injection of contrast media into the guide catheter containing the clot. Following each APA embolization, sequential DSA sequences were acquired, by injection of contrast media through the guide catheter, to assess the degree of APA occlusion and distal perfusion of *rete mirable* using the modified Thrombolysis In Cerebral Infarction (mTICI) scale.

Transcatheter treatment of APA clots

For treatment administration, the end-hole microcatheter was advanced through the 8 F guide catheter to the proximal edge of the APA clot (within 5 mm), or the multi-side-hole microcatheter was advanced across the APA clot, from the coaxial 8 F guide catheter. The microcatheter was infused over 2 hours with either 20 mL normal saline (sham), 20 mL rt-PA (1 mg/mL) only, or 20 mL rt-PA (1 mg/mL) plus Definity® (2 μL/mL) (sonothrombolysis).

In addition to rt-PA and Definity®, the sonothrombolysis treatment arm also was insonated with a 220 kHz ultrasound beam at 0.5 MPa peak-to-peak using an intermittent continuous wave ultrasound scheme (50 seconds on, 30 seconds quiescent) [83]. For 220 kHz ultrasound exposure, the presence of mastoid air cells in the porcine temporal bone prevented a transcranial insonation approach. Porcine temporal bone is an order of magnitude thicker than human temporal bone assessed in stroke patients [144], [146], [189], [191]. A validated computational model [191], [192] with input from cone beam computed tomography (CT) scans of 5 porcine skulls was used to determine an alternative acoustic window. This finite difference method was used to predict the ultrasound field at the location of the APA (Figure II.5A). A CT scan of each porcine head was performed after bilateral embolization of the APAs with preformed clots (XperCT, Philips Healthcare, Best, Netherlands). The ultrasound transducer was positioned within a reservoir of degassed water coupled to each pig's jowl with ultrasound gel. The ultrasound transducer was positioned lateral to the trachea and oriented towards the base of the skull along the APA using integrated needle guidance software (XperGuide 3D tools, Philips) (Figure II.5B). Gentle pressure was applied to the transducer to displace the trachea a few millimeters lateral from the midline to avoid air along the acoustic window. No deleterious bioeffects were noted on gross inspection of the skin and underlying soft tissue due to this transducer coupling procedure.

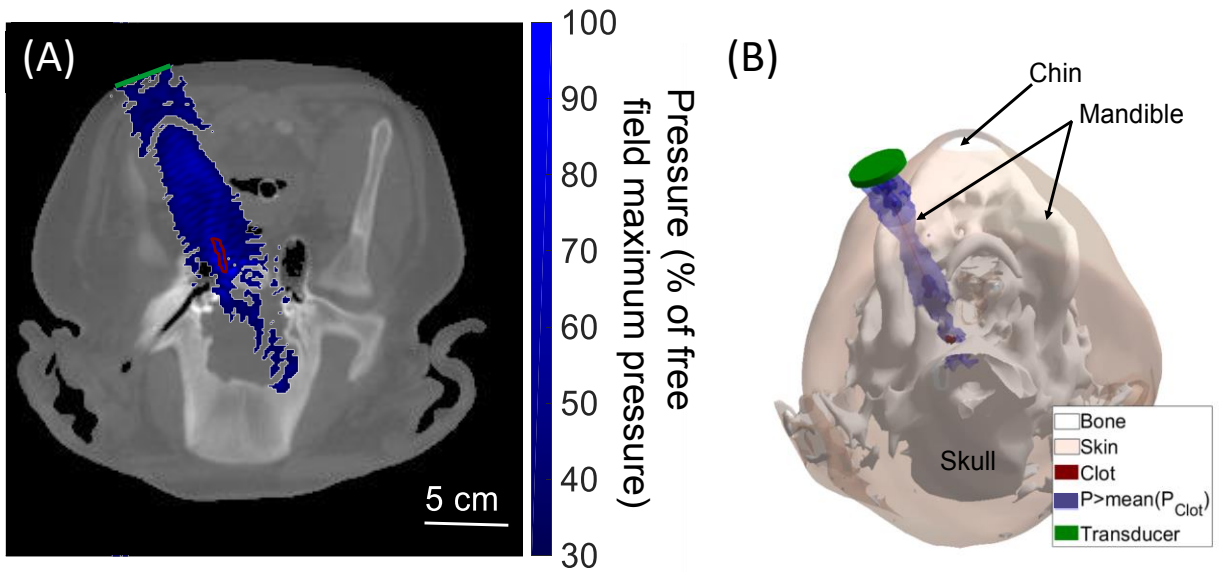

Figure II.5. Computational simulation of the ultrasound field using a validated finite difference code on (A) an axial CT with the ultrasound field overlaid in shades of blue and (B) 3D-rendered display. The transducer (green) is coupled to the skin over the porcine jowls. The clot (outlined in red) is located at the base of the skull, between the two porcine mastoid processes. An unobstructed path for the ultrasound beam was observed medial to the mandible on the ipsilateral side of the clot.

Angiographic assessment of target vessel recanalization and distal reperfusion

Sequential DSAs were obtained every 15 minutes during a 2-hour treatment period. At the conclusion of each experiment, the pig was euthanized and decapitated. APA recanalization and *rete mirable* perfusion at each time point was graded on the mTICI scale by an interventional neuroradiologist blinded to the treatment (Figure II.6). An unblinded mTICI score was determined during the procedure by a trainee. Grading disagreements were settled according to a secondary review conducted by both readers concurrently, without unblinding of the first reader. The reported mTICI score represents the consensus mTICI score agreed upon by the two readers.

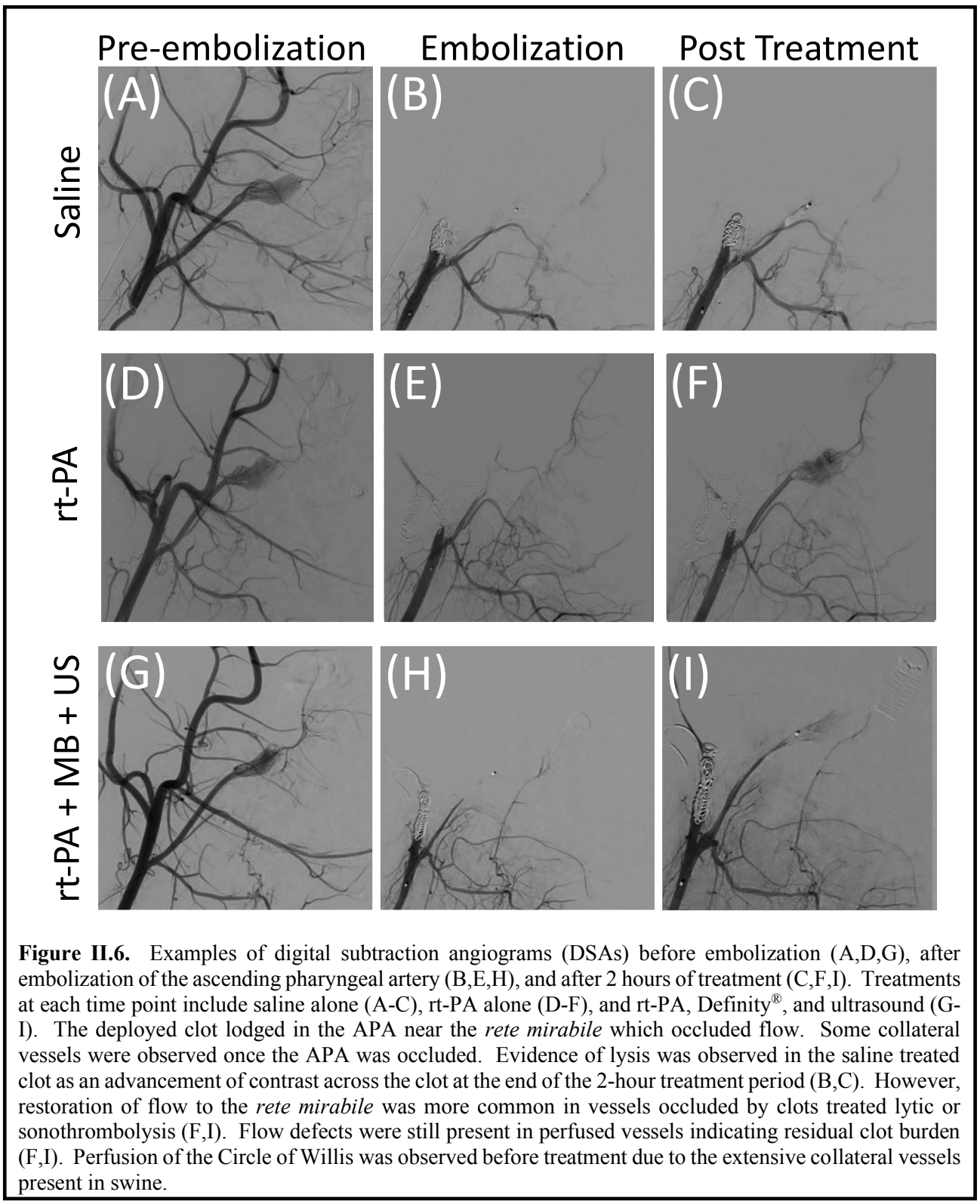

Figure II.6. Examples of digital subtraction angiograms (DSAs) before embolization (A,D,G), after embolization of the ascending pharyngeal artery (B,E,H), and after 2 hours of treatment (C,F,I). Treatments at each time point include saline alone (A-C), rt-PA alone (D-F), and rt-PA, Definity®, and ultrasound (G-I). The deployed clot lodged in the APA near the *rete mirabile* which occluded flow. Some collateral vessels were observed once the APA was occluded. Evidence of lysis was observed in the saline treated clot as an advancement of contrast across the clot at the end of the 2-hour treatment period (B,C). However, restoration of flow to the *rete mirabile* was more common in vessels occluded by clots treated lytic or sonothrombolysis (F,I). Flow defects were still present in perfused vessels indicating residual clot burden (F,I). Perfusion of the Circle of Willis was observed before treatment due to the extensive collateral vessels present in swine.

Histology of APA and associated clot

Each APA was dissected following the protocol developed by Eliyas et al. [208] (Figure II.7). Using a 30 G needle and syringe, each APA was pressurized to 90 mmHg with 10% formalin. Formalin fixed APA specimens were embedded in paraffin, cut longitudinally along the vessel and stained with Verhoeff-Van Gieson stain to highlight the elastin and endothelial layer. The percent patent luminal area of the APA was calculated from the open lumen area and residual clot burden along the length of the vessel using ImageJ (National Institutes of Health, Bethesda, MD).

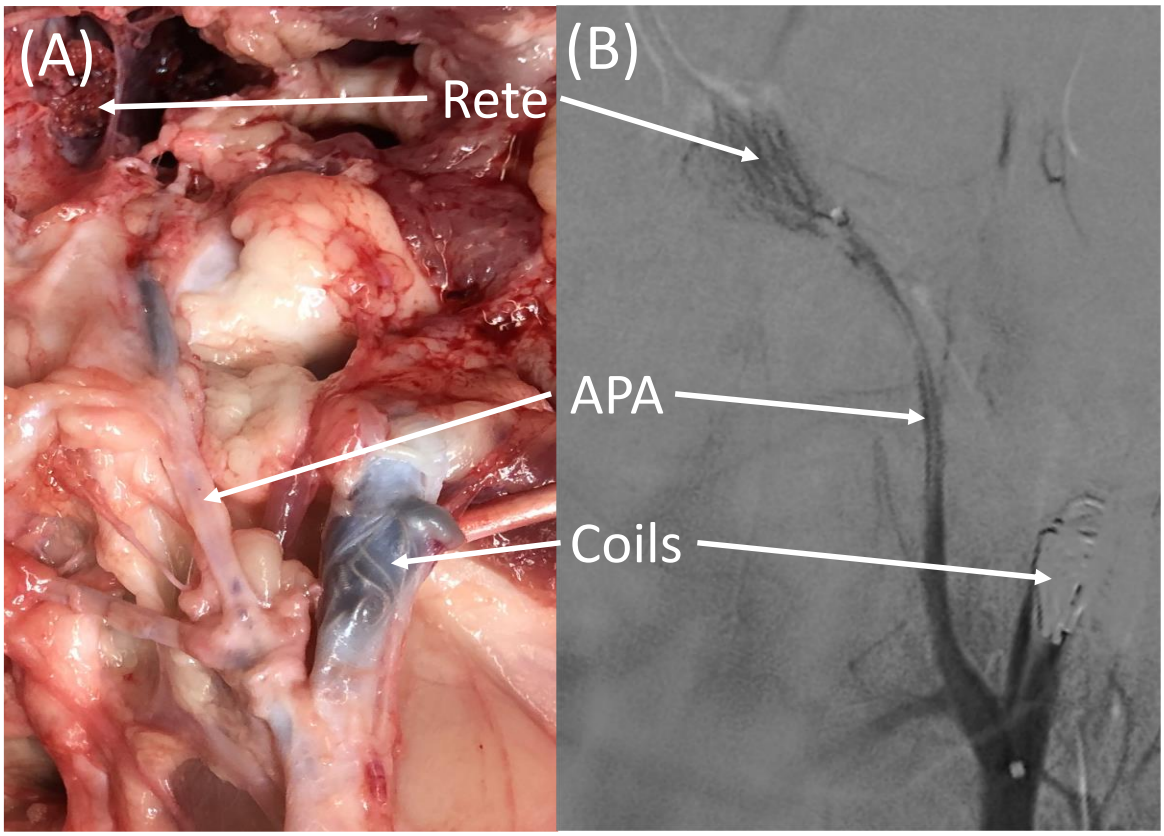

Figure II.7. Dissected left ascending pharyngeal artery (A) with residual clot and (B) the corresponding 120-minute angiogram. The coils in the external carotid artery were visible on the DSA image distal to the APA which ends in the *rete mirabile* embedded in the porcine skull.

II.2.7 Statistics

A one-way (ANOVA) with a Tukey honest significant difference (HSD) test was used to assess CML and percent patent luminal area differences between treatment arms for each microcatheter design. A linear mixed model was used to compare the effect of each microcatheter design and treatment on flow as a function of time *in vitro* and on vasospasm as a function of time *in vivo*. The mTICI scores were dichotomized into failure (mTICI < 2b), or success (mTICI ≥ 2b). The resultant data was fit to a logistic regression model for pairwise comparison between each of the three treatment arms. All statistical computations were done in R (v. 2.14.1, R Foundation for Statistical Computing, Vienna, Austria). A p value < 0.05 was considered statistically significant. Power analysis for the *in vitro* study was performed in MATLAB (2017b) along with the statistical tables in Cohen [212] and *in vivo* study using algorithm described by Demindenko [213], [214].

II.3 Results:

II.3.1 Infusion of Definity® microbubbles through microcatheters

Definity® infused through either the end port or the multiple side port microcatheters exhibited lower attenuation compared to direct measurements, with a 7-8 dB reduction in the attenuation of Definity® at 2 MHz ($p < 0.01$) (Figure II.8). The loss of attenuation was less pronounced at higher frequencies, with the reduction in attenuation approaching 2 dB at 25 MHz. No significant difference in the attenuation from 2 to 25 MHz was observed between Definity® infused through the end port microcatheter or the multiple side port microcatheter ($p > 0.56$).

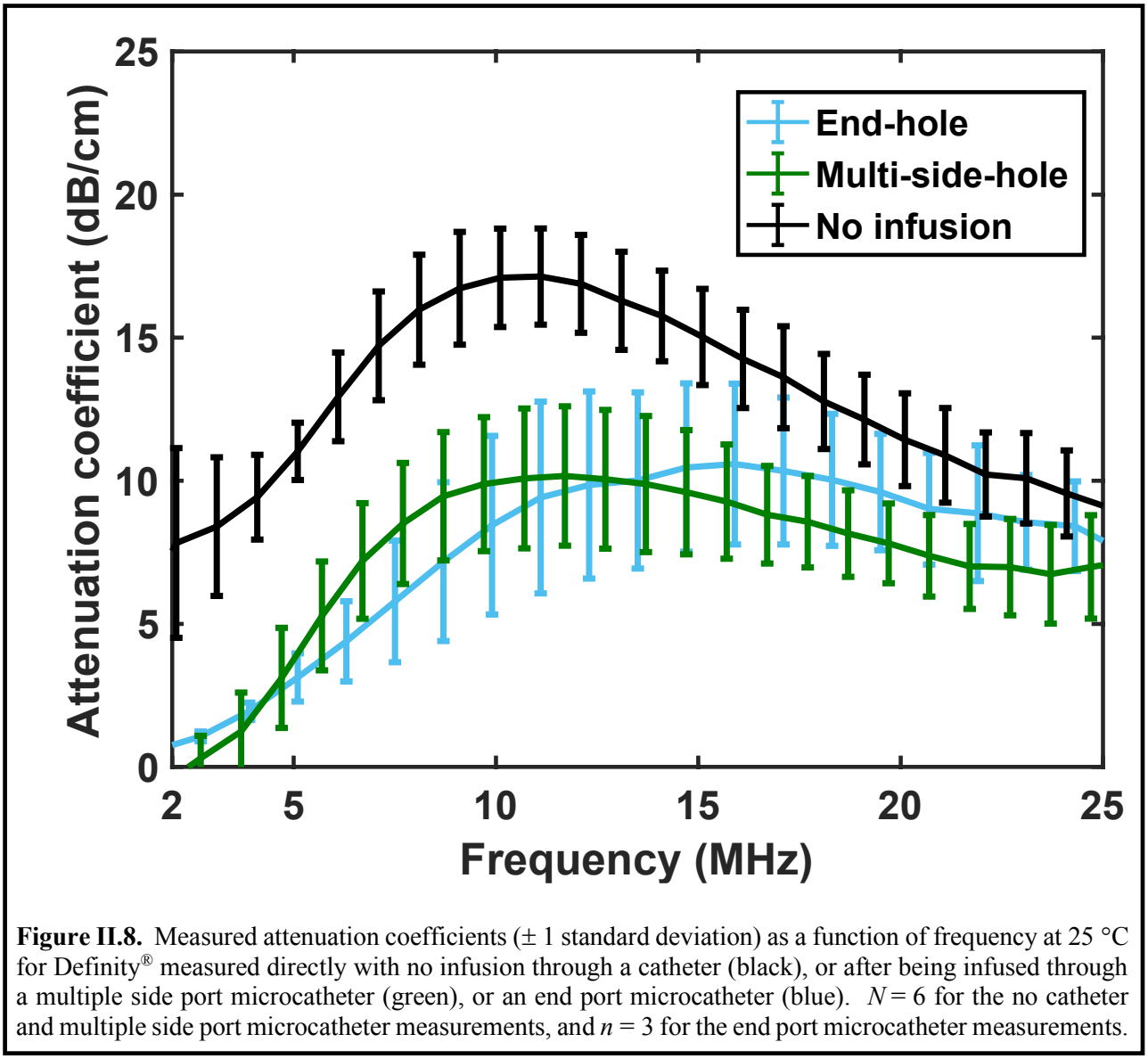

Figure II.8. Measured attenuation coefficients (± 1 standard deviation) as a function of frequency at 25 °C for Definity® measured directly with no infusion through a catheter (black), or after being infused through a multiple side port microcatheter (green), or an end port microcatheter (blue). $N = 6$ for the no catheter and multiple side port microcatheter measurements, and $n = 3$ for the end port microcatheter measurements.

II.3.2 Effects of X-ray Contrast on Lytic Susceptibility results

Recombinant tissue plasminogen activator activity without Optiray was 22.3 ± 4.1 mAbs/min (Figure II.9). X-ray contrast significantly reduced the activity of rt-PA for solutions greater than 25% Optiray by volume compared to 0-10% Optiray ($p < 0.01$) (Figure II.9). Enzymatic activity was even lower at 50% compared to 25% ($p > 0.05$). This reduction in rt-PA activity did not decrease significantly between Optiray volumes of 50 and 85% ($p > 0.91$). The rt-

PA activity was reduced by a factor of 4 (5.3 vs 22.3) at the highest volume of Optiray (85%) compared to 0%.

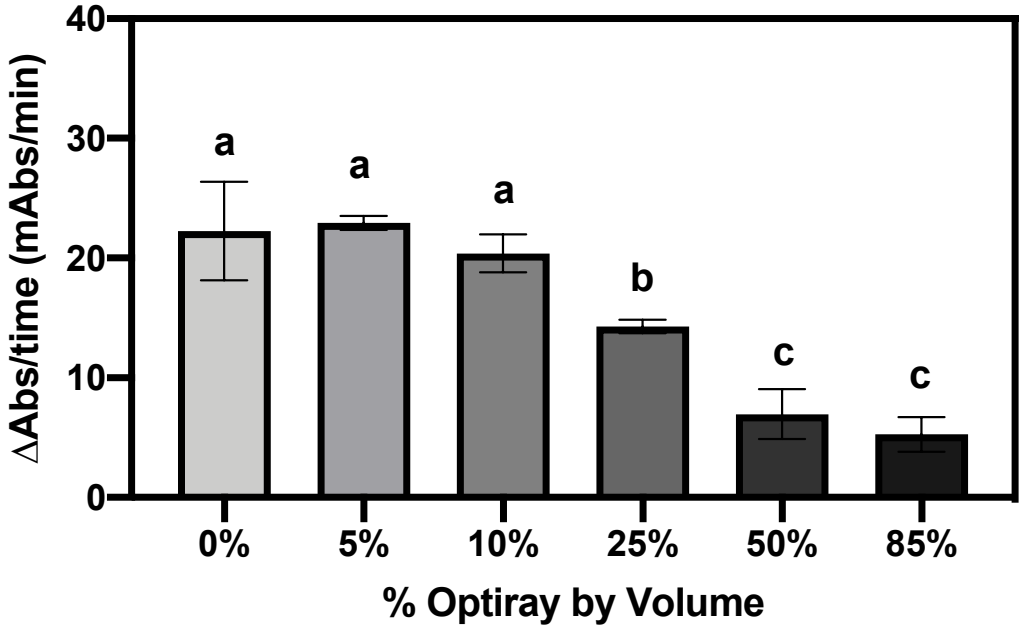

Figure II.9. Change in enzymatic activity of rt-PA (ΔAbs/time) as a function of the percent Optiray by volume. For Optiray volumes 10% or less, the activity of rt-PA to hydrolyze substrate was unaffected ($p > 0.87$). However, as the volume of Optiray increased, the activity of rt-PA significantly decreased. Overall a fourfold reduction in rt-PA activity was observed between the lowest and highest volume of Optiray measured (0-85%) ($p < 0.0001$). A one-way ANOVA was performed and significance was shown using compact letter display to identify statistically equivalent groups.

II.3.2 In vitro flow phantom thromboembolism results

In end-hole microcatheter experiments, CML was 23.5 ± 10.1%, 48.2 ± 15.0%, and 46.0 ± 15.5% for sham, rt-PA only, and sonothrombolysis, respectively (Figure II.10). Sonothrombolysis and rt-PA only treatments showed no significant difference in thrombolytic efficacy ($p > 0.999$). Lytic (rt-PA only) and sonothrombolysis treatments both resulted in significantly greater CML relative to sham ($p < 0.01$).

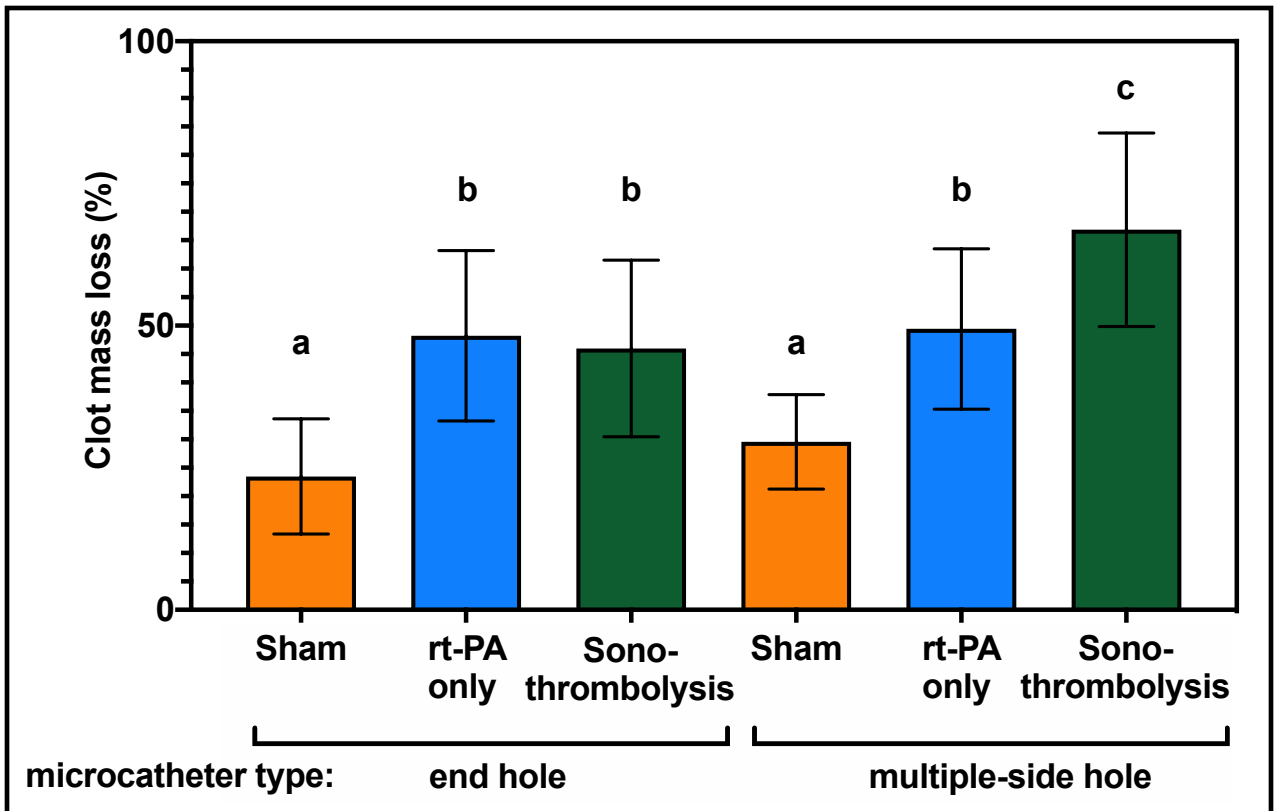

Figure II.10. *In vitro* percent clot mass loss results for human whole blood clots with $n = 10$ for each group. The end port microcatheter was positioned at the proximal face of the clot, and the multiple side port microcatheter crossed the clot axially. Clots treated with rt-PA had increased clot mass loss compared to saline, but no improvement was observed with the addition of the Definity®, and 220 kHz intermittent continuous wave ultrasound exposure for clots treated with the end port microcatheter. Both lytic and sonothrombolysis treatments resulted in significantly greater mass loss compared to clots treated with saline alone ($p < 0.01$ for both). A one-way ANOVA was performed and significance was shown using compact letter display to identify statistically equivalent groups.

CML in the sonothrombolysis arm was significantly higher with the multi-side-hole microcatheter than with the end-hole microcatheter ($p < 0.05$). In multi-side-hole microcatheter experiments, CML was $29.5 \pm 8.3\%$, $49.4 \pm 14.1\%$, and $66.9 \pm 17.0\%$ for sham, rt-PA, and sonothrombolysis treatment arms, respectively (Figure II.10). CML in the sonothrombolysis arm with the multi-side-hole microcatheter was significantly higher than the corresponding CML in the rt-PA only arm ($p < 0.05$), which was significantly higher than sham CML ($p < 0.05$).

Both sonothrombolysis and lytic (rt-PA only) resulted in greater flow restoration when performed through multi-side-hole microcatheters than when performed through end-hole

microcatheters (Figure II.11). Flow distal to the occluding clots was unchanged for all three treatments when administered through an end-hole microcatheter. Sham treatment with the multi-side-hole microcatheter showed no difference compared to sham treatment through the end-hole microcatheter ($p > 0.37$). In contrast, rt-PA or sonothrombolysis treatments treated through a multi-side-hole infusion microcatheter demonstrated partial flow restoration as early as five minutes with complete flow restoration (0.75 mL/min) by 30 min (Figure II.11). The total ultraharmonic energy detected during sonothrombolysis treatments was not significantly different for the end-hole and multi-side hole microcatheters ($12.1 \pm 15.2 \times 10^3$ mV^2 and $12.3 \pm 12.4 \times 10^3$ mV^2 respectively) ($p > 0.77$) (Figure II.12).

II.3.3 In vivo porcine thromboembolism results

Most porcine APA vessels (39/40) were successfully occluded by transcatheter embolization with retracted human clots. Shown in Figure II.13 is the percentage of APA clot treatments achieving successful reperfusion (mTICI 2b or 3) as a function of time for each of the three treatments arms (sham, rt-PA only, sonothrombolysis). In end-hole microcatheter experiments, none of the occluded APA vessels were successfully reperfused during the 120 min treatment period, and no significant difference was found between any of the treatment groups ($p > 0.99$) (Figure II.13A). Five of the 15 clots treated with multi-side-hole microcatheters were successfully reperfused, including 1 sham, 2 rt-PA only, and 2 sonothrombolysis (Figure II.13B). One sham achieved successful reperfusion (mTICI ≥ 2B) at 105-120 min, which was significantly longer than rt-PA only ($p < 0.01$) or sonothrombolysis ($p < 0.01$) treatments (Figure II.13 B). Lytic (rt-PA only) treated clots achieved reperfusion after 75-105 min of treatment, while sonothrombolysis treated clots recanalized the most rapidly, between 0-60 min. The difference in

the degree of recanalization over time between sham and sonothrombolysis treated clots was significant ($p < 0.01$) but not between sham and rt-PA only treated clots ($p = 0.076$)

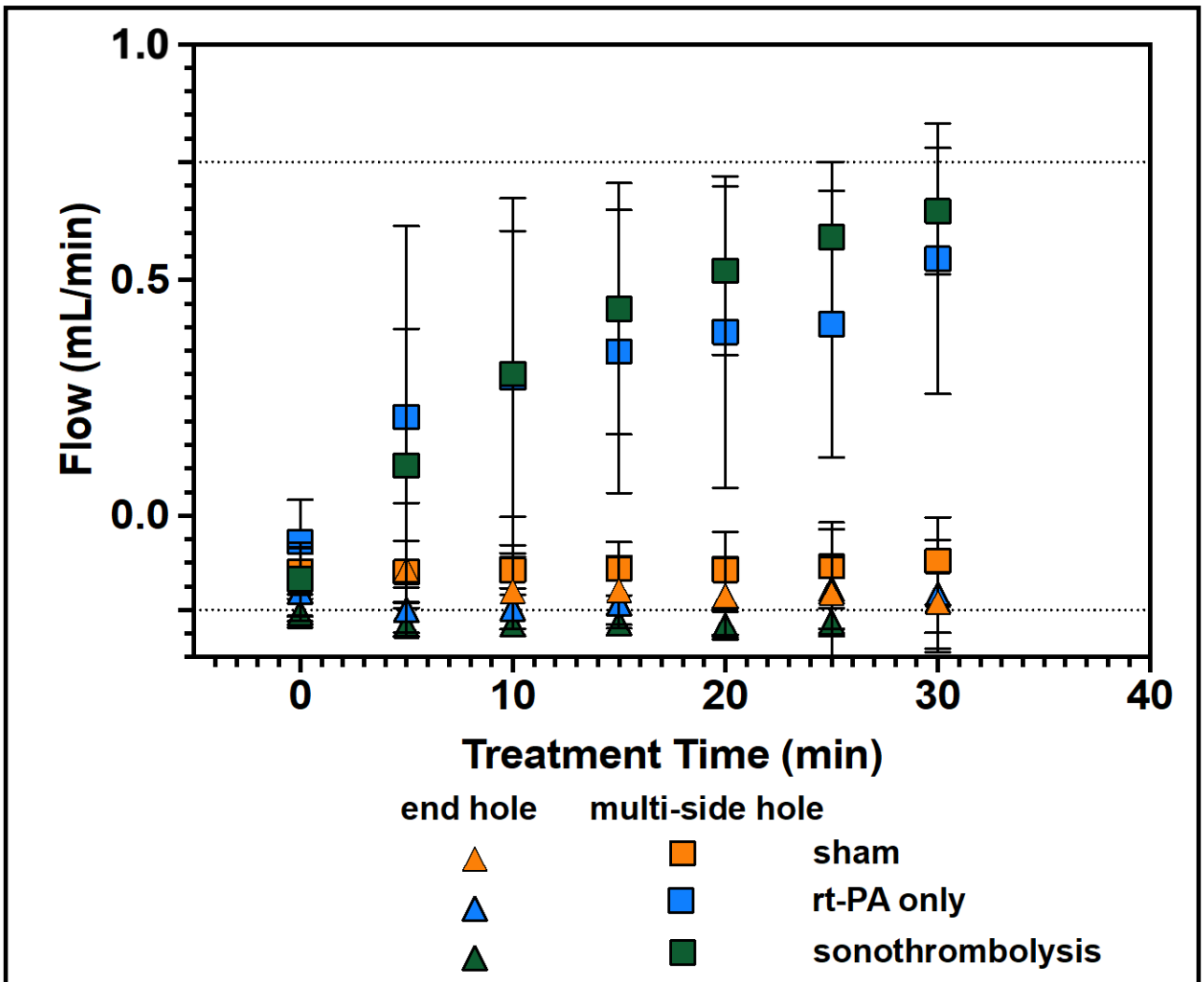

Figure II.11. *In vitro* flow through APA flow model with $n = 10$ for each group. Human whole blood clots were treated with either saline, rt-PA at 1 mg/mL, or rt-PA (1 mg/mL) along with Definity® (2 µL/mL) and 220 kHz intermittent continuous wave ultrasound. Saline, rt-PA, or rt-PA mixed with Definity®, delivered either through an end port microcatheter positioned within 5 mm of the clot or a multiple side port microcatheter which was positioned across the clot. Flow measurements spanned -0.2 mL/min for a fully occluded APA mimic to 0.75 mL for a fully recanalized APA mimic. No increase in flow was observed for clots treated with the end port microcatheter. Flow was observed in clots treated with rt-PA or rt-PA, Definity®, and 220 kHz ultrasound using a multiple side port microcatheter.

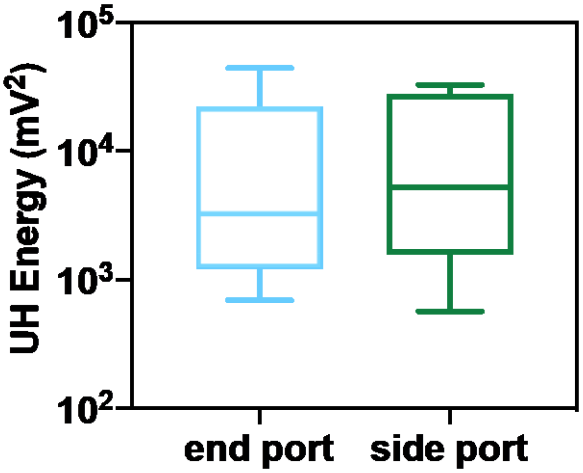

Figure II.12. Total ultraharmonic cavitation emissions between 330-2000 kHz over the 30 minutes treatment period. Cavitation was highly variable for each trial for both the end port microcatheter (blue) and the multiple side port microcatheter (green). No difference in total ultraharmonic emissions was found between the two microcatheters on a Student's t-test ($p > 0.77$).

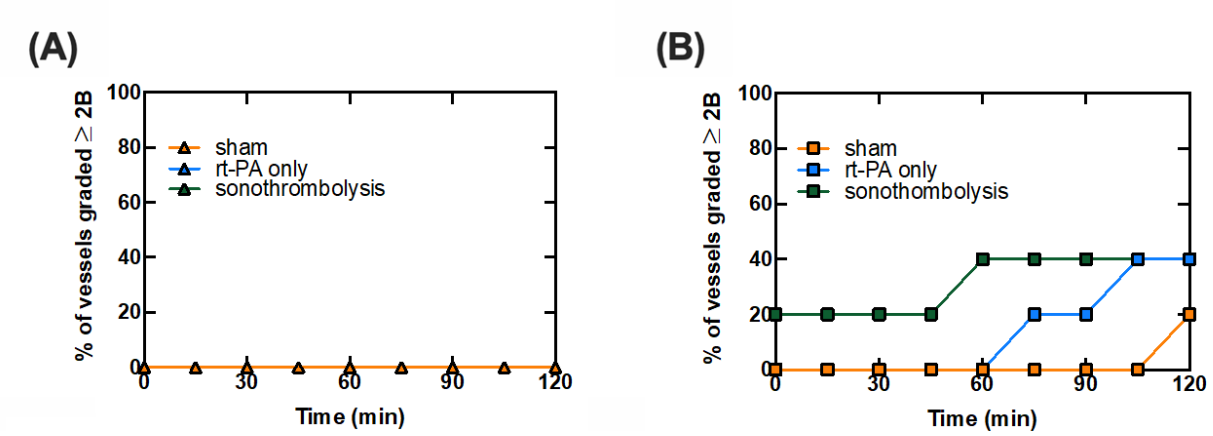

Figure II.13. mTICI scores for (A) clots treated using the end port microcatheter or (B) the multiple side port microcatheter. For plot (A), $n = 12$ for saline alone, $n = 7$ for rt-PA alone, and $n = 5$ for rt-PA, Definity®, and 220 kHz intermittent continuous wave ultrasound. In plot (B), $n = 5$ for all three treatments. No recanalization up to or greater than mTICI = 2b was observed for any clots treated with the end port microcatheter. Clots treated with the multiple side port catheter infused with saline alone showed some improvement in the degree of contrast penetration into the clot and had some mild improvement in downstream perfusion for some cases. The introduction of rt-PA to the clot showed improvement with 2/5 clots showing distal perfusion by 75-105 minutes. Improvement was accelerated with rt-PA, Definity®, and ultrasound, in which 2/5 clots achieved a mTICI score of 2b or greater between 0-60 minutes.

Representative stained longitudinal APA sections differentiated by treatment are shown in Figure II.14(A-C). The percent of patent luminal cross-sectional area (PPLA) was similar for all three treatments (sham, rt-PA only, sonothrombolysis) in end-hole microcatheter experiments ($p > 0.35$) (Figure II.14D). In contrast, multi-side-hole microcatheter experiments showed that PPLA increased in the rt-PA only ($p < 0.05$) and sonothrombolysis ($p < 0.05$) treatment arms.

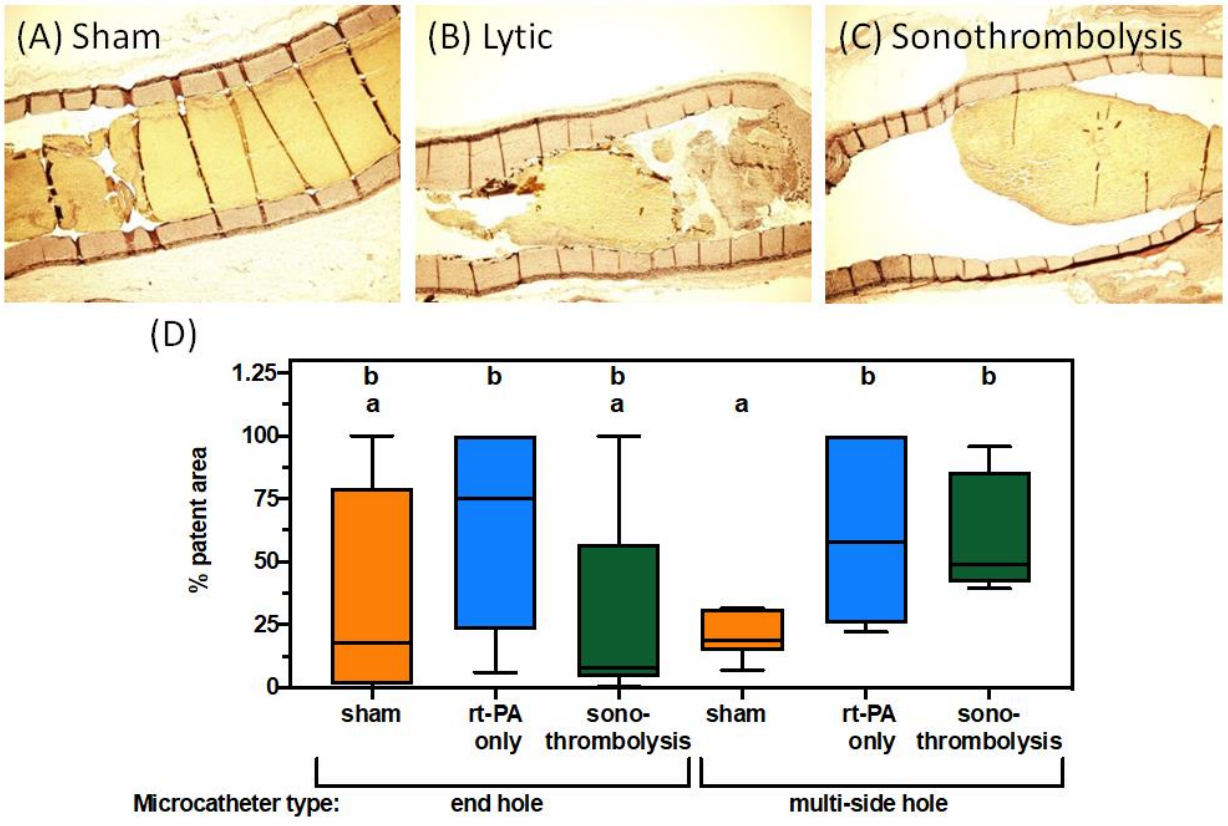

Figure II.14. Representative longitudinal histology images of residual clot burden in APAs with Verhoeff-Van Giessen (VVG) stain, which highlights elastic fibers. Residual clot volume (yellow) is pronounced in clots treated with (A) saline compared to (B) rt-PA only, or (C) rt-PA, Definity®, and ultrasound. The percent patent area within each histology specimen is quantified and compared across the three treatments and two microcatheters (D). A one-way ANOVA was performed and significance was shown using compact letter display to identify statistically equivalent groups.

II.3.4 Vasospasm

Figure II.15 shows the percent APA lumen reduction due to vasospasm for each of the treatment arms as a function of time, using two different APA embolization paradigms (phases 1 and 2 of the study). In phase 1, severe APA vasospasm (> 50% APA lumen reduction) [215] was present throughout the 120 min treatment period for most vessels (Figure II.15A). When severe vasospasm was encountered in phase 2, it decreased significantly within 30 minutes of APA occlusion ($p < 0.05$) (Figure II.15B).

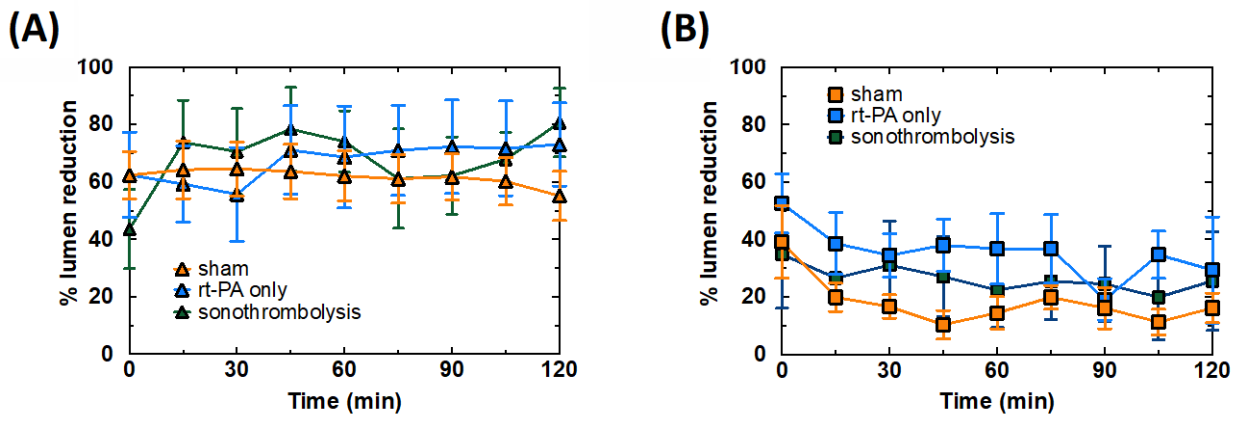

Figure II.15. Percent reduction in vessel diameter monitored during clot delivery and treatment with (A) the end port microcatheter and (B) the multiple side port catheter. All vessel diameters were compared to the diameter before embolization. Vasospasm was highly variable. For occlusions created by directly injecting the clot into the APA and instrumenting the vessel, vasospasm was significantly higher and did not resolve over time (A). For occlusions created by deploying the clot into the common carotid artery, vasospasm and was highest during the first 30 minutes after treatment started (B).

II.4 Discussion:

II.4.1 Catheter effects on ultrasound contrast agents

The changes in the attenuation of Definity® were similar after infusion down either catheter despite the difference in the number, size, and distribution of ports ($p < 0.01$) (Figure II.8). Bubbles that attenuate lower frequencies correspond to larger bubbles, indicating that large

bubbles were preferentially lost during the infusion through each microcatheter. The cause for this reduction in attenuation is not clear and will need to be explored in further studies. Additionally, our attenuation spectroscopy measurements are not sensitive to frequencies below 2 MHz and therefore we cannot confirm if bubbles resonant at 220 kHz were similarly lost (Figure II.8). However, despite this reduction in attenuation, cavitation could still be detected (Figure II.12) with the same order of magnitude detected in previous studies under flow conditions [117], [118], [141]. This may be due to the oscillation of smaller bubbles being driven off resonance, but could also be due to the formation of larger resonant bubbles due to coalescence during insonation [216].

II.4.2 Clot mass loss and flow in vitro

Our *in vitro* experiments show that the design and position of the microcatheter used for the delivery of Definity® is an important modifier of fibrinolytic acceleration. Nonetheless, for sham-treated clots, no difference in CML or flow was observed regardless of microcatheter design and position ($p > 0.99$) (Figure II.10,11). This finding suggests that the mechanical trauma of clot penetration by a microcatheter did not accelerate recanalization in our study. Clots treated with rt-PA had a higher CML compared to sham treated clots regardless of microcatheter design or position, consistent with previous *in vitro* studies (Figure II.10) [79], [81]. On the other hand, sonothrombolysis improved CML only when Definity® was infused directly into clots through multi-side-hole microcatheters (Figure II.10). Definity®, intercalated within the clot, promoted cavitation nucleation and sustained bubble activity similar to previous *in vitro* studies (Figure II.12) [117]. This pattern suggested that the adjuvant effect of Definity® and ultrasound relied on the spatial proximity of bubble activity possibly linked to radial diffusion of Definity® throughout the clot. An increase in CML for a particular treatment was not always accompanied by an increase in flow for the same treatment (Figure II.10,11), possibly due to the low flow velocity or shunting

of flow through the ECA mimic. This data highlights the disparity of these two metrics of thrombolytic efficacy.

II.4.3 Porcine thromboembolism model development

Our APA model was based on the porcine model of vascular occlusion developed by Culp et al. [200]. We modified this approach to accommodate a highly retracted human xenographic clot formed exogenously. In order to deliver the clot without placing a guide catheter into the APA, which caused vasospasm (Figure II.15A), coiling of the external carotid artery was necessary to prevent embolization other than in the APA (Figure II.4). Mechanical irritation of the instrumented APA prior to clot delivery was suspected as a cause of the vasospasm. Nicardipine, a calcium channel blocker, was used successfully to alleviate vasospasm at an infusion of 0.1 mg/kg/hr and was well tolerated [210], [217]. Additionally the ECA provides collateral circulation to the porcine brain unlike the human cerebral vasculature (Figure II.4) [207]. Without occluding the ECA, mTICI scoring of flow restoration in the APA was difficult as distal perfusion from the APA could not be differentiated from collateral circulation. The occlusion of the ECA, which likely would not be suitable for survival studies, was well tolerated for a up to 6 hours in these non-survival studies and eliminated collateral cerebral circulation not found in humans.

Following occlusion of the ECA, delivery of the clot into the common carotid led to rapid and complete occlusion of the APA. Despite no attempt to control for various blood types and antigens, human xenographic clots did not cause any obvious distress to the pig. However, the effects of human whole blood clots in the porcine vasculature over longer periods (greater than 8 hours) are unclear. Additionally, the highly retracted, fibrin dominant exterior of the clots may limit the presentation of foreign antigens in the porcine blood, reducing the incidence of immunologic reactions [82], [141], [157]. The methylprednisolone and carprofen, given to prevent

porcine hypersensitivity to Definity®, may also have suppressed the immune response to the human whole blood clots.

II.4.4 Restoration of Perfusion in vivo

We modified the porcine model described developed by Culp et al. [200] to accommodate a highly retracted human xenographic clot formed exogenously. However, in our phase 1 study, no reperfusion was observed in any of the three treatment arms. This lack of rt-PA efficacy was hypothesized to come from vasospasm. Grading perfusion based on the mTICI scale was complicated by severe vasospasm (Figure II.15). During each DSA, it was difficult to tell if a vessel was truly occluded by a clot, or simply spasmed shut. This vasospasm could also have obstructed the clot surface from being exposed to rt-PA, delaying or stopping lysis entirely.

To deliver the clot percutaneously into the APA without provoking severe vasospasm, we performed APA embolization from a catheter stationed in the CCA (Figure II.4). Initial occlusion of the ECA by coil embolization facilitated targeted delivery of clot into the APA, a vessel that is much smaller than the ECA. The ECA is a major source of collateral blood flow to the brain when the APA is occluded (Figure II.4). In our model, coil embolization of the ECA places the burden for anterograde *rete mirable* perfusion exclusively on the APA, removing competitive flow that might otherwise complicate assessment of angiographic reperfusion according to the mTICI scale. Thus, the advantages of ECA occlusion in our model are multifold. We observed an increase in perfusion of the *target vessel territory* during a two-hour treatment period for all three treatment arms (Figure II.13B). The adjuvant effect of Definity® and 220 kHz continuous wave ultrasound exposure was most prominent early in the treatment process. Adjuvant Definity® plus ultrasound increased the percentage of occluded vessels achieving successful reperfusion in the first 60 minutes of treatment by 20% and reduced the minimum time to successful reperfusion with rt-PA

only by 45 minutes. Khatri et al. [218] showed that the probability of a good clinical outcome is increased by 10% for every 30-min reduction in the time to successful angiographic reperfusion (TICI 2 or 3) during treatment with transcatheter intra-arterial rt-PA. Consequently, the quantitative acceleration of successful reperfusion observed in our study has the potential to translate into improved clinical outcomes.

An improvement in mTICI scores for 20% of sham treated clots was noted in the final 15 minutes of treatment (Figure II.13B). Culp et al. [178], [200] observed similar results for saline treated porcine thrombi. *In vivo*, spontaneous complete recanalization without any treatment has been observed in clinical trials such as the PROACT II trial (18-30%), but was not noted in our study [39].

As observed in our *in vitro* study, the design and position of the microcatheter used for delivery of Definity® was an important modifier of fibrinolytic acceleration in our *in vivo* studies. Overall, two thirds of the vessels treated with multi-side-hole microcatheters did not successfully reperfuse regardless of the therapy arm. Conversely, none of the vessels treated with the end-hole microcatheter were successfully reperfused, regardless of the therapy arm. Vasospasm was an important factor associated with reperfusion failure, particularly in phase 1 of our study (Figure II.13,15). Vasospasm likely inhibited angiographic reperfusion, as constriction of the APA around the intraluminal blood clot prevented downstream flow, even if the intraluminal blood clot were enzymatically degraded. Nonetheless, our *in vitro* study suggests that even without vasospasm, delivery of rt-PA through an end-hole microcatheter at the proximal face of an occlusive clot does not effectively achieve successful reperfusion (Figure II.11). This is consistent with the results of prior clinical trials that employed a similar treatment strategy [45].

Our experimental design was intended to disadvantage treatment with rt-PA only, so that the differential benefit provided by adjuvant treatment with Definity® and ultrasound could be quantified. Toward that end, our study employed clots with a length of 15 mm. Such clots are known to be resistant to treatment with intravenous rt-PA [202]. In addition to the degree of retraction affecting lytic resistance, the clot location could also have contributed to this high percentage of vessels which fail to reperfuse. The porcine cranial circulation has extensive collaterals, some of which can only be observed on DSA after the primary vessel is occluded. One explanation for the low degree of reperfusion in our model was slow exchange of plasminogen between circulating blood and the stagnation zone at the proximal face of experimental clots. Prolonged stasis of flow in this region was confirmed angiographically in our study.

II.4.5 Limitations

The *in vitro* flow model had several differences compared to the porcine thromboembolism model. The *in vitro* system utilized continuous flow, rather than physiological pulsatile flow, although the hydrodynamic pressure in the flow model was chosen as the mean arterial pressures observed in our in vivo studies and consistent with published values [209], [219]. Our continuous flow velocity was 4 cm/s based on the plug flow assumption, which is in the range of velocities of a partially occluded middle cerebral arteries in humans [159]. However, flow velocity can vary widely during recanalization and pulsatile flow can reach peak velocities greater than 100 cm/s in a patent middle cerebral artery [159]. Also lacking in the flow model was vasospasm, which was assessed in vivo.

In phase 1 of our *in vivo* study, the degree of vasospasm prevented accurate assessment of vessel recanalization. The lack of recanalization observed in vessels occluded by clots treated with rt-PA in phase 1 may have bene due may be due to the vessel narrowing following clot deployment.

Furthermore, in phase 2, recanalization was a product of both mechanical agitation due to the microcatheter and enzymatic thrombolysis due to rt-PA with or without ultrasound and Definity®. The rapid recanalization seen in phase 2 near the start time was likely a product of the initial mechanical agitation (Figure II.13). However, the clot in this vessel continued to break down and no reduction in the mTICI score was noted in that trial, although the mTICI score was observed to decrease in several other runs following recanalization.

Our computational simulations were conducted on porcine CT images acquired before insertion of the coils in the ECAs, as well as embolization of the APAs with human whole blood clots. Thus, the simulations also did not account for the attenuation caused by the coils or the precise location of each deployed clot. The presence of x-ray contrast in the CT images would have been interpreted as bone in the derivation of acoustic parameters used as input to the computational model and thus was avoided.

The porcine cranial thromboembolism model is not representative of ischemic stroke as the porcine cranial collateral circulation is more robust than the human cranial circulation. This feature added to the complexity of the mTICI scoring from DSA images. Additionally, it is unknown what effect occluding the external carotid artery had on the porcine physiology. Due to the attenuation of ultrasound along the acoustic pathway and limited signal to noise, we were not able to monitor cavitation during our study in vivo. However, the predicted pressures were adequate to achieve robust stable cavitation nucleated by Definity® during the treatment as demonstrated in our *in vitro* and *in silico* studies (Figure II.5, II.12).

II.5 Conclusions:

This study demonstrates that concurrent administration of Definity® and 220 kHz ultrasound significantly accelerates resolution of thromboembolic vessel occlusions treated with

rt-PA *in vitro* and *in vivo*. Using widely accepted clinical criteria for technically successful reperfusion, concurrent Definity® and 220 kHz ultrasound reduced the time to successful angiographic reperfusion *in vivo* by 45 minutes, a time savings with potential for clinically significant positive impact. Thus, we accepted our hypothesis that intermittent continuous wave 220 kHz ultrasound and Definity® enhances rt-PA lysis of human retracted clots and improves recanalization of occluded vessels. Given that clinically proven modern paradigms of stroke therapy are based on mechanical revascularization of large vessel occlusions and administration of rt-PA, further study is needed to understand how adjuvant ultrasound therapies can be used to improve these therapies.

CHAPTER III: THROMBOLYTIC EFFICACY OF TRANSCRANIAL ULTRASOUND IN A PORCINE INTRACEREBRAL HEMORRHAGE MODEL [3]

III.1 Introduction:

Submegahertz (220 kHz) ultrasound successfully restored flow in an occluded vessel *in vivo* (Chapter II), however, insonation through the skull is key challenge in human translation. To test the efficacy of transcranial ultrasound *in vivo*, a porcine model of intracerebral hemorrhage developed by Wagner et al. was used [220], [221]. The juvenile porcine skull in this model has approximately the same thickness as the adult human temporal bone (1.4-4.0 mm) and provides a platform model to test the efficacy of transcranial sonothrombolysis for human translation [189], [190]. Wagner et al. assessed thrombolytic efficacy by measuring the volume of the fibrin degradation products aspirated through a catheter 30 minutes after rt-PA infusion [221]. *In vivo* ICH studies were performed in 2009-2010 by Ammi et al. [222] to assess whether ultrasound enhanced thrombolysis using D-dimer, a breakdown product of blood clots, as a metric of thrombolytic efficacy. However, neither human nor porcine D-dimer assays were sensitive to porcine clot lysis [188], and thus these *in vivo* specimens were analyzed using alternate metrics as part of this dissertation.

Several *in vitro* studies of sonothrombolysis have used metrics such as clot mass loss [79], [81], [106], [120], [172] to assess clot break-down. Clot mass loss, a robust metric of lytic efficacy *in vitro* [100], [106], [172], [223], is challenging to implement *in vivo* because the initial thrombus mass cannot be assessed. However, the link between the thrombus size and improvements in the

[3] *This chapter contains sections adapted from a manuscript in preparation for submission to an academic journal. Its use in this dissertation will be declared to the journal upon submission. Quoted text is identified by a vertical dashed line in the left margin.*

modified Rankin Scale score suggest that residual thrombus mass and residual thrombus volume might be used as predictors of clinical success [17]. Furthermore, volume aspiration is a clinically relevant metric as it is used in minimally invasive thrombus removal and has been associated with improved outcomes [17]. Therefore, the fluid portion of the clot would also be expected to be increase as the clot breaks down. In thrombi treated with rt-PA and gently aspirated, Wagner et al. observed that the volume of blood aspirated was greater, the volume of perihematomal edema and thrombus volume smaller, and the intracranial pressure lower, compared to untreated thrombi [221].

We proposed to look at residual thrombus mass, volume, and density as metrics of thrombolysis in the porcine ICH model and choose one to assess the thrombolytic efficacy of transcranial ultrasound in conjunction with rt-PA *in vivo*. The objective of this chapter was to develop a metric of thrombolytic efficacy and assess the degree of lytic enhancement caused by 120 kHz ultrasound exposure in the porcine ICH model. Mass was selected based on its use in *in vitro* studies [106] and volume was selected based on the prior work by Wagner et al. [221] in a similar porcine model. However, Wagner et al. also aspirated clots prior to measuring the volume, therefore thrombus density was included as it may provide a metric normalized to the initial thrombus size, analogous to *in vitro* metrics such as clot mass loss or fractional clot width [83], [204]. We hypothesized that the residual thrombus mass, volume, and density would be adequate metrics of thrombolytic efficacy to differentiate treatment arms *in vitro* and *ex vivo*.

In vitro studies were performed to assess the sensitivity of residual thrombus mass, volume, and density as a metrics for thrombolytic efficacy and choose which metric to use *in vivo*. Several methods were tested to assess residual thrombus mass by removing excess water. Blotting, a previously established protocol, works well for whole thrombi, but can be difficult to use for

thrombus fragments which can adhere to the blotting paper. Centrifugation (spinning) and lyophilization were developed to address this limitation in blotting fragmented clots and separate the liquid and solid portions of the thrombi. Residual thrombus volume was also assessed using two different methods, Optical imaging was used based on the protocol established by Wagner et al. for frozen clots [221]. These were compared with volumes calculated using displacement of PBS. The three metrics of thrombolytic efficacy were also tested in an *ex vivo* porcine ICH model to verify the results.

Residual thrombus mass and residual thrombus volume were compared to thrombus mass loss, which was used *in vitro* (see Chapter I.3.4). Due to limitations in the *in vivo* study, it was impossible to measure the initial thrombus mass to normalize the post-treatment mass as the thrombus is formed *in situ*. We hypothesized that residual thrombus density would have less variability and would be more sensitive to thrombolysis than residual thrombus mass or volume alone *in vitro* and *ex vivo*. After determining the metric of thrombolytic efficacy which differentiated between sham and rt-PA treatment arms *in vitro* and *ex vivo*, residual thrombus density was chosen as a metric of thrombolytic efficacy in the ICH porcine model. The central hypothesis in this chapter was that transcranial 120 kHz pulsed ultrasound exposure without Definity® enhances rt-PA lysis of intracranial thrombi in juvenile pigs.

III.2 Methods:

III.2.1 In vitro thrombolytic assay

Fresh porcine blood was collected from swine during the *in vivo* procedure described below (Chapter III.2.5) and 3 mL aliquots of blood were then placed in glass vacutainers with a siliconized interior (366430, Becton Dickinson and Company, Franklin Lakes, NJ, USA). Tubes were sealed with a rubber stopper and the blood was incubated in a 37 °C water bath for 3 hours

to allow the aliquots to clot. Clots were stored at room temperature (22 °C) for up to 8 hours while experiments were performed.

To assess residual thrombus mass, volume, and density as metrics for rt-PA mediated thrombolytic efficacy, an *in vitro* study was performed. Clot mass was measured following a protocol developed by Datta et al. before and after treatment to assess mass loss and residual clot mass [81], [204]. Each clot was removed from its glass vacutainer, blotted with a Kimwipe to remove excess water (Kimtech, 34155, Kimberly-Clark Professional, Roswell, GA, USA) and weighed in a weigh boat. Clots were divided into a no treatment arm (sham) and three treatment arms: rt-PA only (lytic), rt-PA and 120 kHz ultrasound (sonothrombolysis without Definity®), or rt-PA, Definity®, and 120 kHz ultrasound (sonothrombolysis with Definity®). Each clot was treated for 30 minutes while incubated in a condom filled with thawed fresh-frozen pooled porcine plasma (Lampire Biological Laboratories, Pipersville, PA, USA) which had been allowed to gas for 2 hours to equilibrate with the surrounding air in an open container based on the protocol published by Bader et al. [224]. Clots receiving rt-PA with or without Definity® were pierced with a plastic 20 G catheter (SR*FF2032, Sureflash, Terumo, Vaughan, Ontario, Canada) and had 0.3 mL 1 mg/mL rt-PA and 0.15 mL Definity® as appropriate injected into the center of the clot over 20 seconds. Clots treated with ultrasound as well were placed in a condom whose tip was positioned 3 cm from the 120 kHz therapy transducer face and centered to receive the maximum pressure at that distance. The pressure at this location was set to 0.5 MPa_{p-p} as this measurement is within the range of pressures which enhance clot mass loss [81], [106], [204].

After treatment, clots were removed from the condom and rinsed in PBS to remove plasma, lose red blood cells, and rt-PA from the exterior. Three different methods were used to remove excess water from the clot and obtain a clot mass: blotting, centrifugation (spinning), and

lyophilization. Each clot was blotted again and reweighed to obtain a "blotted" mass, then placed in a centrifuge tube of known mass and spun at 1000 rpm and 4 °C for 15 minutes. Following centrifugation, the supernatant was removed with a 1000 μL pipette (Pipet-Lite 1000-LTS, Mettler-Toledo Rainin, Oakland, CA, USA), and the clot was weighed again to obtain a post-centrifugation "spun" mass. Each clot was then placed in a lyophilizer (Freezone 2.5 L, Labconco, Kansas City, MO, USA) to further dehydrate the clot (-40 °C, 0.015 bar) and incubated for 15 hours. The clot mass was measured once more after lyophilization to obtain a "lyophilized" mass. Clot mass loss was calculated by comparing each post-treatment mass (blotted, spun, lyophilized) to the pre-treatment blotted mass. Residual clot mass was obtained by using the blotted, spun, and lyophilized masses measured.

Clot volume was calculated using two methods: displacement and optical imaging. The displacement volume was determined by filling a graduated cylinder (20025, TEKK, Toledo, OH, USA) partially with PBS. The clot was then added to the graduated cylinder and the difference between the initial and final volume was determined. The displacement volume was measured after the clot had been treated and the clot blotted to obtain the final mass. The optical imaging volume was determined both before and after treatment by photographing the clot in a glass plate of PBS with a millimeter ruler. The clots were cylindrical and the volume was determined by measuring the radius and the length of each clot.

III.2.2 Comparison of clots incubated with plasma or artificial cerebrospinal fluid

Artificial cerebrospinal fluid (a-CSF) was made following the protocol published by Hitchcock et al. and fresh frozen porcine plasma was obtained from Lampire and thawed prior to each experiment [105]. Each clot was blotted and weighed, then clots were either incubated in a-CSF, or thawed porcine plasma within a condom and incubated at 37 °C for 30 minutes following

a previously described protocol (Chapter III.2.1) [81]. Clots treated with rt-PA were punctured with a 20 G catheter and had 0.3 mg of 1 mg/mL rt-PA injected into the clot parenchyma prior to incubation. After treatment, clots were removed from the condom and blotted or centrifuged to obtain a final mass.

III.2.3 Ex vivo thrombolysis protocol[4]

A whole juvenile (20 kg total body weight) porcine head (Wayne's Meats, Milan, IN, USA) was obtained within 3 hours of death using an electric shock. Heads were stored at 4 °C for up to three days before use. Each head was placed in a 37 °C water bath and allowed time to warm for 3 hours. An incision was made at the midsagittal and coronally planes using a #10 scalpel to expose the periosteum on the top of the skull. The periosteum was removed to identify the coronal and sagittal sutures. A ruler was used to measure 11 mm to the right of the sagittal and 11 mm anterior to the coronal sutures. The location identified was marked using an awl and mallet to create an indentation in the skull. A power drill (DC730, DeWALT, Baltimore, MD, USA) with 1/16" high-speed steel tip was used to drill a cranial burr hole at the marked location. An IV Catheter (Sureflash, Terumo, 20 G x 1.25") was inserted into the burr hole stereotactically and into the cerebral cortex of the right frontal lobe. The depth was controlled by using a spacer to insert the catheter 15 mm into the brain.

The infusion apparatus was set up just prior to infusion (Figure III.1). The catheter was connected to the pressure transducer using a three-way valve. A heparin lock was prepared in a

[4] *This section is adapted from a paper coauthored by the author of this dissertation and submitted as part of a summer program along with Samantha Ford and Christy Holland for the WISE program at the University of Cincinnati. It is included with permission from all authors. Quoted text is demarcated by a vertical solid line in the margin.*

1 mL plastic BD (Becton, Dickson, and Company, Franklin Lakes, NJ, USA) syringe 1:9 dilution of heparin in PBS. The heparin lock syringe was connected to the three-way valve and the three-way valve was closed to the syringe to prevent heparin contaminating the catheter during infusion. Note that this volume of heparinized saline is enough to fill the dead space between the three-way valve and the catheter. On the other side of the pressure transducer, 30 cm of silicone tubing was connected to another three valve and two 5 mL syringes, one loaded with 4.5 mL anticoagulated porcine blood, and one loaded 0.5 mL 0.16 M $CaCl_2$.

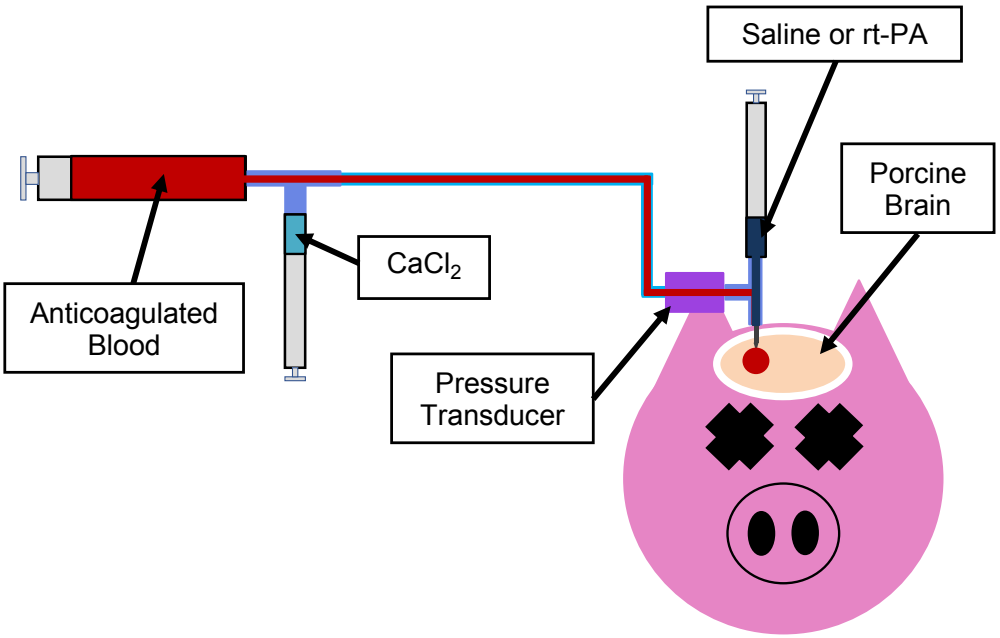

Figure III.1. Diagram of *ex vivo* porcine intracerebral hemorrhage model with infusion apparatus. Pressure is monitored during infusion using the pressure transducer before the catheter.

The citrated porcine blood was recalcified by injecting the $CaCl_2$ into the porcine blood syringe through the three-way valve. Once mixed, the three-way valve was opened to the catheter and the tubing primed with the recalcified blood. Once finished, the syringe was placed into a syringe pump (Harvard Apparatus, Pump 11 Elite, Holliston, MA, USA) and infusion started.

Pressure was monitored throughout the infusion. After infusion was complete, the three-way valve was opened, and the heparin lock was infused by hand to prevent clotting within the catheter. The blood was incubated at 37 °C in the brain for 3 hours.

Once 3 hours had passed, the thrombus was treated according to the two treatment arms: rt-PA only (lytic) and saline only (sham), with an $n = 5$ for each arm. For the lytic treatment arm, rt-PA (Activase, Genentech, San Francisco, CA, USA) was warmed in a 37 °C water bath 20 minutes prior to treatment infusion. 0.65 mL of rt-PA (1 mg/mL) or saline was loaded into a 1 mL plastic syringe in preparation for treatment. The heparin lock was disconnected from the three-way valve and the treatment infused down the catheter by hand over 1 minute. After infusing the treatment, the thrombus was incubated for 30 minutes, then the porcine head was placed into a 2-gallon freezer bag and put into a -80 °C freezer for 3 days. On the day before head sectioning, the head was placed in a -20 °C freezer. The head was sectioned using a bandsaw into 0.5-1.0 cm sections (Figure III.2) and thawed at 4 °C in a walk-in refrigerator. The thrombus was then dissected out from the surrounding brain tissue and placed in pre-weighed centrifuge tubes and centrifuged for 15 minutes at 1000 rpm and 4 °C. Supernatant was removed using a pipette and the residual mass was measured.

Digital photographs were downloaded and processed using ImageJ (v1.8.0, U.S. National Institutes of Health, Bethesda, Maryland, USA). Operators blinded to the treatment outlined the intracerebral hemorrhage on both anterior and posterior aspects of each brain section. Lesion volume was determined using equation (1)

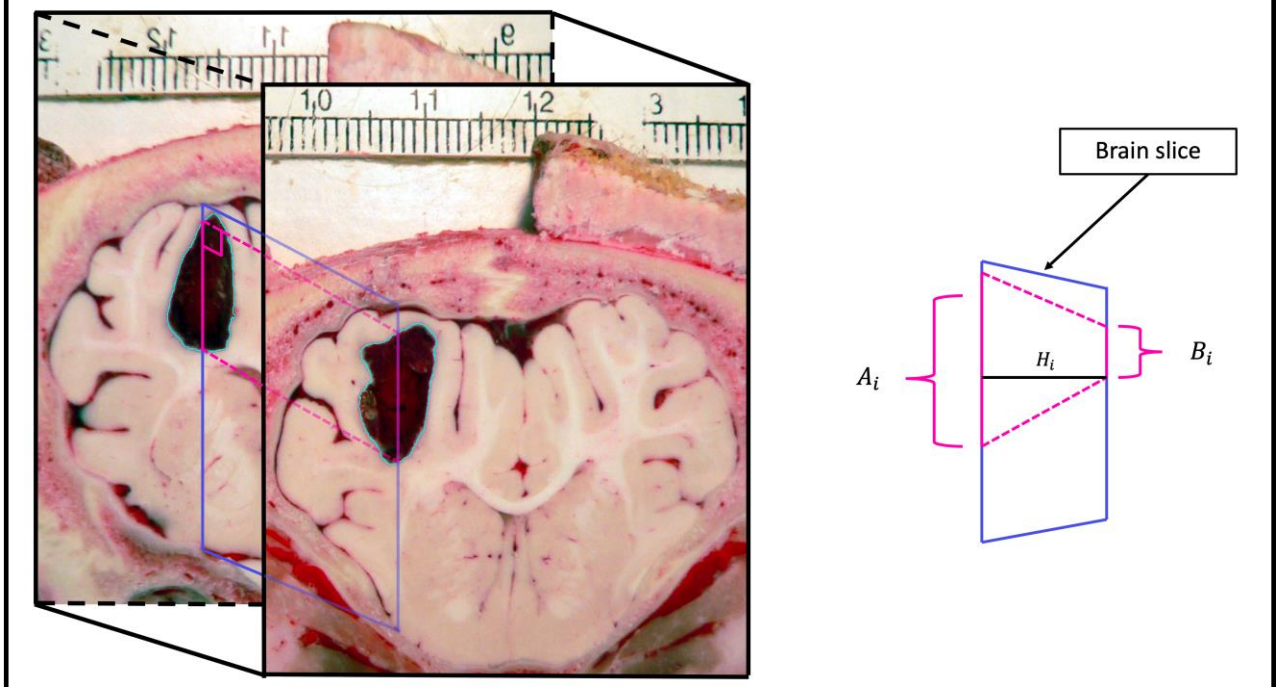

Figure III.2. Thrombus volume estimation based on optical imaging. Thrombus area on both the anterior and posterior sections of each slice were measured and the volume determined using equation (1).

$$V_{clot} = \sum_{n=1}^{i} \frac{A_i + B_i}{2} H_i \qquad \text{(III.1)}$$

where A_i and B_i are the areas of the thrombus measured on the anterior and posterior sides of slice i, respectively, and H_i is the thickness of slice i [221] measured using digital calipers (No. 147, General, New York, NY, USA). The volumes of each slice were then summed to derive the lesion's total volume estimate [225].

III.2.4 In vivo thrombolysis protocol

Details of the surgical methods to induce ICH in pigs are described in several publications by Wagner et al. [220], [221]. All animal experiments were conducted using a protocol approved by the University of Cincinnati Institutional Animal Care and Use Committee. In brief, pigs (~20 kg) were initially anesthetized with an intramuscular (IM) injection of ketamine, 33 mg/kg, acepromazine 1.1 mg/kg, and atropine 0.04 mg/kg and analgesia was provided with an IM

injection of buprenorphine (0.1-0.3 mg/kg). An endotracheal tube was inserted orally, and pigs were mechanically ventilated using a pediatric respirator. Respiration rate and tidal volume were adjusted to achieve arterial blood gases within physiologic limits: $pO_2 > 100$ and $pCO_2 = 35\text{-}45$. Following sedation and intubation, Isoflurane (1-3%) was administered to maintain a surgical plane of anesthesia. A femoral artery catheter was placed using the Seldinger technique under ultrasound imaging guidance using an (EPIQ 7G, Philips, Bothell, Washington, USA) and L12-5 array. Femoral access was used to provide continuous blood pressure monitoring and blood for intracerebral infusion [226]. Core temperature was measured using a rectal thermistor probe and was maintained at 38.5 ± 1.0 °C using a warm water blanket.

Prior to infusion, the animal's head was shaved and disinfected using aseptic techniques. A cranial burr hole was made 11 mm to the right of the sagittal and 11 mm anterior to the coronal sutures (Figure III.3). A 20 G sterile plastic, 16.5 mm long catheter was cut to 14 mm in length, inserted stereotactically into the frontal cerebral white matter at the caudate nucleus level, and cemented in place using cyanoacrylate surgical adhesive (Vetclose, Henry Schein, Dublin, OH). A 5 mL aliquot of autologous porcine blood was used to prime a 30 cm length of silastic tubing (1.58 mm ID, 2.41 mm OD, HelixMark, Carpinteria, CA, USA). A 3 mL bolus of blood was slowly infused over 10 min through the 20 G catheter into the frontal cerebral white matter using a syringe pump (Pump 11 Elite, Harvard Apparatus, Holliston, MA) (Figure III.3). The blood was allowed to form an intracerebral thrombus for three hours.

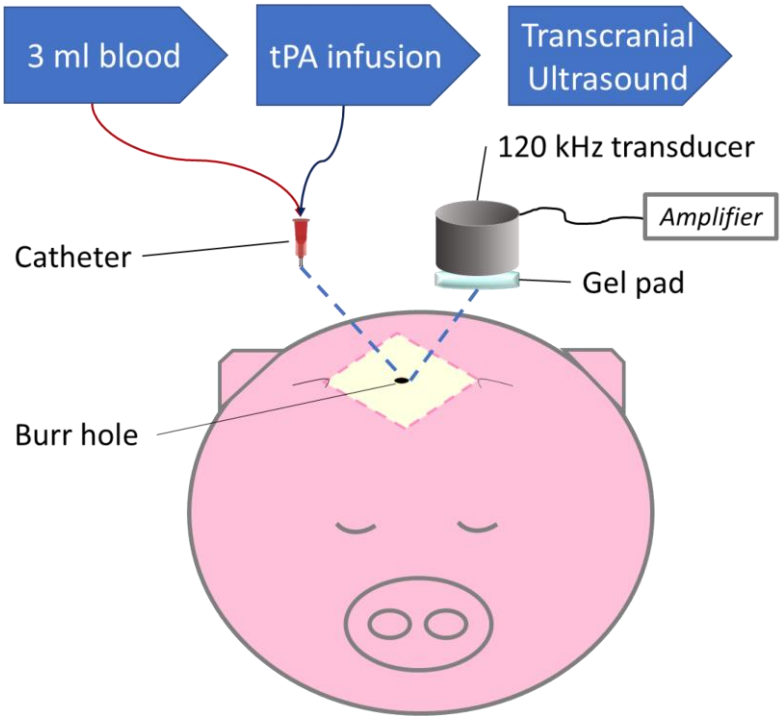

Figure III.3. *In vivo* protocol of porcine ICH. ICH was infused through a catheter placed in the frontal white matter of an anesthetized crossbred pig (~20 kg). The catheter was positioned 11 mm anterior and 11 mm right of the coronal and sagittal sutures, respectively. After a 3-hour incubation period, rt-PA was injected into the thrombus (for treatment arms only) and then the catheter removed. The burr hole was sealed with bone wax and for ultrasound treated pigs, and ultrasound transducer was then positioned above the thrombus and coupled to the skull using ultrasound gel.

Three hours after intracerebral blood injection, the thrombi were exposed to either no treatment (sham), ultrasound alone (ultrasound), rt-PA alone (lytic), or 120 kHz ultrasound and rt-PA (sonothrombolysis). Those pigs treated with rt-PA received 0.3 mL solution of rt-PA (1 mg/ml) infused slowly by hand during 10 minutes through the same catheter used for blood injection (Figure III.3). After the drug infusion, the catheter was removed and the borehole was filled with bone wax. For pigs receiving ultrasound therapy (sonothrombolysis), an unfocused ultrasound transducer (120 kHz, 40-mm diameter disk, Sonic Concepts Inc., Seattle, WA, USA) was placed in a holder and attached to the pig head. The transducer was aligned parallel to the skull, coupled to the skull with a custom 3D printed standoff (15 mm) and acoustic gel pad (04-

02, Aquaflex, Parker Laboratories, Fairfield, NJ, USA), and centered at 8-mm distance from the burr hole in the craniocaudal direction (Figure III.3). The transducer was driven for 30 minutes (80% duty cycle, 1667 Hz pulse repetition frequency) with a free-field acoustic pressure amplitude of 625 kPa peak-to-peak.

Following termination, pigs were decapitated and the heads placed in liquid nitrogen and placed in a -80 °C freezer. After 24 hours, the frozen heads were then cut using a band saw into 5 mm thick coronal sections and the slices were examined in a refrigerated glove box (-20 °C) for hematoma location. The thickness of the frozen brain slices was measured and all slices through the brain were digitally photographed with a millimeter scale ruler (Figure III.2). Thrombus volume was measured using the same protocol described above (Section III.2.4)

Frozen brain sections were thawed and processed at 4 °C. Each thrombus was carefully excised using a scalpel and forceps to pull the brain tissue from the thrombus. The extracted frozen thrombus fragments were placed into 15 mL centrifuge tubes of known mass. Once all of the thrombus was excised, the tube with the thrombus was centrifuged (Beckman Coulter Allegra Z-15R Centrifuge) for 15 minutes at 1000 rpm at 4 °C. Following centrifugation, the supernatant was removed with a pipette and the solid portion of the thrombus was weighed to obtain a residual thrombus mass. The residual thrombus density was calculated according to Equation (III.1).

III.2.7 Ultrasound field measurements and simulations

To estimate the ultrasound pressure field in the intracranial cavity of the porcine model, the heads of three animals were removed after euthanasia. The intracranial acoustic pressure field was measured post mortem using the material and methods described by Ammi et al. [189]. The brain was removed from the heads so that the cranial cavity could be accessed through the foramen

magnum by a calibrated hydrophone (TC4038, Teledyne Reson Inc. Goleta, CA, USA) mounted on a 3D positioning arm (NF-90, Velmex, Bloomfield, NY, USA).

To estimate the ultrasound field outside the small area that was accessible to the hydrophone, simulations based on CT-scans of the porcine skulls (voxel size 0.43 x 0.43 mm^2 x 5 mm, LightSpeed Pro 16 scanner, GE Healthcare, Chalfont St Giles, UK) were conducted using the finite-difference model described and validated by Bouchoux et al. [191], [192]. All simulations were implemented in MATLAB (2011b, Mathworks, Natick, , MA, USA), C and CUDA, a parallel computing platform and run on a computer with 10GB memory, a 3.4 GHz processor with four cores (i7-2600, Intel, Santa Clara, CA, USA) and a graphics processing unit (GTX 550 Ti, NVIDIA, Santa Clara, CA, USA). Pressure amplitudes were normalized to the maximum amplitude in the free field for both free field and intracranial simulations. The excitation field from the transducer was positioned 1 cm from the skull above the burr hole.

III.2.8 Statistical Analysis

All statistical analysis was conducted in PRISM (GraphPad Software, San Diego, CA, USA) except for the power analysis. Power analysis for the *in vitro* study was performed using MATLAB (2017b) and the statistical tables published by Cohen [212]. Normality of the *in vivo* residual thrombus mass data was determined using a Shapiro-Wilk test. A one-way analysis of variance (ANOVA) with a Tukey post-hoc analysis was used to compare differences between treatment arms for residual thrombus mass, volume, and density.

III.3 Results:

III.3.1 Development of a thrombolytic assay in vitro

Initial clot mass (blotted) was not different for any of the four treatment groups ($p > 0.13$, Figure III.4). Clot mass loss was significantly different between sham, rt-PA only, and

sonothrombolysis with Definity®, with significant differences between all three treatment arms for the blotted and spun clots ($p < 0.05$, Figure III.5). However, no significant increase in thrombolysis was observed between rt-PA only and sonothrombolysis without Definity® ($p > 0.37$) for either blotted, spun, or lyophilized clots (Figure III.5). Additionally, there was no difference in the clot mass loss between sonothrombolysis with and without Definity® for any of the three water removal methods ($p > 0.34$) (Figure III.5). There was a significant difference in the clot mass loss for rt-PA only compared to sonothrombolysis with Definity® for the blotted mass ($p < 0.05$) and spun mass ($p < 0.05$), but not for the lyophilized mass ($p > 0.34$).

Residual thrombus mass was also assessed as a metric of thrombolysis (Figure III.6). Comparing the residual mass based on the blotted mass measurement, no difference was detected in the mass for any groups except between sham and sonothrombolysis with Definity® ($p < 0.05$)

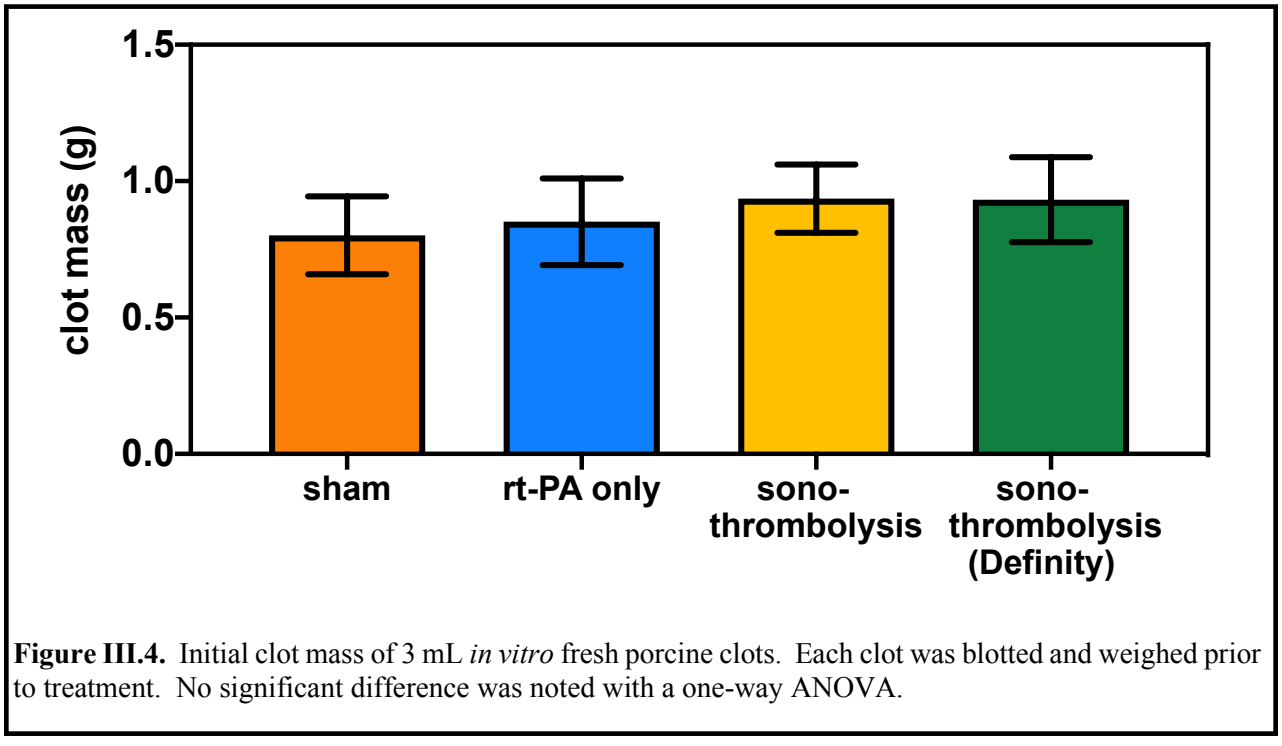

Figure III.4. Initial clot mass of 3 mL *in vitro* fresh porcine clots. Each clot was blotted and weighed prior to treatment. No significant difference was noted with a one-way ANOVA.

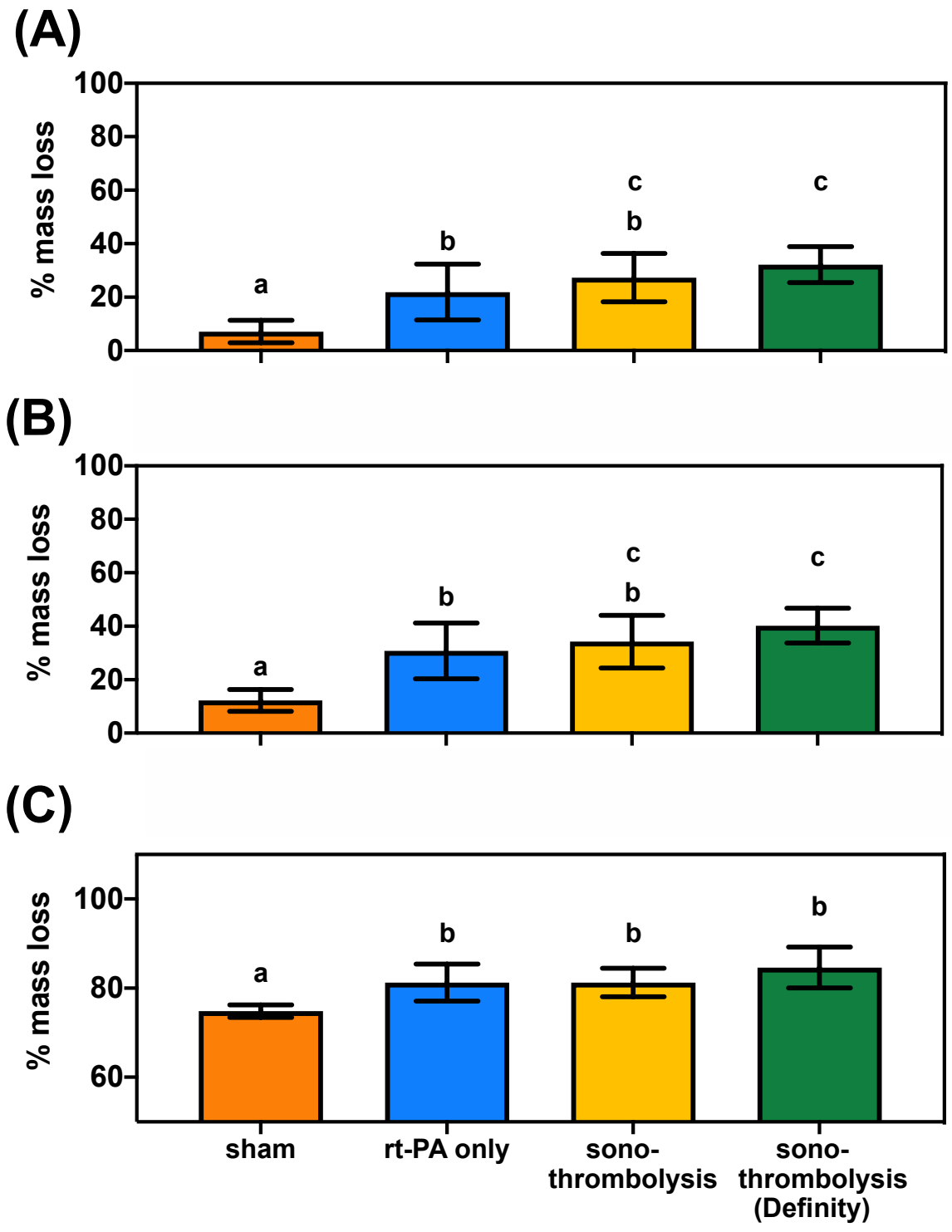

Figure III.5. Clot mass loss for 3 mL *in vitro* fresh porcine clots measured using blotting (A), spinning (B), or lyophilization (C). All clots were incubated in 30 mL thawed fresh-frozen porcine plasma gassed for 30 minutes. A one-way ANOVA was used to compare treatments and compact letter display used to identify statistically equivalent groups.

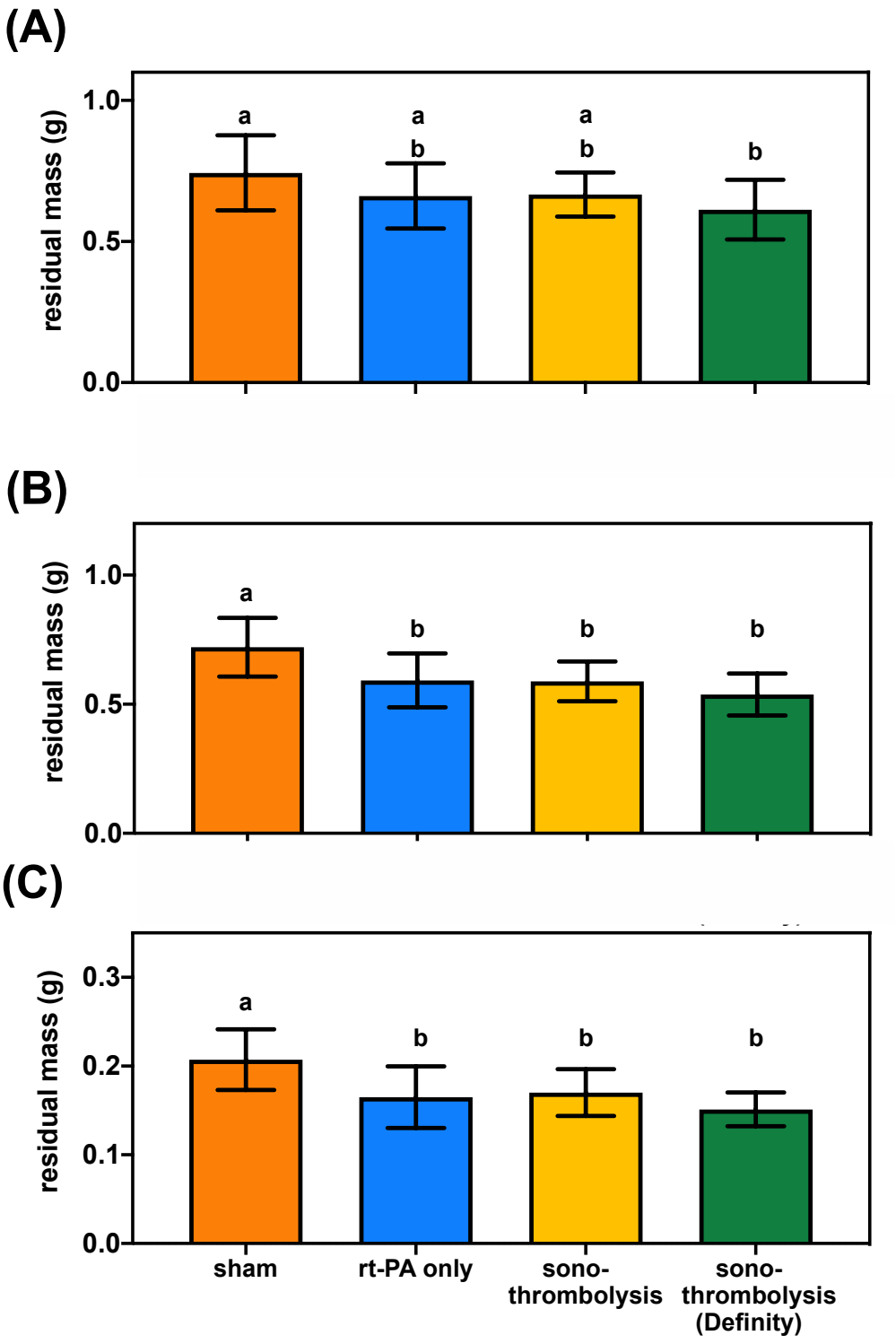

Figure III.6. Residual clot mass for 3 mL fresh porcine clots measured using blotting (A), spinning (B), or lyophilization (C). All clots were incubated in 30 mL thawed fresh-frozen porcine plasma gassed for 30 minutes. A one-way ANOVA was used to compare treatments and compact letter display used to identify statistically equivalent groups.

(Figure III.6). The residual masses measured using the spun or lyophilized clots did not change the results compared to blotted clots, with significant differences in the residual mass observed between sham and all three treatment groups ($p < 0.05$), but no difference between the three treatment groups ($p > 0.55$).

Clot volume also varied with the metric used with larger volumes measured using imaging techniques compared with the volume displacement (Figure III.7). Volumes measured using displacement ranged between 0.6-1.0 mL and volumes measured using optical imaging ranged from 0.9-1.8 mL before treatment and 0.7-1.6 mL after treatment. There was no significant difference in clot volumes prior to treatment ($p > 0.19$). Following treatment, volume measured by displacement was significantly lower for rt-PA only and sonothrombolysis compared to sham ($p < 0.05$). In contrast, volume calculated using optical imaging was significantly higher when comparing sham to rt-PA only and sonothrombolysis without Definity® ($p < 0.05$).

Comparing the clot volumes measured before and after treatment (optical imagining volume), clots lost volume following treatment, with a decrease in volume measured optically seen in the sonothrombolysis with Definity® treatment group (0.50 ± 0.26 mL) (Figure III.7). Sham clots also reduced in volume following treatment (0.26 ± 0.30 mL). Both the clots in the rt-PA only and sonothrombolysis without Definity® groups change as well, but were just as likely to increase in volume as decrease with a difference in their initial and final volumes of 0.02 ± 0.30 mL and -0.05 ± 0.13 mL respectively (Figure III.7). This difference in volumes was significant comparing all four treatments ($p < 0.05$), however, a multiple comparisons test was not significant for any single pairwise comparison ($p > 0.07$).

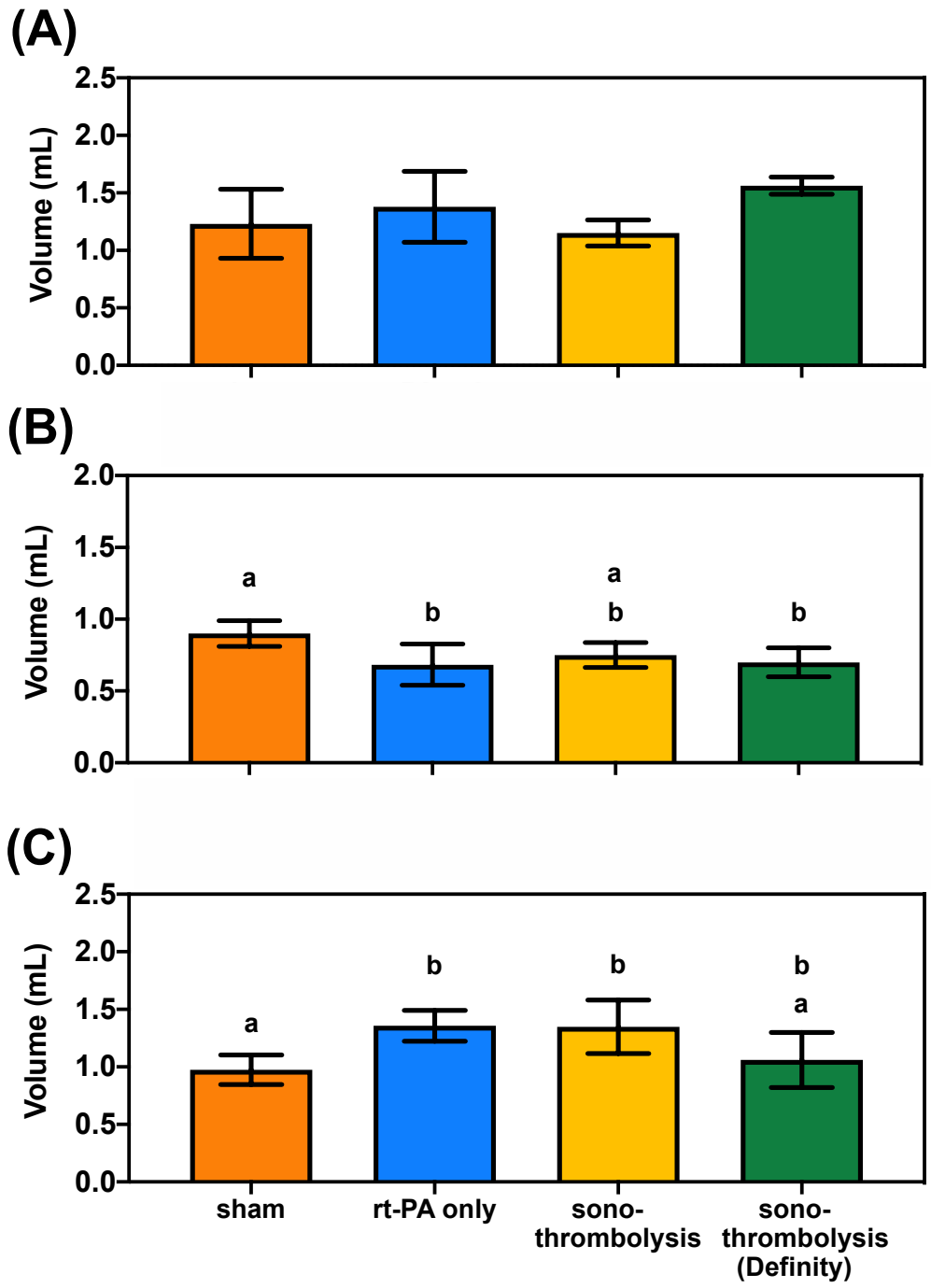

Figure III.7. Clot volumes for 3 mL *in vitro* fresh porcine clots measured before treatment using optical imaging (A), or after treatment using displacement (B) or optical imaging (C). All clots were incubated in 30 mL thawed fresh-frozen porcine plasma gassed for 30 minute. Sham clots received no treatment, and were compared to rt-PA only (0.3 mg rt-PA), sonothrombolysis without Definity® (120 kHz, 0.5 MPa_{p-p}, 0.3 mg rt-PA), sonothrombolysis with Definity® (120 kHz, 0.5 MPa_{p-p}, 0.3 mg rt-PA, 0.15 mL Definity®). A one-way ANOVA was used to compare treatments and compact letter display used to identify statistically equivalent groups.

Spun clots, which showed contrast between the treatment groups, were then normalized by the post-treatment volume determined both by displacement, and by optical imaging (Figure III.8). Normalizing by the volume calculated from displacement resulted in no difference between any of the treatment groups ($p > 0.14$) (Figure III.8A). In contrast, normalizing by the volume calculated from the optical image provided contrast between sham, and each of the three treatment groups ($p < 0.0001$), but still no difference was found between the three treatment groups ($p > 0.17$) (Figure III.8B).

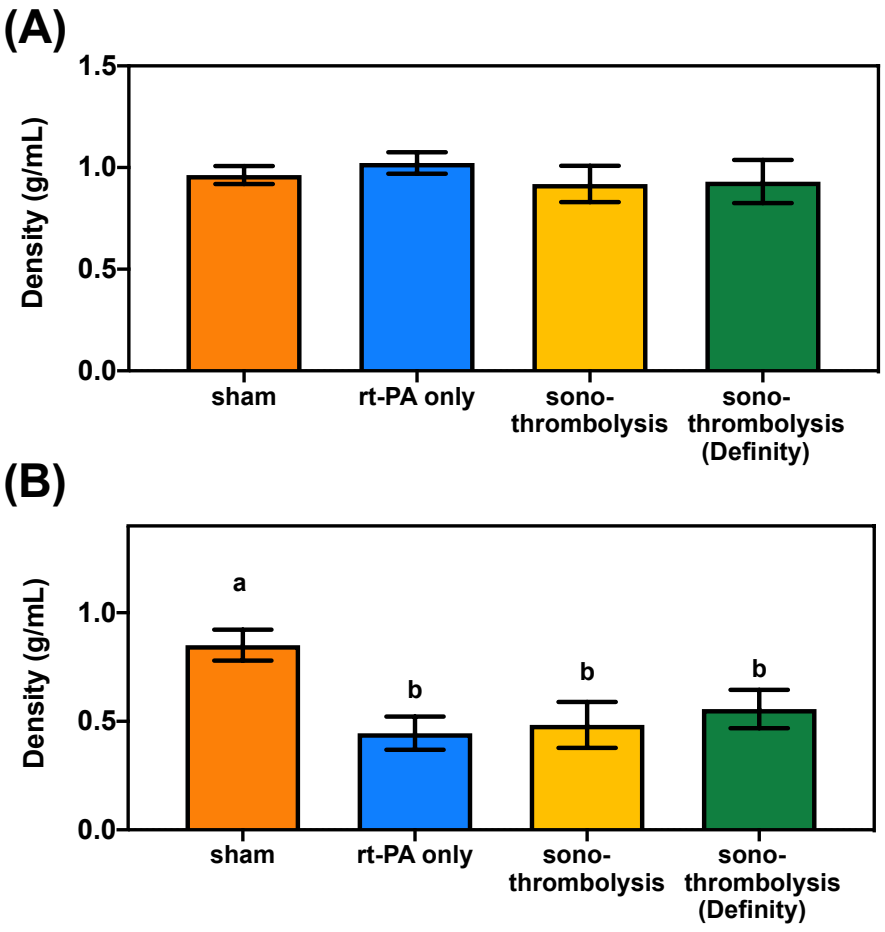

Figure III.8. Fresh 3 mL porcine clots density after treatment with clot volume calculated using displacement (A) or optical imaging (B). All clots were incubated in 30 mL thawed fresh-frozen porcine plasma gassed for 30 minute. Sham clots received no treatment, and were compared to rt-PA only (0.3 mg rt-PA), sonothrombolysis without Definity® (120 kHz, 0.5 MPa_{p-p}, 0.3 mg rt-PA), sonothrombolysis with Definity® (120 kHz, 0.5 MPa_{pp}, 0.3 mg rt-PA, 0.15 mL Definity®). A one-way ANOVA was used to compare treatments and compact letter display used to identify statistically equivalent groups.

III.3.2 Comparison of clots incubated with plasma or artificial cerebrospinal fluid

Clots treated with rt-PA only (lytic) showed a significant increase in the clot mass loss compared to the corresponding shams in both porcine plasma and a-CSF ($p < 0.0001$) (Figure III.9). Additionally, the incubation media (either porcine plasma or a-CSF) made no difference to the clot mass loss for the same treatment with a $p > 0.94$ and $p > 0.05$ for the no treatment, and rt-PA treatment groups respectively. However, a-CSF clot mass loss was almost significantly greater ($p = 0.0509$) (Figure III.9) than porcine plasma for the rt-PA treated group.

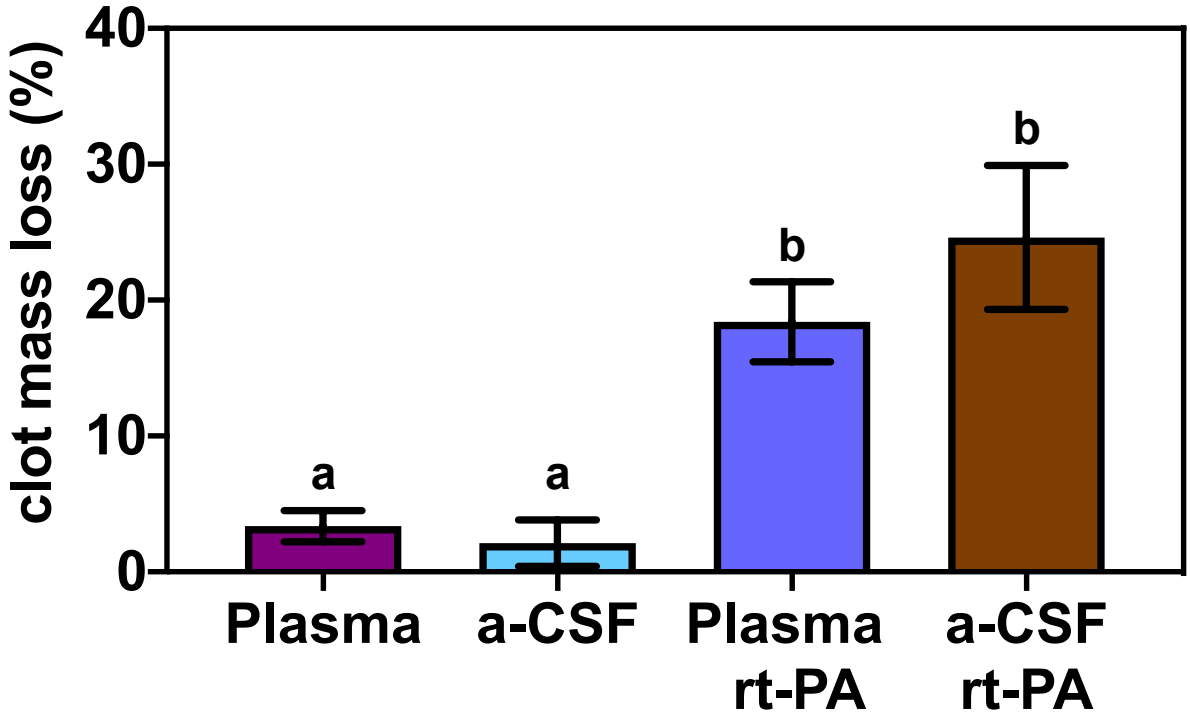

Figure III.9. Clot mass loss for clots incubated in porcine plasma and artificial CSF. Clots were treated either with a direct inject of 0.3 mg rt-PA into the center of the clot (both rt-PA groups), or received no treatment (plasma, a-CSF). Artificial CSF did not result in a significant change in clot mass loss for clots receiving no treatment or clots receiving treatment with rt-PA. For both plasma and a-CSF, clots treated with rt-PA had significantly greater clot mass loss ($p < 0.0001$). A one-way ANOVA was used to compare treatments and compact letter display used to identify statistically equivalent groups.

III.3.3 Validation of thrombolytic assay ex vivo

During infusion, some pigs had blood flow out of the burr hole and into the water bath. This volume varied and was not able to be quantified. Blood was also noted to form a bruise in the bone 15 minutes after the injection in some pigs. Following sectioning, intracerebral hemorrhages were confirmed in porcine brains exposed to either saline or rt-PA. Intracerebral thrombi and subarachnoid thrombi were both present in each *ex vivo* brain.

The residual thrombus mass from *ex vivo* studies is shown in Figure III.10A. Sham thrombi had a significantly greater residual thrombus mass than rt-PA alone ($p < 0.05$) (Figure III.10A). The average volume was 2.16 ± 0.61 cm^3 and there was no significant difference between groups ($p > 0.12$) (Figure III.10B). The residual thrombus density was similarly significantly lower for rt-PA alone compared to sham ($p < 0.01$) (Figure III.10C). A power analysis showed, with 80% power and $\alpha = 0.05$, only an n of 3 was required to show thrombolytic efficacy of rt-PA alone compared to sham.

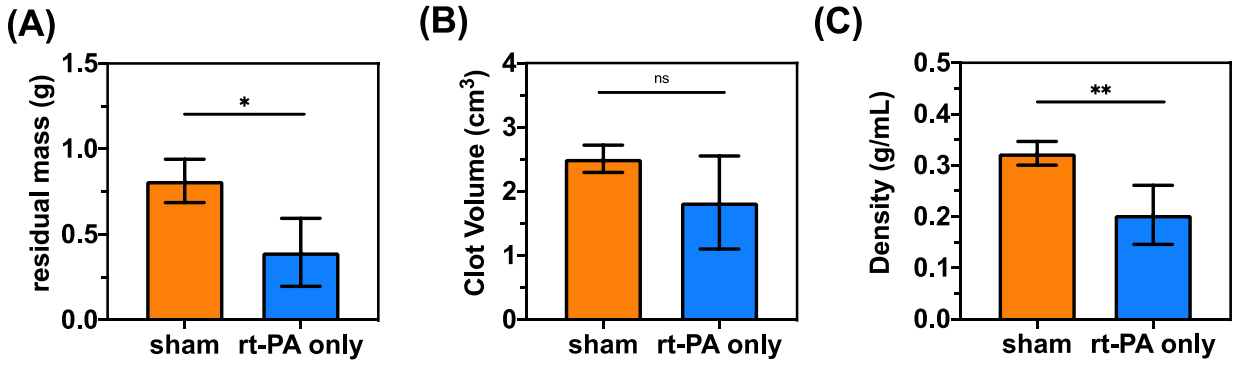

Figure III.10. Residual thrombus mass (A), thrombus volume (B), and residual thrombus density (C) for frozen porcine thrombi formed in an *ex vivo* porcine model of ICH. Saline treated thrombi exhibited higher residual thrombus mass and density after extraction than rt-PA treated thrombi with a significance of $p = 0.012$, and $p < 0.0083$ respectively and a power of 80% with an n of 3. A Student's t-test was used to compare treatments and statistical significance is shown with Asterix *: $p < 0.05$, **: $p < 0.01$.

III.3.4 In vivo thrombolysis

Representative coronal sections of porcine brains from studies performed for this dissertation are shown in Figure III.11. Similar to the *ex vivo* data, subarachnoid hemorrhage (SAH) was present in addition to the intracerebral hemorrhage (Figure III.11). No thrombi crossed the midline. Any thrombi that extended into the ventricles were removed from the study.

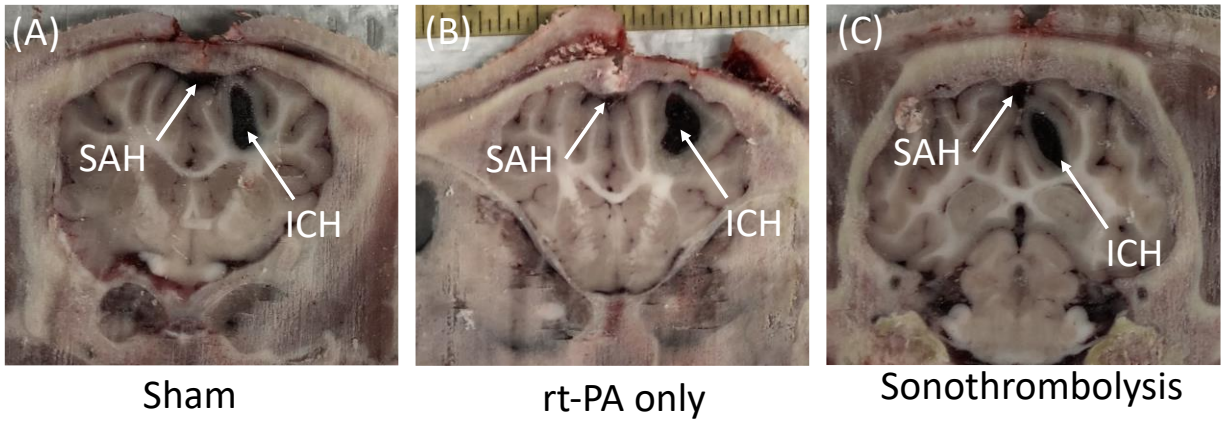

Figure III.11. Images of coronal sections for sham (A), rt-PA only (B), and sonothrombolysis without Definity® (C) *in vivo* porcine studies. Note the presence of intracerebral hemorrhage (ICH) in the right frontal white matter of the porcine brain as well as the presence of subarachnoid hemorrhage (SAH).

Thrombus density was chosen as the metric of thrombolytic efficacy to be employed *in vivo* based on *in vitro* and *ex vivo* results. Out of 108 porcine brain samples from the *in vivo* studies performed by Ammi et al. [222], 87 were lost due to thrombus removal or sampling for other assays prior to this study. The remaining samples included 4 sham, 3 rt-PA only, and 11 sonothrombolysis without Definity®. Further studies were performed in this dissertation to increase the power of the study. A comparison of data acquired by Ammi et al. [222] and data acquired for this dissertation, is shown in Figure III.12. No significant difference between the data analyzed from the porcine studies performed by Ammi et al. and those performed for this dissertation was found for any of the three treatment arms ($p > 0.29$).

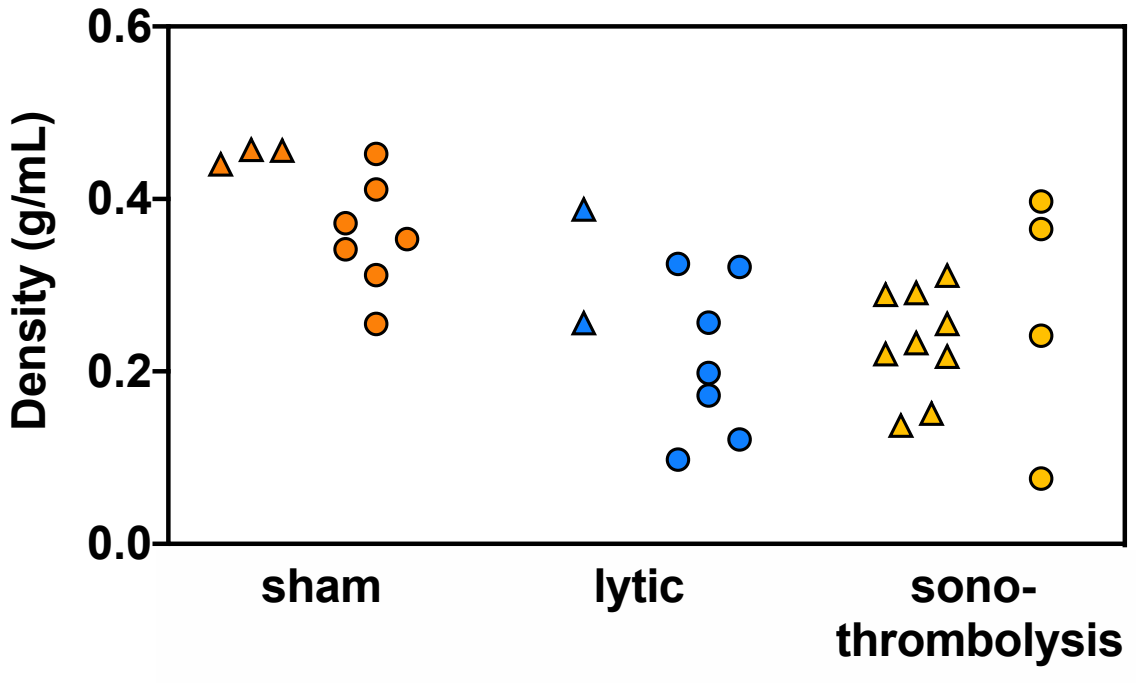

Figure III.12. Comparison between the residual thrombus density data acquired from porcine studies performed by Ammi et al. and for this dissertation. Data analyzed from the studies performed by Ammi et al. is shown in triangles and data analyzed from porcine studies performed in this dissertation are shown in circles. No groups were significantly different on two-way ANOVA.

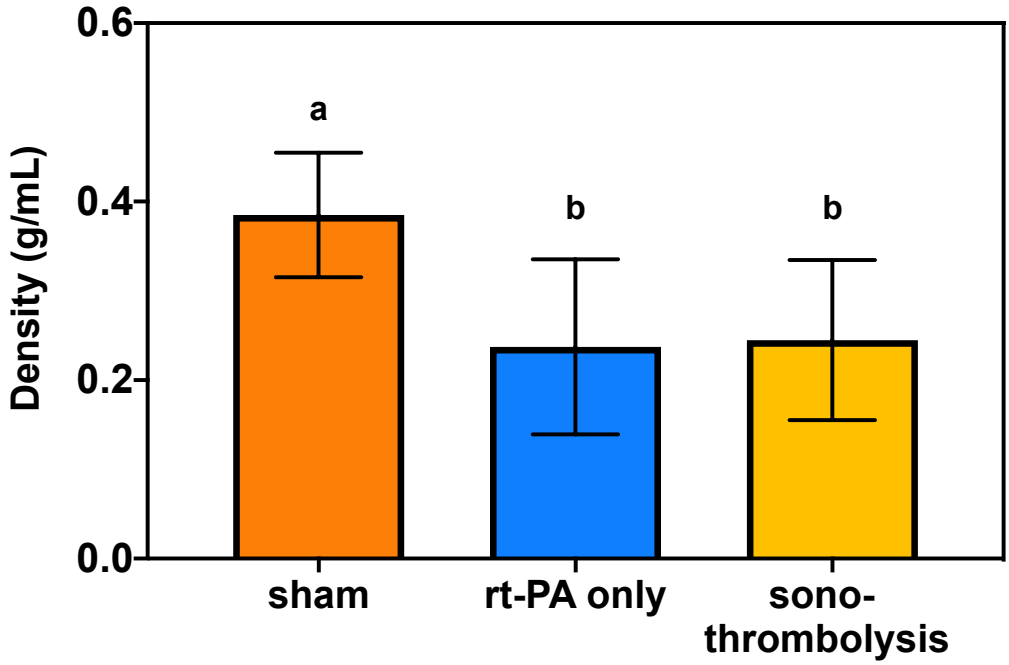

Figure III.13. Combined *in vivo* residual thrombus density. A one-way ANOVA was used to compare treatments and statistically equivalent groups are shown by compact letter display.

The analyzed data from Ammi et al. was combined with data analyzed from the surgeries performed for this dissertation as no difference was found between the data sets for each treatment arm ($p > 0.29$) (Figure III.13). A Grubbs' Outlier test was performed to remove outliers and one point was removed from each data set. A significant difference in residual thrombus density between sham treated thrombi and both rt-PA only and sonothrombolysis without Definity® treated thrombi was detected ($p < 0.01$, $p < 0.05$ respectively) (Figure III.13). No significant difference in thrombus density was found between rt-PA only and sonothrombolysis without Definity® treated thrombi ($p > 0.98$).

III.3.5 Ultrasound field measurements and simulations

The acoustic pressure measured *in vitro* in the cranial cavity at the predicted position of the center of the hematoma was 504 ± 51 kPa peak to peak (Table III.1). The free-field maximum, at the same position was 625 ± 20 kPa, and the acoustic pressure reduction at 120 kHz due to the presence of the skull was 19 ± 6%. An ultrasound field obtained by simulation is shown in Figure III.14. The relative standard deviation of the simulated acoustic pressure in the typical thrombus volume was 27%. The simulations also confirmed the presence of acoustic interference due to the reflections of the wave in the cranial cavity (up to 0.64 MPa_{p-p}).

Table III.1. Intracranial field measurements in 3 porcine skulls. The free field was first measured, then the porcine skull positioned relative to the transducer as described in the *in vivo* thrombolysis methods.

Skull Number	Free Field Max (MPa_{p-p})	Skull Free Field Max (MPa_{p-p})	Percent Pressure Reduction at Free Field Max (%)
1	0.606	0.446	26
2	0.649	0.540	17
3	0.621	0.525	15

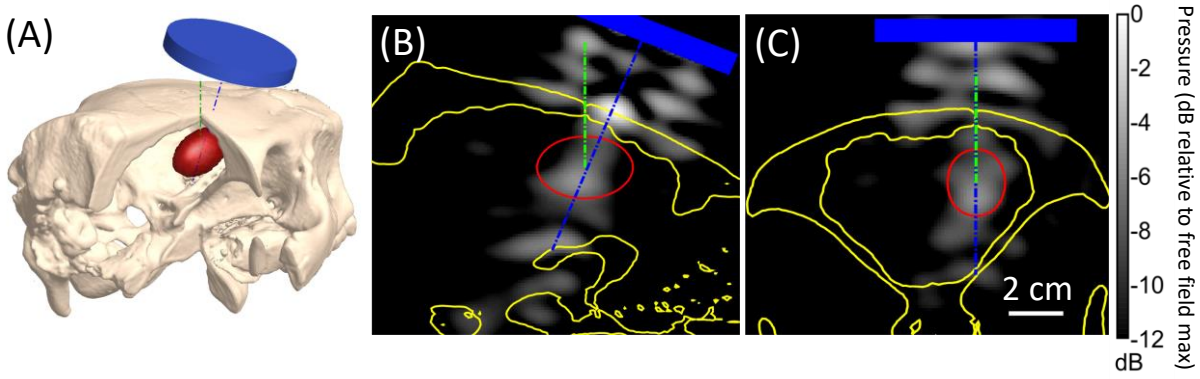

Figure III.14. Computational model of acoustic propagation through porcine skull using 3D rendered (A) model (A), and sagittal (B) and coronal (C) views. The ultrasound transducer was positioned parallel to the bone, using a plastic holder and an acoustic gel pad for transmission (not shown on the diagram). The position of the catheter used for blood injection and treatment administration is indicated by the green line (the catheter was removed during ultrasound exposure). The average thrombus size is represented by the red spheroid. (B) The map of the acoustic pressure obtained in the cranial cavity was obtained by simulation and is shown relatively to the pig skull (yellow contours).

III.4 Discussion:

III.4.1 Development of thrombolytic assay in vitro

All clots started within the same range of masses based on their initial measurements (Figure III.4). This initial mass was obtained using blotting as this has been used previously in similar studies [81], [106], [204]. One critical difference with these previous studies is that they used aged, retracted clots (3-14 days old), while the clots in this study were made from fresh porcine blood and used the same day. After incubation at 37 °C for 3 hours, the clots were transferred to room temperature (22 °C) while studies were conducted. Some of the clots waited as long as 6 hours after incubation until they were included in the study. For the fresh clots, this time period may have contributed to the variation observed in the initial clot mass. Effort was made to distribute the treatment arms throughout the study so that this variation would be equally spread among all the treatment arms, however, this may contribute to a higher variability than would be predicted *in vivo* where clots are treated after 3 hours of incubation at 37 °C.

Clot mass loss provided sufficient contrast to differentiate between sham and treatment arms (rt-PA only, sonothrombolysis without Definity®, sonothrombolysis with Definity®) for freshly created porcine clots (Figure III.5). This effect has been observed in multiple models using mass, d-dimer, and clot width [81], [83], [172]. Ultrasound in conjunction with rt-PA in the absence of microbubbles (sonothrombolysis without Definity®) has similarly been observed to augment thrombolysis, however, it was less efficacious than with an exogenous bubble source [81], [86], [106], [227]. The clot mass loss assay provided better contrast between the treatment arms than the residual clot mass assay likely due to decreased variability in clot size (Figure III.4,5). Residual clot mass and density were able to detect thrombolysis due to rt-PA which agreed with our hypothesis.

Clot volume was assessed using two different metrics *in vitro*, an optical imaging technique that was also employed in the *in vivo* study and a displacement technique. The displacement technique resulted in lower volumes measured than those observed using the optical technique ($p < 0.05$) (Figure III.7). Measuring volume by displacement assumes that volumes are additive, which is not necessarily true in this study. It is possible that the process of blotting removes more water than would normally be lost by syneresis (fluid expulsion) during normal clot retraction [228]. Therefore, the lower volumes measured during displacement may be partially attributed to the absorption of water into the clot, reducing the overall displacement of water to a value less than the true volume of the clot. Additionally, the optical imaging method loses some information by compressing a 3D volume into a 2D image. This loss of information may result in over- or underestimates based on the unique shape of each clot. The assumption that the clot is a cylinder breaks down at the bottom of the clot which is rounded (following the shape of the bottom of the

test tube) which means that the optical imaging technique would overestimate the volume of the clot to some degree.

The initial volumes calculated using the optical imaging technique were not different from each other for the four treatment arms ($p > 0.19$) (Figure III.7A) consistent with the initial masses measured using blotting (Figure III.4). After treatment, differences were observed in the clot volume using either displacement ($p < 0.05$) or optical imaging ($p > 0.01$), (Figure III.7B,C). Using displacement, volume decreased for both sonothrombolysis with and without Definity® compared to sham ($p < 0.05$) (Figure III.7B). This result is consistent with the decrease in mass observed after each treatment and suggests that the volume measured by displacement does not capture the pre-treatment variability in clot mass well (Figure III.5, Figure III.6). Using optical imaging however, volume actually increased for clots treated with rt-PA alone, or rt-PA and ultrasound compared to sham (Figure III.7C). This effect has also been observed by Kleven et al. (see also Chapter IV) who noted that clot swelling occurred in the initial phase of clot breakdown and was more prominent in rt-PA alone treated clots than in controls or rt-PA, Definity®, and ultrasound treated clots (sonothrombolysis with Definity®) [117]. One possible explanation of these two opposite volume measurements is that the increase in volume observed optically could be due to the breakdown of the retracted fibrin superstructure causing clot swelling, which was not observed on the volume measured by displacement, as the density of the clot may have decreased and it absorbed more water. Overall, residual clot volume was not an adequate thrombolytic metric due to its variability and we accepted the null hypothesis for this metric.

The residual thrombus density was more effective than the residual thrombus mass alone at detecting mass loss due to rt-PA, but not superior to clot mass loss (Figure III.5,III.6, III.8). The clot volume, while accounting for some of the variation observed in the clot size, was unable to

cancel out this variation and may have added some additional sources of variability as the clots changed shape during treatment. Residual clot mass is not as sensitive as clot mass loss at detecting thrombolysis due to rt-PA, likely because of the variability in the initial clot mass. Thus, we found that residual thrombus mass and residual thrombus density were adequate metrics of thrombolytic efficacy *in vitro* as we hypothesized, however, residual thrombus volume was not an adequate metric of thrombolysis contrary to our hypothesis.

III.4.2 Comparison of clots incubated with plasma or artificial cerebrospinal fluid

Clots in the brain parenchyma are surrounded by a serous environment composed of CSF, rather than the plasma or blood which forms the environment of clots in the vasculature. Clots incubated in a-CSF which contains no added plasminogen showed similar degrees of thrombolysis as clots incubated in plasma (Figure III.9). This was in contrast to results published by Huang et al. who have shown that the surrounding fluid plays a role in the observed thrombolysis using clot width [141]. However, Huang et al. only compared different plasminogen sources (porcine and human plasma), not the presence or absence of plasminogen (plasma to a-CSF). Additionally, the direct injection of rt-PA into the clot parenchyma may enhance thrombolysis regardless of the medium as the rt-PA is readily able to interact with both fibrin and plasminogen intercalated within the clot. It was noted that the clots treated with rt-PA and incubated in a-CSF tended to have ($p > 0.0509$) a higher clot mass loss than those clots incubated in porcine plasma (Figure III.9). Osmolar differences could account for this change as porcine plasma as an osmolality of 260-290 mOsm/kg [229] and our artificial CSF, in line with literature values, has an osmolality of 310 mOsm/kg [230], [231]. This difference in solutes could pull some water out of the RBC's in the blood clot and further decrease the mass. However, this effect was not observed for those clots which received no treatment (Figure III.9).

III.4.3 Validation of thrombolytic assay ex vivo

The residual thrombus masses observed in our *ex vivo* study were within the range of our *in vitro* studies (Figure III.6, III.10). Saline treated thrombi had a significantly greater mass, but did not have a significantly larger volume although a trend was visible ($p > 0.12$) (Figure III.10B), similar to what we observed in our initial optically measured volumes *in vitro*, but in contrast to the post-treatment optical imaging volume (Figure III.7A,C). It is possible that the freezing process captures the majority of the lysed blood which has not yet been reabsorbed into the brain. This lysed blood would contribute to the *ex vivo* thrombus volume but would not have been detected *in vitro* as part of the post-treatment volume. This is even more likely as the deceased state of the brain means it could not react to the physiological disturbance of the thrombus by resorbing fluid or actively trying to break down the thrombus as would be seen *in vivo* [5], [13].

Using a similar porcine intracerebral hemorrhage model, Wagner et al. noted a smaller thrombus volume (1.3 ± 0.2 mL) compared to the thrombus volume observed in our *ex vivo* study (2.2 ± 0.6 mL) ($p < 0.05$) (Figure III.10B) [221]. Wagner et al. used a 2.5 mL infusion volume, 83% of the volume of blood infused in our *ex vivo* study, but their mean thrombus volume was 60% of the *ex vivo* thrombus volume measured in this study. In an earlier study, Wagner et al. infused 1.7 mL of blood and observed thrombus volumes of 1.57 ± 0.47 mL which was closer to the infused volume [220]. This variation in the final thrombus volume, both approximately the infused volume [220], and two thirds of the infused volume [221] puts our *ex vivo* thrombus volumes within the range observed based on the 3 mL infusion.

These *ex vivo* thrombus volumes also differed from our *in vitro* study based on a 3 mL aliquot of blood (Figure III.7, III.10B). Sham volumes were significantly larger for the *ex vivo* study than the *in vitro* ($p < 0.001$), however, there was no difference in thrombus volumes for rt-

PA only treated clots ($p > 0.19$). As the *ex* vivo study used the brain of a previously deceased pig, it is possible that other sources of blood from the damaged tissue and vessels contributed to the larger thrombus observed. Also, the use of recalcified citrated porcine blood, as opposed to fresh autologous blood could contribute to the difference seen between the *ex vivo* and *in vitro* studies.

Despite these differences, we were able to detect a difference in the residual mass and residual thrombus density between the sham and rt-PA only treatment arms as we hypothesized, and no difference was found with residual thrombus volume, as was observed *in vitro*. The frozen hematomas were able to be extracted from the surrounding brain tissue and excess water was removed using centrifugation as performed *in vitro.*

III.4.4 In vivo thrombolysis

A significant difference was found between rt-PA only and sham treatments ($p < 0.01$) which agreed with studies published by Wagner et al. [220], [221]. Thus, we replicated the effects of rt-PA measured in this model previously. Sonothrombolysis showed a similar degree of lysis as rt-PA, offering no significant enhancement of thrombolysis in this transcranial porcine model. Greater variation in this data was noted than that observed by Wagner et al. which may have obscured the thrombolytic efficacy of ultrasound from being detected [221]. Freezing the clots after treatment could cause variable amounts of clot lysis which would increase the variability in the data. In future studies, aspirating the thrombus could be performed before freezing to confirm replication of Wagner's results, and the residual density protocol could be implemented following freezing. Additionally, a critical difference between Wagner et al. and this study is the mechanical agitation of the clot by the catheter during aspiration which occurred. This could have induced further lysis, especially in clots which had been partially broken down by rt-PA. Thrombi treated with rt-PA only in Wagner et al. [221] also were exposed to rt-PA 10 minutes (10 minutes initial

rt-PA infusion, 20 minutes treatment, 10 minutes aspiration) longer than the 30 minute treatment period used in this study.

III.4.6 Ultrasound field measurements and simulations

In vitro measurements showed that the broad 120-kHz beam homogeneously insonified the hematoma (Table III.I). An acoustic pressure of 504 ± 51 kPa was reproducibly obtained *in situ* which has been shown to cause sustained cavitation bubble oscillation correlated with thrombolysis enhancement [83]. The acoustic pressure reduction due to the intervening bone (19 ± 6%) was slightly lower than similar measurements performed through human temporal bone (33 ± 10%) [189]. The difference could be due to the flatter bone surface of the pig cranium compared to the human temporal bone. Local acoustic pressure maxima situated close to the contralateral bone were observed. These local maxima are likely due to the reflections of the ultrasound wave in the cranial cavity, and were also reported in simulations of ultrasound propagation within the human skull [117], [191], [194].

III.5 Conclusions:

Residual thrombus mass and residual thrombus volume was designed, tested, and validated *in vitro* and *ex vivo*. Using the residual thrombus mass assay, the effect of rt-PA, with or without Definity® or ultrasound was detectable compared to no treatment, however the results were not as robust as those seen using clot mass loss which is typically used. Normalization of each clot mass to its initial clot mass reduces variability in the data and improves the resolution between treatment arms. Given the limitations of the *in vivo* study, where the initial thrombus mass could not be measured, normalizing the residual thrombus mass by the residual thrombus volume to determine a residual thrombus density was tested and found to effective at reduce variability in the data *in vitro* and *ex vivo*. Thus, the hypothesis that residual thrombus mass,

volume, and density were adequate metrics of thrombolytic efficacy was accepted for thrombus mass and density, but not for residual thrombus volume.

Porcine clots from studies performed by Ammi et al. [222] were analyzed using residual thrombus density. Further studies were performed due to the low number of samples with moderate success in replicating data from Ammi et al. [222]. Using thrombus density, the thrombolytic efficacy of rt-PA with or without ultrasound was assessed *in vivo*. Sonothrombolysis without Definity® effectively reduced the thrombus density compared to sham, but not compared to rt-PA only. Thus, we rejected our overall hypothesis that transcranial 120 kHz pulsed ultrasound exposure without Definity® enhances rt-PA lysis of intracranial thrombi in juvenile pigs.

CHAPTER IV: THE EFFECT OF INSONATION SCHEME ON LYTIC EFFICACY AND PREDICTED INTRACRANIAL PRESSURE AND TEMPERATURE[5]

IV.1 Introduction:

Abstract of full article

Ultrasound-enhanced recombinant tissue plasminogen activator (rt-PA) thrombolysis is under development as an adjuvant to ischemic stroke therapy. The goal of this study was to design a pulsed ultrasound (US) exposure scheme that reduced intracranial constructive interference and tissue heating, and maintained thrombolytic efficacy relative to continuous wave (CW) insonation. Three 220 kHz US schemes were evaluated, two pulsed insonation schemes (15 cycles, 68 μs pulse duration, 33% or 62.5% duty cycle) and an intermittent CW insonation scheme (50 s active, 30 s quiescent) over a 30-min treatment period. An in silico study using a finite-difference model of transcranial US propagation was performed to estimate the intracranial acoustic field and temperature rise in the skull for each insonation scheme. In vitro measurements with flow were performed to assess thrombolysis using time-lapse microscopy. Intracranial constructive interference was not reduced with pulsed US using a pulse length of 15 cycles compared to intermittent CW US. The 33.3% duty cycle pulsed US scheme reduced heating in the temporal bone as much as 60% relative to the intermittent CW scheme. All

[5] *Chapter IV is published in Physics in Medicine and Biology 64(16),* ***Kleven*** *et al. The effect of 220 kHz insonation scheme on rt-PA thrombolytic efficacy in vitro. © (2019) Institute of Physics and Engineering in Medicine. DOI* 10.1088/1361-6560/ab293b. Abstract is marked with a solid vertical line. Additional methods, results, and discussion is printed here.

insonation schemes promoted sustained stable cavitation in vitro and augmented thrombolysis compared to rt-PA alone ($p < 0.05$). Ultraharmonic (UH) and harmonic cumulative energy over a 30 min treatment period was significantly higher ($p < 0.05$) for the intermittent CW US scheme compared to either pulsed US scheme. Despite the difference in cavitation emissions, no difference was observed in the clot lysis between the three US schemes. These findings demonstrate that a 33.3% duty cycle pulsed US scheme with a 15-cycle burst can reduce bone heating and achieve equivalent thrombolytic efficacy as an intermittent CW scheme.

IV.2 Methods:

To assess what parameters contributed to temperature and pressure rises, several characteristics of the skulls and the acoustic path optimized were recorded. There parameters included, bone thickness (mm) and mean bone density (averaged over the temporal bone in the acoustic path) (kg/m^3), and the incident angle the transducer made with the temporal bone (θ). Additionally, the free field pressure maximum based on the driving pressure required to achieve 0.44 MPa at the clot was also included to assess its contribution as well. These parameters were then correlated to the pressure and temperature at each region (soft tissue, bone, brain, clot). A linear fit was applied to each correlation and the R^2 value was determined.

IV.3 Results:

Little correlation was observed between the maximum pressure in any of the tissues (external soft tissue, bone, or brain), and the bone thickness, bone density ($R^2 < 0.46$, Table IV.I, Figure IV.8). This effect was even less prominent for the incident angle ($R^2 < 0.09$, Table IV.I, Figure IV.8). Similar results were observed for the maximum temperature with relationship to the bone thickness, bone density, and angle of incidence ($R^2 < 0.45$, $R^2 < 0.38$, $R^2 < 0.18$ respectively, Table IV.II), and was better correlated with the free field pressure ($R^2 > 0.77$, Table IV.II).

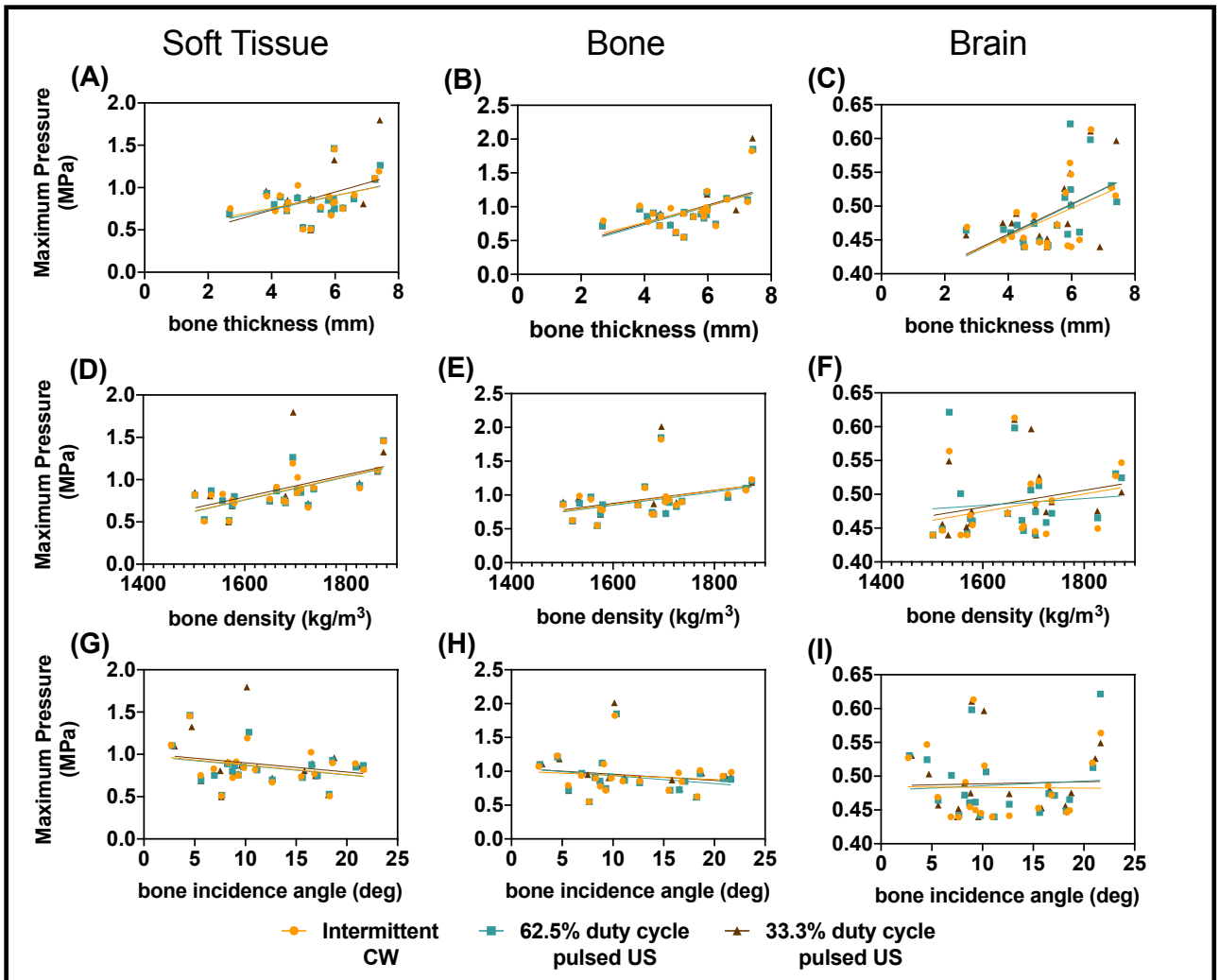

Figure IV.8. Comparison of various patient specific parameters including bone thickness (A-C), bone density (D-F), and incident angle between transducer and bone (G-I) and the maximum pressure in the external soft tissue (A,D,G), bone (B,E,H), and brain (C,F,I) for 20 simulations. A linear fit was applied to each relationship. Table IV.I contains the R^2 values for each correlation.

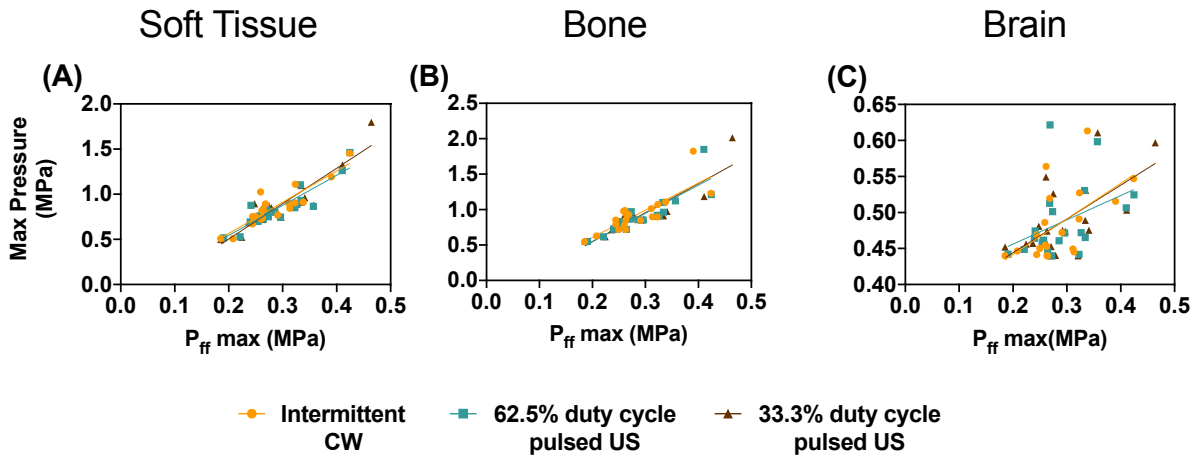

Figure IV.9. Maximum peak-to-peak pressure in the soft tissue (A), bone (B), and brain (C) as a function of the free field maximum peak-to-peak pressure. A linear fit was applied to each relationship. Table IV.I contains the R^2 values for each correlation.

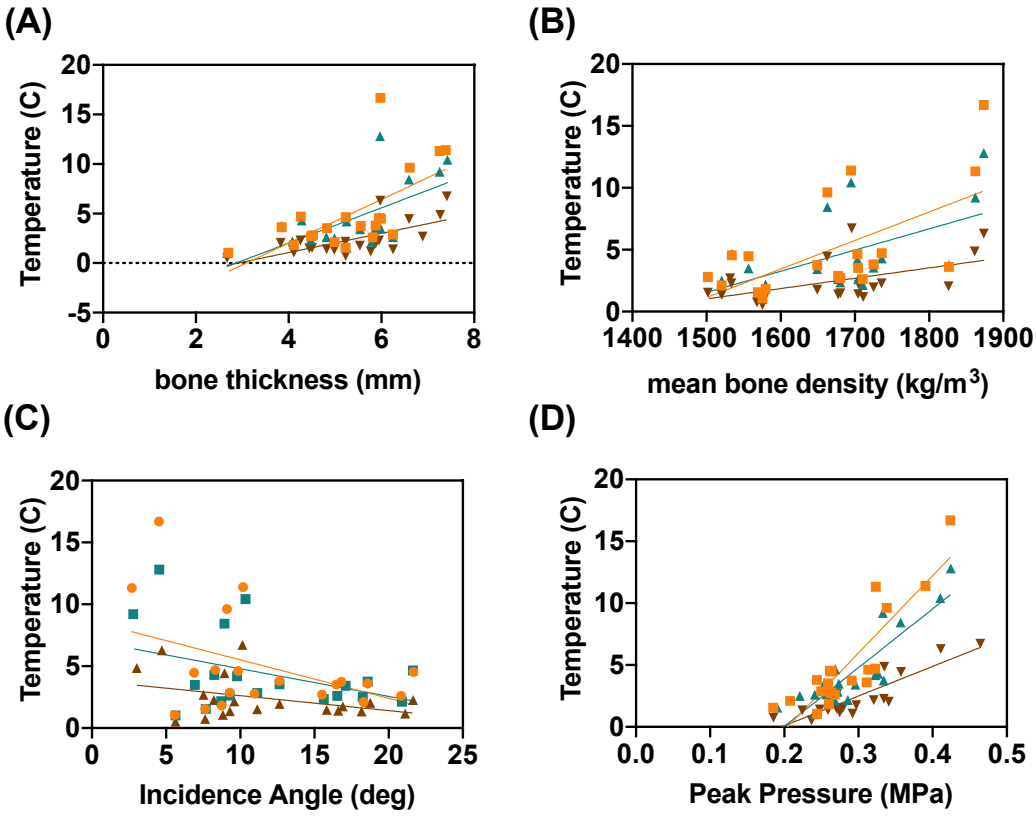

Figure IV.10. The maximum temperature for 20 simulations as a function of four variables: bone thickness (A), bone density (B), incident angle (C), and the acoustic pressure at the transducer surface (D). All temperature maximums occurred in the bone. A linear fit was applied to each relationship. Table IV.I contains the R^2 values for each correlation.

Table IV.I. Correlation of patient and ultrasound parameters on the maximum pressure measured *in silico*. The bone thickness, mean bone density, incident angle between transducer and bone, and the free field maximum peak-to-peak pressure required to achieve 0.44 MPa peak-to-peak pressure at the clot were all compared to the peak-to-peak pressure maximum in each tissue type (external soft tissue, bone, and brain). P_{ff} is the pressure in the free field.

	Treatment Type	Soft Tissue	Bone	Brain
Bone Thickness	Intermittent CW US	0.16	0.29	0.24
	62.5% Duty Cycle Pulsed US	0.18	0.33	0.28
	33.3% Duty Cycle Pulsed US	0.21	0.30	0.29
Mean Bone Density	Intermittent CW US	0.46	0.17	0.08
	62.5% Duty Cycle Pulsed US	0.45	0.15	0.01
	33.3% Duty Cycle Pulsed US	0.27	0.13	0.08
Incident Angle with Bone	Intermittent CW US	0.09	0.02	0.00
	62.5% Duty Cycle Pulsed US	0.08	0.06	0.00
	33.3% Duty Cycle Pulsed US	0.05	0.03	0.00
P_{ff} maximum	Intermittent CW US	0.81	0.67	0.32
	62.5% Duty Cycle Pulsed US	0.80	0.74	0.18
	33.3% Duty Cycle Pulsed US	0.83	0.80	0.37

Table IV.II. Correlation of patient and ultrasound parameters on the maximum temperature measured *in silico*. The bone thickness, mean bone density, incident angle between transducer and bone, and the free field maximum peak-to-peak pressure required to achieve 0.44 MPa peak-to-peak pressure at the clot were all compared to maximum temperature in the bone. P_{ff} is the pressure in the free field.

	Intermittent CW US	62.5% Duty Cycle Pulsed US	33.3% Duty Cycle Pulsed US
Bone Thickness	0.398	0.421	0.446
Mean Bone Density	0.381	0.337	0.271
Incident Angle with Bone	0.181	0.150	0.144
P_{ff} maximum	0.769	0.776	0.769

IV.4 Discussion

Patient specific characteristics did not correlate well with either the pressure or temperatures observed *in silico*. Bone thickness, and density both had weak correlations ($R^2 < 0.46$, Table IV.I) with the magnitude of the pressures measured in the external soft tissue or the bone. This correlation was even worse for pressures in the brain ($R^2 < 0.29$, Table IV.I). Similar outcomes were observed with the temperature (Table IV.II, Figure IV.10). However, better correlation ($R^2 > 0.67$) was observed between the maximum pressure in soft tissue or bone and the driving pressure of the ultrasound transducer determined by the free field pressure maximum (Figure IV.9, Table IV.II). This result was surprising as parameters such as bone density and thickness are expected to determine the acoustic transparency of the temporal bone [189]. Therefore, thinner bone and less dense bone would be expected to cause less attenuation, reducing the driving pressure required to achieve adequate insonation of the clot. This was not observed in our study and may indicate the multi-variate nature of the acoustic field propagation to the clot. One limitation of these metrics is that they do not capture the heterogeneity in the values of bone density, thickness, or angle of incidence which may explain the discrepancy between this data and previously published data. Our analysis shows that these parameters are not major contributors to

the predicted pressure and temperature peaks. The angle of incidence between the transducer and the temporal bone had no correlation at all with the maximum pressure ($R^2 < 0.09$).

CHAPTER V: CONCLUSIONS AND FUTURE DIRECTIONS

V.1 Goals of Study

One of the long-term goals of the Image guided Ultrasound Therapeutics Laboratory is to use ultrasound to accelerate the breakdown of blood clots. To that end the studies described in this dissertation were conducted to assess the efficacy of sonothrombolysis using unfocused 120 kHz ultrasound *in vivo* and 220 kHz ultrasound *in vitro* and *in vivo*. Both 120 kHz [81]–[83], [106], [117]–[119], [141], [204], [224] and 220 kHz [117], [118] unfocused ultrasound have been shown to be effective in breaking up blood clots *in vitro*. A necessary next step in the translation of sonothrombolysis to the clinic was to demonstrate enhanced therapeutic efficacy over standard clinical care techniques in preclinical models. Two *in vivo* models of thrombolysis were developed in swine to assess sonothrombolysis efficacy. In Chapter II, a porcine occlusive thromboembolism model was established in the ascending pharyngeal artery. In Chapter III, a porcine model of intracerebral hemorrhage was established to assess thrombolytic enhancement transcranially. Chapter IV summarizes *in silico* and *in vitro* studies adapting 220 kHz ultrasound therapy to human transcranial insonation to provide safe and effective thrombolysis clinically.

V.2 Summary of findings in Chapter II

V.2.1 In vitro findings

The porcine cranial circulation was modeled *in vitro* to compare saline (sham), rt-PA alone (lytic), and rt-PA, Definity®, and 220 kHz ultrasound (sonothrombolysis) effects on an occlusive human clot. Flow was restored for clots in the lytic and sonothrombolysis treatment arms when delivered through a multi-side-hole microcatheter. Sonothrombolysis with the multi-side-hole microcatheter was significantly better than sonothrombolysis with the end-hole microcatheter and both lytic and sham with either catheter. In addition, direct delivery of the rt-PA into the clot

parenchyma enhanced thrombolysis and improved flow as seen in both the lytic and sonothrombolysis treatment arms.

V.2.2 In vivo findings

A model of vascular occlusion of cranial vessels was developed in swine based on a previously published model of vascular occlusion by Culp et al. [178], [200]. The ascending pharyngeal artery (APA) was successfully occluded with a preformed retracted human whole blood clot delivered using two delivery methods: direct deployment into the APA using an 8 F guide catheter, and deployment upstream in the common carotid to avoid instrumenting the APA. For the upstream delivery method, the porcine cranial circulation was modified bilaterally by occluding the external carotid arteries with hydrogel coils which was well tolerated for a non-survival study up to 6 hours. Significant vasospasm was noted in the APA for clots delivered directly into the APA and was significantly less for clots delivered into the common carotid following occlusion of the ECA. Occluding the ECA blocked collateral circulation that feeds the anterior portion of the Circle of Willis. By occluding this collateral, the porcine cranial circulation more closely modeled the human circulation, which has fewer collaterals feeding the Circle of Willis, and facilitated grading of porcine cranial perfusion using a clinical metric (mTICI).

No improvement in perfusion was observed *in vivo* over 2 hours for clots treated with either lytic or sonothrombolysis delivered through an end-hole microcatheter at the clot face. We hypothesized that rt-PA was not reaching the clot due to the small surface area of the clot exposed to rt-PA and the severe vasospasm observed in early pigs. A multi-side-hole microcatheter was introduced which significantly improved recanalization times for both lytic and sonothrombolysis treatment arms compared to sham. Thus, we accepted our hypothesis that intermittent continuous wave 220 kHz ultrasound and Definity® enhances rt-PA lysis of human retracted clots and

improves recanalization of occluded vessels. Following insertion of a wire and microcatheter into the APA, most vessels showed significant vasospasm (>50%) which Kassel et al. characterize as "severe" [215]. A combination of intravenous nicardipine and a modified clot delivery method which reduced instrumentation of the vessel by delivering the clot upstream in the common carotid was found to be effective in reducing vasospasm. Using the modified protocol, vasospasm resolved over the first 15-30 minutes. It is unclear to what degree each of these changes reduced the vasospasm as both variables were changed concurrently. This study is being submitted for publication.

V.3 Summary of findings in Chapter III

V.3.1 Metrics of Thrombolysis

In Chapter III, an intraventricular hemorrhage model in swine was used to assess thrombolytic efficacy of transcranial ultrasound combined with rt-PA. Several metrics were tested to quantify thrombolysis *in vitro* and in an *ex vivo* model of porcine ICH: residual thrombus volume, residual thrombus mass, and residual thrombus density. The residual thrombus density was the most sensitive of the three assays to detect thrombolysis by comparing sham and rt-PA alone thrombi *in vitro* and *ex vivo*. Following the validation of the residual thrombus density thrombolytic assay, porcine thrombus samples collected by Ammi et al. [222]were analyzed and 14 more porcine studies were conducted *in vivo*. Combining the data from Ammi et al. and new data, the residual thrombus density was significantly different comparing sham treated thrombi to rt-PA only or sonothrombolysis without Definity®. However, no significant difference in thrombus density was found for the sonothrombolysis treatment arm compared to rt-PA only. Thus, we rejected our overall hypothesis that transcranial 120 kHz pulsed ultrasound exposure

without Definity® enhances rt-PA lysis of intracranial thrombi in juvenile pigs. This study will be submitted for publication.

V.4 Summary of findings in Chapter IV

In Chapter IV, we adapted the insonation scheme used *in vitro* and in porcine studies to the human skull. Using a previously validated finite difference method, three pulsing schemes were assessed using CT data from 20 patients. *In silico* simulations showed a decrease in the acoustic field during transit through the bone. This required modification of the driving voltage of the ultrasound transducer to achieve an appropriate pressure at the location of each clot in the MCA. Temperature rise was significantly higher in the bone and external soft tissue for the intermittent continuous wave (CW) insonation scheme used in both porcine studies than the pulsed scheme with an equivalent duty cycle (62.5%). *In vitro* studies were then performed in a previously established time-lapse microscopy setup to assess if using a pulsed ultrasound scheme (especially with a reduced duty cycle) would affect thrombolytic efficacy. No difference was detected in thrombolytic efficacy using any of the three pulsing schemes. Thus, we accepted our hypothesis that pulsed 220 kHz ultrasound exposure of cranial tissues produces less constructive interference and causes lower thermal deposition compared to intermittent continuous wave ultrasound. This study has been published in Physics in Medicine and Biology [117].

V.5 Impact on field

The studies described here provide several advances in the field of sonothrombolysis. Chapter II describes a critical link in the understanding of thrombolysis and flow. A common metric for lysis *in vitro* is clot mass loss. We demonstrate that clot mass loss and flow do not correlate well *in vitro*. In particular, mass loss of up to 60% did not result in a change in flow over time. Additionally, we showed that flow is not correlated to thrombolysis due to rt-PA alone in

our model of vascular occlusion, but that flow does correlate with thrombolysis for rt-PA in conjunction with Definity® and 220 kHz ultrasound. Further study is needed to understand this effect. We anticipate that this data will encourage using metrics such as flow for thrombolysis to better understand the clinical outcomes each therapy will provide. Additionally, the occlusion of the external carotid artery circulation eliminates many of the collateral vessels which feed the brain of many ruminants and other mammals, but not humans [207]. Clinical grading sores such as mTICI, which are based on human vasculature, do not anticipate the extensive collaterals observed in porcine cranial circulation, which makes these scores difficult to use in animal studies. This study provides an important step in humanizing the porcine circulation for future studies, both in the field of sonothrombolysis and other disciplines. In Chapter II we also provided a porcine model of thrombolysis using a clot with a susceptibility to rt-PA similar to that seen in human clinical studies [151], [153]. The introduction of a xenographic clot into the porcine circulation, and its subsequent treatment, provides an improved model of clinical thrombolysis in a large animal model compared to porcine clot models.

In Chapter III, the porcine ICH model enables testing of ultrasound therapy across the skull. The development of an *ex vivo* model enables testing and optimization of approaches before performing animal studies. Additionally, in Chapter III, physical properties of the thrombus such as mass and volume are compared across treatments. The use of a thrombus mass assay *in vivo* provides more direct comparison to the breadth of published results where thrombus mass is a common assay (Chapter I.3).

In Chapter IV, a pulsing scheme that maintains efficacy and reduces total ultrasound exposure was designed and tested *in vitro*. We demonstrated that three different insonation schemes resulted in similar rates of lysis. Ultrasound enhanced thrombolysis despite lower

cavitation amplitude detected and decreased total exposure to ultrasound with the 33.3% duty cycle pulsed ultrasound scheme compared with the other two insonations schemes. The ALARA (as low as reasonably achievable) principle encourages reducing exposure to as little as necessary to achieve an effect. The results of Chapter IV provide impetus to further explore insonation scheme based on the physical constraints of human anatomy.

V.6 Recommendations for Future Studies

In Chapter II and III, the introduction of passive cavitation monitoring would benefit both models as it is unclear the degree of cavitation that was present during the treatment period, or how the cavitation changed over time *in vivo*. It is known that ultraharmonic signals persist over the duration of the intermittent continuous wave (CW) insonation scheme in vitro and this effect was replicated in the study described in Chapter IV [105]. However, in the APA model, the microcatheters which contain Definity® were exposed to ultrasound before arriving at the clot (as the path of the APA is close to the acoustic path). Therefore, it is possible Definity® was destroyed as it traveled down the catheter before even reaching the clot. Passive cavitation imaging could assist in this evaluation [133]. The quiescent period should allow Definity to reach the clot without being exposed to potentially destructive ultrasound, however, the quiescent period limits the therapeutic time of exposure. Optimization of the cavitation activity, either through predetermined insonation schemes, or an active feedback loop would enhance bubble mediated thrombolysis [105]. Furthermore, Hitchcock et al. have demonstrated that cavitation activity decreases with time, even in the stable cavitation regime [105]. Datta et al. performed serial injections (every 3 minutes) of Definity® down a catheter protected by a layer of air to provide fresh Definity [204]. Other studies have provided a continuous source of cavitation nuclei from flow [83], [117]. Further development is needed to evaluate the time course of cavitation in these studies and

improve delivery of nucleation agents to the therapeutic region. Monitoring the cavitation in real time and adjusting the ultrasound input based on the received cavitation could also address this limitation while reducing exposure. To effectively monitor cavitation for stroke therapy, a detector with sufficient sensitivity to detect cavitation across the skull could be incorporated.

The porcine APA model can be used to assist further therapeutic strategies for thrombi refractory to treatment. One future step would be the development of intravascular ultrasound contained in a catheter. Percutaneous sonothrombolysis was limited by the thick bone and presence of air along most approaches to the deep vessels at the base of the brain such as the APA. Intravascular sonothrombolysis using the EkoSonic Endovascular System (Boston Scientific, Marlborough, MA, USA) would be better positioned to treat thrombi seated in these difficult to reach vessels.

In Chapter III, the use of ultrasound in conjunction with rt-PA was not significantly better than rt-PA alone *in vitro* (rt-PA only vs sonothrombolysis without Definity®). The addition of Definity® was shown to improve clot lysis *in vitro* in this and other studies (Chapter III.3.1) [204], [227]. This improvement in clot lysis in the presence of exogenous nucleation agents should be verified *in vivo* using the porcine ICH model. Based on our *in vitro* studies, as well as published literature, we expect that the addition of Definity® to the sonothrombolysis treatment arm *in vivo* would enhance thrombolysis and could improve the contrast between sham, rt-PA only, and sonothrombolysis treatment arms *in vivo*. Additionally, the bioeffects due to insonation should be assessed in sham, rt-PA only, and sonothrombolysis studies. 2,3,5-Triphenyltetrazolium chloride (TTC) and silver staining provide early viability markers for brain tissue, both adjacent to the infarct and on the contralateral brain. Edema can also be assessed using optical imaging [265].

Given the success of treating a xenographic human clot in the porcine APA model, the use of a human thrombus in the porcine ICH model is also warranted. A human thrombus would further "humanize" the lytic response measured in the porcine ICH model. However, the effects of introducing liquid human blood into the porcine brain is not well understood and could elicit immunologic or allergic responses in the brain. Furthermore, pairing a residual thrombus mass assay with the volume aspiration assay described in Wagner et al. could provide unique insights into the ICH model [220], [221]. This would enable a better understanding of what degree of the fluid portion of the thrombus is able to be evacuated during surgical aspiration and how much is left behind.

The ICH model also provides an opportunity to assess neuroprotective potential of xenon delivered directly into the thrombus and surrounding brain parenchyma. Britton et al. have demonstrated a rescue effect of xenon captured in a microbubble and released using ultrasound on rat brains after an intracerebral hemorrhage [266]. The use of a large animal model with a larger distribution of white matter would be relevant to explore neuroprotection. Survival studies would be key to assessing long term outcomes for clinical translation.

Given the similar efficacy of the pulsing schemes tested in Chapter IV to the intermittent CW insonation scheme, 33.3% duty cycle pulsed ultrasound (15 cycles) could be applied *in vivo* to verify the *in vitro* results. MRI based temperature monitoring could be performed as described by McDannold et al. to assess *in vivo* tissue heating predicted *in silico*. Histological analysis of tissue would also be important and survival studies would provide a necessary step for clinical translation. More work is needed to understand which patient factors predict tissue heating and constructive interference as the correlation with any single patient parameter was low ($R^2 = 0.46$). Treatment of patients with ultrasound would benefit from a rapid predictive model based on initial

CT which could exclude patients for which the pressure and temperature rises are too great to be safely applied. The finite difference method used in Chapter IV takes over an hour to provide the predicted pressure and temperature fields in a simulated skull which is too long for clinical use. Further study on a wider sampling of patients would be beneficial. Additionally, other patient specific characteristics could be explored such as the degree of curvature of the contralateral skull which may affect the focusing or dispersion of reflected waves.

BIBLIOGRAPHY

[1] E. J. Benjamin *et al.*, "Heart Disease and Stroke Statistics—2019 Update: A Report From the American Heart Association," *Circulation*, vol. 139, no. 10, 2019.

[2] H. S. Markus, "Cerebral perfusion and stroke," *J. Neurol. Neurosurg. Psychiatry*, vol. 75, no. 3, pp. 353–361, 2004.

[3] P. Lipton, "Ischemic cell death in brain neurons," *Physiol. Rev.*, vol. 79, no. 4, pp. 1431–1568, 1999.

[4] A. I. Qureshi, S. Tuhrim, J. P. Broderick, H. H. Batjer, H. Hondo, and D. F. Hanley, "Spontaneous Intracerebral Hemorrhage," *N. Engl. J. Med.*, vol. 344, no. 19, pp. 1450–1460, 2001.

[5] A. I. Qureshi, A. D. Mendelow, and D. F. Hanley, "Intracerebral haemorrhage," *Lancet*, vol. 373, no. 9675, pp. 1632–1644, 2009.

[6] G. R. Sutherland and R. N. Auer, "Primary intracerebral hemorrhage," *J. Clin. Neurosci.*, vol. 13, no. 5, pp. 511–517, 2006.

[7] S. Prabhakaran and A. M. Naidech, "Ischemic brain injury after intracerebral hemorrhage: A critical review," *Stroke*, vol. 43, no. 8, pp. 2258–2263, 2012.

[8] J. Ögren, A. L. Irewall, L. Bergström, and T. Mooe, "Intracranial Hemorrhage after Ischemic Stroke: Incidence, Time Trends, and Predictors in a Swedish Nationwide Cohort of 196 765 Patients," *Circ. Cardiovasc. Qual. Outcomes*, vol. 8, no. 4, pp. 413–420, 2015.

[9] M. G. Lansberg, G. W. Albers, and C. A. C. Wijman, "Symptomatic intracerebral hemorrhage following thrombolytic therapy for acute ischemic stroke: A review of the risk factors," *Cerebrovasc. Dis.*, vol. 24, no. 1, pp. 1–10, 2007.

[10] K. D. Kim, C. H. Chang, B. Y. Choi, and Y. J. Jung, "Mortality and real cause of death from the nonlesional intracerebral hemorrhage," *J. Korean Neurosurg. Soc.*, vol. 55, no. 1, pp. 1–4, 2014.

[11] J. P. Broderick, T. G. Brott, J. E. Duldner, T. Tomsick, and G. Huster, "Volume of intracerebral hemorrhage: A powerful and easy-to-use predictor of 30-day mortality," *Stroke*, vol. 24, no. 7, pp. 987–993, 1993.

[12] H. N. Panchal, M. S. Shah, and D. S. Shah, "Intracerebral Hemorrhage Score and Volume as an Independent Predictor of Mortality in Primary Intracerebral Hemorrhage Patients," *Indian J. Surg.*, vol. 77, no. Suppl 2, pp. 302–304, 2015.

[13] C. Righy, M. T. Bozza, M. F. Oliveira, and F. A. Bozza, "Molecular, Cellular and Clinical Aspects of Intracerebral Hemorrhage: Are the Enemies Within?," *Curr. Neuropharmacol.*, vol. 14, no. 4, pp. 392–402, 2016.

[14] J. Aronowski and X. Zhao, "Molecular pathophysiology of cerebral hemorrhage: Secondary brain injury," *Stroke*, vol. 42, no. 6, pp. 1781–1786, 2011.

[15] J. Scaggiante, X. Zhang, J. Mocco, and C. P. Kellner, "Minimally invasive surgery for Intracerebral hemorrhage an updated meta-analysis of randomized controlled trials," *Stroke*, vol. 49, no. 11, pp. 2612–2620, 2018.

[16] Z. Xia *et al.*, "Minimally Invasive Surgery is Superior to Conventional Craniotomy in Patients with Spontaneous Supratentorial Intracerebral Hemorrhage: A Systematic Review and Meta-Analysis," *World Neurosurg.*, vol. 115, pp. 266–273, 2018.

[17] D. F. Hanley *et al.*, "Efficacy and safety of minimally invasive surgery with thrombolysis in intracerebral haemorrhage evacuation (MISTIE III): a randomised, controlled, open-label, blinded endpoint phase 3 trial," *Lancet*, vol. 393, no. 10175, pp. 1021–1032, 2019.

[18] H. P. Adams *et al.*, “Guidelines for thrombolytic therapy for acute stroke: A supplement to the guidelines for the management of patients with acute ischemic stroke,” *Stroke*, vol. 27, no. 9, pp. 1711–1718, 1996.
[19] W. Hacke *et al.*, “European Stroke Initiative Recommendations for Stroke Management - Update 2003,” *Cerebrovasc. Dis.*, vol. 16, no. 4, pp. 311–337, 2003.
[20] P. A. Ringleb *et al.*, “Guidelines for management of ischaemic stroke and transient ischaemic attack 2008,” *Cerebrovasc. Dis.*, vol. 25, no. 5, pp. 457–507, 2008.
[21] W. S. Tillett and R. L. Garner, “The fibrinolytic activity of hemolytic streptococci,” *J. Exp. Med.*, vol. 58, no. 4, pp. 485–502, 1933.
[22] “GISSI-2: A factorial randomised trial of alteplase versus streptokinase and heparin versus no heparin among 12 490 patients with acute myocardial infarction. Gruppo Italiano per lo Studio della Sopravvivenza nell’Infarto Miocardico,” *Lancet*, vol. 336, no. 8707, pp. 65–71, 1990.
[23] “ISIS-3: a randomised comparison of streptokinase vs tissue plasminogen activator vs anistreplase and of aspirin plus heparin vs aspirin alone among 41,299 cases of suspected acute myocardial infarction.,” *Lancet*, vol. 339, no. 8796, pp. 753–70, 1992.
[24] GUSTO, “An International Randomized Trial Comparing Four Thrombolytic Strategies for Acute Myocardial Infarction,” *N Engl J Med*, vol. 329, no. 10, pp. 987–94, 1993.
[25] The National Institute of Neurological Disorders and Stroke rt-PA Stroke Study Group, “Tissue Plasminogen Activator for Acute Ischemic Stroke,” *N. Engl. J. Med.*, vol. 333, no. 24, pp. 1581–1587, 1995.
[26] W. Hacke *et al.*, “Intravenous thrombolysis with recombinant tissue plasminogen activator for acute hemispheric stroke. The European Cooperative Acute Stroke Study (ECASS),” *J. Am. Med. Assoc.*, vol. 274, no. 13, pp. 1017–1025, 1995.
[27] W. Hacke *et al.*, “Randomised double-blind placebo-controlled trial of thrombolytic therapy with intravenous alteplase in acute ischaemic stroke (ECASS II),” *Lancet*, vol. 352, no. 9136, pp. 1245–1251, 1998.
[28] G. J. Del Zoppo, J. L. Saver, E. C. Jauch, and H. P. Adams, “Expansion of the time window for treatment of acute ischemic stroke with intravenous tissue plasminogen activator: A science advisory from the American Heart Association/American Stroke Association,” *Stroke*, vol. 40, no. 8, pp. 2945–2948, 2009.
[29] W. Hacke *et al.*, “Thrombolysis with Alteplase 3 to 4.5 Hours after Acute Ischemic Stroke,” *New Engl. J. Med.*, vol. 359, no. 13, pp. 1543–1554, 2008.
[30] D. Mozaffarian *et al.*, “Executive summary: Heart disease and stroke statistics-2016 update: A Report from the American Heart Association,” *Circulation*, vol. 133, no. 4, pp. 447–454, 2016.
[31] J. Emberson *et al.*, “Effect of treatment delay, age, and stroke severity on the effects of intravenous thrombolysis with alteplase for acute ischaemic stroke: A meta-analysis of individual patient data from randomised trials,” *Lancet*, vol. 384, no. 9958, pp. 1929–1935, 2014.
[32] E. C. Jauch *et al.*, “Guidelines for the early management of patients with acute ischemic stroke: A guideline for healthcare professionals from the American Heart Association/American Stroke Association,” *Stroke*, vol. 44, no. 3, pp. 870–947, 2013.
[33] G. J. Del Zoppo *et al.*, “Recombinant tissue plasminogen activator in acute thrombotic and embolic stroke,” *Ann. Neurol.*, vol. 32, no. 1, 1992.
[34] M. R. Heldner *et al.*, “National Institutes of Health Stroke Scale Score and Vessel

Occlusion in 2152 Patients With Acute Ischemic Stroke," *Stroke*, vol. 44, no. 4, pp. 1153–1157, 2013.
[35] B. K. Menon *et al.*, "Association of clinical, imaging, and thrombus characteristics with recanalization of visible intracranial occlusion in patients with acute ischemic stroke," *JAMA*, vol. 320, no. 10, pp. 1017–1026, 2018.
[36] J. I. Suarez *et al.*, "Predictors of Clinical Improvement, Angiographic Recanalization, and Intracranial Hemorrhage After Intra-Arterial Thrombolysis for Acute Ischemic Stroke," *Stroke*, vol. 30, no. 10, pp. 2094–2100, 1999.
[37] I. Linfante *et al.*, "Clinical and Vascular Outcome in Internal Carotid Artery Versus Middle Cerebral Artery Occlusions After Intravenous Tissue Plasminogen Activator," *Stroke*, vol. 33, no. 8, pp. 2066–2071, 2002.
[38] M. Saqqur *et al.*, "Site of arterial occlusion identified by transcranial Doppler predicts the response to intravenous thrombolysis for stroke," *Stroke*, vol. 38, no. 3, pp. 948–954, 2007.
[39] A. Furlan *et al.*, "Intra-arterial prourokinase for acute ischemic stroke.," *J. Am. Med. Assoc.*, vol. 282, no. 21, pp. 2003–2011, 1999.
[40] G. J. Del Zoppo, R. T. Higashida, A. J. Furlan, M. S. Pessin, H. A. Rowley, and M. Gent, "PROACT: A phase II randomized trial of recombinant pro-urokinase by direct arterial delivery in acute middle cerebral artery stroke," *Stroke*, vol. 29, no. 1, pp. 4–11, 1998.
[41] G. W. Albers *et al.*, "Thrombectomy for Stroke at 6 to 16 Hours with Selection by Perfusion Imaging," *N. Engl. J. Med.*, vol. 378, no. 8, pp. 708–718, 2018.
[42] A. P. Jadhav *et al.*, "Eligibility for Endovascular Trial Enrollment in the 6- to 24-Hour Time Window," *Stroke*, vol. 49, no. 4, pp. 1015–1017, 2018.
[43] W. S. Smith *et al.*, "Safety and efficacy of mechanical embolectomy in acute ischemic stroke: Results of the MERCI trial," *Stroke*, vol. 36, no. 7, pp. 1432–1438, 2005.
[44] W. S. Smith *et al.*, "Mechanical thrombectomy for acute ischemic stroke: Final results of the multi MERCI trial," *Stroke*, vol. 39, no. 4, pp. 1205–1212, 2008.
[45] J. P. Broderick *et al.*, "Endovascular therapy after intravenous t-PA versus t-PA alone for stroke," *N. Engl. J. Med.*, vol. 368, no. 10, pp. 893–903, 2013.
[46] A. Ciccone *et al.*, "Endovascular treatment for acute ischemic stroke," *N. Engl. J. Med.*, vol. 368, no. 10, pp. 904–913, 2013.
[47] C. S. Kidwell *et al.*, "A trial of imaging selection and endovascular treatment for ischemic stroke," *N. Engl. J. Med.*, vol. 368, no. 10, pp. 914–923, 2013.
[48] M. E. Kelly, A. J. Furlan, and D. Fiorella, "Recanalization of an acute middle cerebral artery occlusion using a self-expanding, reconstrainable, intracranial microstent as a temporary endovascular bypass," *Stroke*, vol. 39, no. 6, pp. 1770–1773, 2008.
[49] C. Castaño, J. Serena, and A. Dávalos, "Use of the new solitaire™ AB device for mechanical thrombectomy when merci clot retriever has failed to remove the clot: A case report," *Interv. Neuroradiol.*, vol. 15, no. 2, pp. 209–214, 2009.
[50] J. L. Saver *et al.*, "Time to Treatment with Intravenous Tissue Plasminogen Activator and Outcome From Acute Ischemic Stroke," *JAMA*, vol. 309, no. 23, pp. 2480–88, 2013.
[51] J. L. Saver *et al.*, "Solitaire flow restoration device versus the Merci Retriever in patients with acute ischaemic stroke (SWIFT): A randomised, parallel-group, non-inferiority trial," *Lancet*, vol. 380, no. 9849, pp. 1241–1249, 2012.
[52] O. A. Berkhemer *et al.*, "A randomized trial of intraarterial treatment for acute ischemic stroke," *N. Engl. J. Med.*, vol. 372, no. 1, pp. 11–20, 2015.

[53] B. C. V. Campbell *et al.*, "Endovascular stent thrombectomy: The new standard of care for large vessel ischaemic stroke," *Lancet Neurol.*, vol. 14, no. 8, pp. 846–854, 2015.
[54] M. Goyal *et al.*, "Randomized assessment of rapid endovascular treatment of ischemic stroke," *N. Engl. J. Med.*, vol. 372, no. 11, pp. 1019–1030, 2015.
[55] J. L. Saver *et al.*, "Stent-retriever thrombectomy after intravenous t-PA vs. t-PA alone in stroke," *N. Engl. J. Med.*, vol. 372, no. 24, pp. 2285–2295, 2015.
[56] T. G. Jovin *et al.*, "Thrombectomy within 8 hours after symptom onset in ischemic stroke," *N. Engl. J. Med.*, vol. 372, no. 24, pp. 2296–2306, 2015.
[57] R. G. Nogueira *et al.*, "Thrombectomy 6 to 24 Hours after Stroke with a Mismatch between Deficit and Infarct," *N. Engl. J. Med.*, vol. 378, no. 1, pp. 11–21, 2017.
[58] D. L. Cohen, R. Kearney, M. Griffiths, V. Nadesalingam, and R. Bathula, "Around 9% of patients with ischaemic stroke are suitable for thrombectomy," *BMJ*, vol. 351, p. 4757, 2015.
[59] N. H. Chia, J. M. Leyden, J. Newbury, J. Jannes, and T. J. Kleinig, "Determining the Number of Ischemic Strokes Potentially Eligible for Endovascular Thrombectomy: A Population-Based Study," *Stroke*, vol. 47, no. 5, pp. 1377–1380, 2016.
[60] K. B. Bader, G. Bouchoux, and C. K. Holland, "Sonothrombolysis," *Adv. Exp. Med. Biol.*, vol. 880, pp. 339–362, 2016.
[61] A. Sobbe, U. Stumpff, and G. Truebestein, "Die Ultraschall Auflosung Von Thromben," *Wien. Klin. Wochenschr.*, vol. 52, no. 23, pp. 1117–1121, 1974.
[62] G. Truebestein, C. Engel, F. Etzel, A. Sobbe, H. Cremer, and U. Stumpff, "Thrombolysis by ultrasound," *Clin. Sci. Mol. Med.*, vol. 3, pp. 697s-698s, 1976.
[63] A. D. Maxwell, C. A. Cain, A. P. Duryea, L. Yuan, H. S. Gurm, and Z. Xu, "Noninvasive Thrombolysis Using Pulsed Ultrasound Cavitation Therapy - Histotripsy," *Ultrasound Med. Biol.*, vol. 35, no. 12, pp. 1982–1994, 2009.
[64] K. B. Bader *et al.*, "Efficacy of histotripsy combined with rt-PA in vitro," *Phys. Med. Biol.*, vol. 61, no. 14, pp. 5253–5274, 2016.
[65] C. C. Wright, K. Hynynen, and D. E. Goertz, "Pulsed focused ultrasound-induced displacements in confined in vitro blood clots," *IEEE Trans. Biomed. Eng.*, vol. 59, no. 3, pp. 842–851, 2012.
[66] C. Wright, K. Hynynen, and D. Goertz, "In vitro and in vivo high-intensity focused ultrasound thrombolysis," *Invest. Radiol.*, vol. 47, no. 4, pp. 217–225, 2012.
[67] U. Rosenschein, V. Furman, E. Kerner, I. Fabian, J. Bernheim, and Y. Eshel, "Ultrasound Imaging – Guided Noninvasive Ultrasound Thrombolysis," *Circulation*, vol. 102, no. 2, pp. 238–245, 2000.
[68] A. Burgess, Y. Huang, A. C. Waspe, M. Ganguly, D. E. Goertz, and K. Hynynen, "High-intensity focused ultrasound (HIFU) for dissolution of clots in a rabbit model of embolic stroke," *PLoS One*, vol. 7, no. 8, pp. 1–7, 2012.
[69] M. Ariani *et al.*, "Dissolution of peripheral arterial thrombi by ultrasound," *Circulation*, vol. 84, no. 4, pp. 1680–1688, 1991.
[70] R. J. Siegel *et al.*, "Ultrasonic Plaque Ablation: A New Method for Recanalization of Partially or Totally Occluded Arteries," *Circulation*, vol. 78, no. 6, pp. 1443–1448, 1988.
[71] U. Rosenschein, J. J. Bernstein, E. DiSegni, E. Kaplinsky, J. Bernheim, and L. A. Rozenzsajn, "Experimental ultrasonic angioplasty: Disruption of atherosclerotic plaques and thrombi in vitro and arterial recanalization in vivo," *J. Am. Coll. Cardiol.*, vol. 15, no. 3, pp. 711–717, 1990.

[72] H. Shankar and P. S. Pagel, “Potential Adverse Ultrasound-related Biological Effects: A Critical Review,” *Anesthesiology*, vol. 115, no. 5, pp. 1109–1124, 2011.
[73] Z. Izadifar, P. Babyn, and D. Chapman, “Mechanical and Biological Effects of Ultrasound: A Review of Present Knowledge,” *Ultrasound Med. Biol.*, vol. 43, no. 6, pp. 1085–1104, 2017.
[74] C. K. Holland, G. J. Shaw, and S. Datta, “Ultrasound-Enhanced Thrombolysis,” in *Therpeutic Ultrasound: Mechanisms to Applications*, 1st ed., V. Frenkel, Ed. New York: Nova Science, 2011.
[75] J. B. Fowlkes and C. K. Holland, “Biologic Effects and Safety,” in *Diagnostic Ultrasound*, 5th ed., C. M. Rumack and D. Levine, Eds. Philadelphia: Elsevier, 2017.
[76] A. S. Hong, J. S. Chae, S. B. Dubin, S. Lee, M. C. Fishbein, and R. J. Siegel, “Ultrasonic clot disruption: An in vitro study,” *Am. Heart J.*, vol. 120, no. 2, pp. 418–422, 1990.
[77] K. Tachibana, “Enhancement of Fibrinolysis with Ultrasound Energy,” *J. Vasc. Interv. Radiol.*, vol. 3, no. 2, pp. 299–303, 1992.
[78] C. W. Francis *et al.*, “Enhancement of fibrinolysis in vitro by ultrasound,” *J. Clin. Invest.*, vol. 90, no. 5, pp. 2063–2068, 1992.
[79] Y. H. Chuang, P. O. W. Cheng, S. C. Chen, J. L. Ruan, and P. C. Li, “Effects of ultrasound-induced inertial cavitation on enzymatic thrombolysis,” *Ultrason. Imaging*, vol. 32, no. 2, pp. 81–90, 2010.
[80] J. E. Leeman *et al.*, “Effect of Acoustic Conditions on Microbubble-Mediated Microvascular Sonothrombolysis,” *Ultrasound Med. Biol.*, vol. 38, no. 9, pp. 1589–1598, 2012.
[81] S. Datta *et al.*, “Correlation of cavitation with ultrasound enhancement of thrombolysis,” *Ultrasound Med. Biol.*, vol. 32, no. 8, pp. 1257–1267, 2006.
[82] J. T. Sutton, N. M. Ivancevich, S. R. Perrin, D. C. Vela, and C. K. Holland, “Clot Retraction Affects the Extent of Ultrasound-Enhanced Thrombolysis in an Ex Vivo Porcine Thrombosis Model,” *Ultrasound Med. Biol.*, vol. 39, no. 5, pp. 813–824, 2013.
[83] K. B. Bader, M. J. Gruber, and C. K. Holland, “Shaken and Stirred: Mechanisms of Ultrasound-Enhanced Thrombolysis,” *Ultrasound Med. Biol.*, vol. 41, no. 1, pp. 187–196, 2015.
[84] A. V. Alexandrov, A. W. Wojner, and J. C. Grotta, “CLOTBUST: Design of a Randomized Trial of Ultrasound-Enhanced Thrombolysis for Acute Ischemic Stroke,” *J. Neuroimaging*, vol. 14, no. 2, pp. 108–112, 2004.
[85] A. V. Alexandrov, A. M. Demchuk, W. S. Burgin, D. J. Robinson, and J. C. Grotta, “Ultrasound-Enhanced Thrombolysis for Acute Ischemic Stroke: Phase I. Findings of the CLOTBUST Trial,” *J. Neuroimaging*, vol. 14, no. 2, pp. 113–117, 2004.
[86] C. A. Molina *et al.*, “Microbubble administration accelerates clot lysis during continuous 2-MHz ultrasound monitoring in stroke patients treated with intravenous tissue plasminogen activator,” *Stroke*, vol. 37, no. 2, pp. 425–429, 2006.
[87] Z. Chen *et al.*, “Efficacy and safety of sonothombolysis versus non-sonothombolysis in patients with acute ischemic stroke: A meta-analysis of randomized controlled trials,” *PLoS One*, vol. 14, no. 1, pp. 1–15, 2019.
[88] W. Mathias *et al.*, “Diagnostic Ultrasound Impulses Improve Microvascular Flow in Patients with STEMI Receiving Intravenous Microbubbles,” *J. Am. Coll. Cardiol.*, vol. 67, no. 21, pp. 2506–2515, 2016.
[89] W. Mathias *et al.*, “Sonothrombolysis in ST-Segment Elevation Myocardial Infarction

Treated With Primary Percutaneous Coronary Intervention," *J. Am. Coll. Cardiol.*, vol. 73, no. 22, pp. 2832–2842, 2019.
[90] J. Slikkerveer, L. J. Juffermans, N. van Royen, Y. Appelman, T. R. Porter, and O. Kamp, "Therapeutic application of contrast ultrasound in ST elevation myocardial infarction: Role in coronary thrombosis and microvascular obstruction," *Eur. Hear. journal. Acute Cardiovasc. care*, vol. 8, no. 1, pp. 45–53, 2019.
[91] H. P. Ebben, J. H. Nederhoed, R. J. Lely, W. Wisselink, and K. Yeung, "Microbubbles and UltraSound-accelerated Thrombolysis (MUST) for peripheral arterial occlusions: Protocol for a phase II single-arm trial," *BMJ Open*, vol. 7, no. 8, pp. 1–7, 2017.
[92] Y. Shi, W. Shi, L. Chen, and J. Gu, "A systematic review of ultrasound-accelerated catheter-directed thrombolysis in the treatment of deep vein thrombosis," *J. Thromb. Thrombolysis*, vol. 45, no. 3, pp. 440–451, 2018.
[93] M. Dumantepe, I. Uyar, B. Teymen, O. Ugur, and Y. Enc, "Improvements in pulmonary artery pressure and right ventricular function after ultrasound-accelerated catheter-directed thrombolysis for the treatment of pulmonary embolism," *J. Card. Surg.*, vol. 29, no. 4, pp. 455–463, 2014.
[94] R. P. Engelberger and N. Kucher, "Ultrasound-assisted thrombolysis for acute pulmonary embolism: A systematic review," *Eur. Heart J.*, vol. 35, no. 12, pp. 758–764, 2014.
[95] K. A. Lee, A. Cha, M. H. Kumar, C. Rezayat, and C. M. Sales, "Catheter-directed, ultrasound-assisted thrombolysis is a safe and effective treatment for pulmonary embolism, even in high-risk patients," *J. Vasc. Surg. Venous Lymphat. Disord.*, vol. 5, no. 2, pp. 165–170, 2017.
[96] K. Valji and J. Bookstein, "Fibrinolysis with Intrathrombic Injection of Urokinase and Tissue-Type Plasminogen Activator Results in a New Model of Subacute Venous Thrombosis," *Invest. Radiol.*, vol. 22, no. 1, pp. 23–27, 1987.
[97] G. M. Lim and J. J. Bookstein, "Augmented Pulse-Spray Thrombolysis with tPA by Early Pulsed Intrathrombic Plasminogen Enrichment," *J. Vasc. Interv. Radiol.*, vol. 9, pp. 618–25, 1998.
[98] A. F. Prokop, A. Soltani, and R. A. Roy, "Cavitational Mechanisms in Ultrasound-Accelerated Fibrinolysis," *Ultrasound Med. Biol.*, vol. 33, no. 6, pp. 924–933, 2007.
[99] B. Petit *et al.*, "Sonothrombolysis: The Contribution of Stable and Inertial Cavitation to Clot Lysis," *Ultrasound Med. Biol.*, vol. 41, no. 5, pp. 1402–1410, 2015.
[100] K. Tachibana and S. Tachibana, "Albumin microbubble echo-contrast material as an enhancer for ultrasound accelerated thrombolysis," *Circulation*, vol. 92, no. 5, pp. 1148–1150, 1995.
[101] C. W. Francis, A. Blinc, S. Lee, and C. Cox, "Ultrasound accelerates transport of recombinant tissue plasminogen activator into clots," *Ultrasound Med. Biol.*, vol. 21, no. 3, pp. 419–424, 1995.
[102] V. N. Suchkova, R. B. Baggs, and C. W. Francis, "Effect of 40-kHz Ultrasound on Acute Thrombotic Ischemia in a Rabbit Femoral Artery Thrombosis Model," *Circulation*, vol. 101, no. 19, pp. 2296–2301, 2000.
[103] V. Suchkova, E. L. Carstensen, and C. W. Francis, "Ultrasound enhancement of fibrinolysis at frequencies of 27 to 100 kHz," *Ultrasound Med. Biol.*, vol. 28, no. 3, pp. 377–382, 2002.
[104] A. F. Prokop, A. Soltani, and R. A. Roy, "Mechanisms responsible for ultrasound-accelerated fibrinolysis in the presence and absence of optison™," *Proc. - IEEE Ultrason.*

Symp., vol. 1, pp. 289–292, 2006.
[105] K. E. Hitchcock *et al.*, "Ultrasound-enhanced rt-PA thrombolysis in an ex vivo porcine carotid artery model," *Ultrasound Med. Biol.*, vol. 37, no. 8, pp. 1240–1251, 2011.
[106] C. K. Holland, S. S. Vaidya, S. Datta, C.-C. Coussios, and G. J. Shaw, "Ultrasound-enhanced tissue plasminogen activator thrombolysis in an in vitro porcine clot model," *Thromb. Res.*, vol. 121, no. 5, pp. 663–673, 2008.
[107] S. A. Elder, "Cavitation microstreaming," *J. Acoust. Soc. Am.*, vol. 31, pp. 54–64, 1959.
[108] H. Flynn, "Physics of acoustic cavitation in liquids," in *Physical Acoustics*, Vol 1-B., W. Mason, Ed. New York: Academic Press, 1964, pp. 58–172.
[109] K. B. Bader and C. K. Holland, "Gauging the likelihood of stable cavitation from ultrasound contrast agents," *Phys. Med. Biol.*, vol. 58, no. 1, pp. 127–44, 2013.
[110] A. D. Phelps and T. G. Leighton, "The Subharmonic Oscillations and Combination-Frequency Subharmonic Emissions from a Resonant Bubble: Their Properties and Generation Mechanisms," *Acustica*, vol. 83, no. 1. pp. 59–66, 1997.
[111] E. L. Carstensen and H. Flynn, "The potential for transient cavitation with microsecond pulses of ultrasound," *Ultrasound Med. Biol.*, vol. 8, no. 6, pp. L720-24, 1982.
[112] H. G. Flynn, "Generation of transient cavities in liquids by microsecond pulses of ultrasound," *J. Acoust. Soc. Am.*, vol. 72, no. 6, pp. 1926–1932, 1982.
[113] W. S. Chen, A. A. Brayman, T. J. Matula, and L. A. Crum, "Inertial cavitation dose and hemolysis produced in vitro with or without Optison," *Ultrasound Med. Biol.*, vol. 29, no. 5, pp. 725–737, 2003.
[114] A. A. Brayman, M. Azadniv, C. Cox, and M. W. Miller, "Hemolysis of Albunex-supplemented, 40% Hematocrit Human Erythrocytes in Vitro By 1-MHz Pulsed Ultrasound: Acoustic Pressure and Pulse Length Dependence," *Ultrasound Med. Biol.*, vol. 22, no. 7, pp. 927–938, 1996.
[115] A. Goyal *et al.*, "Inertial Cavitation Ultrasound with Microbubbles Improves Reperfusion Efficacy When Combined with Tissue Plasminogen Activator in an In Vitro Model of Microvascular Obstruction," *Ultrasound Med. Biol.*, vol. 43, no. 7, pp. 1391–1400, 2017.
[116] G. E. R. Weller, F. S. Villanueva, A. L. Klibanov, and W. R. Wagner, "Modulating targeted adhesion of an ultrasound contrast agent to dysfunctional endothelium," *Ann. Biomed. Eng.*, vol. 30, no. 8, pp. 1012–1019, 2002.
[117] R. T. Kleven *et al.*, "The effect of 220 kHz insonation scheme on rt-PA thrombolytic efficacy in vitro," *Phys. Med. Biol.*, vol. 64, no. 16, 2019.
[118] H. Shekhar *et al.*, "In vitro characterization of sonothrombolysis and echocontrast agents to treat ischemic stroke," *Sci. Rep.*, vol. 9, no. 1, pp. 1–13, 2019.
[119] H. Shekhar *et al.*, "In vitro thrombolytic efficacy of echogenic liposomes loaded with tissue plasminogen activator and octafluoropropane gas," *Phys. Med. Biol.*, vol. 62, no. 2, pp. 517–38, 2017.
[120] J. Brüßler *et al.*, "Nanoscaled ultrasound contrast agents for enhanced sonothrombolysis," *Colloids Surfaces B Biointerfaces*, vol. 172, pp. 728–733, 2018.
[121] M. de Saint Victor, L. C. Barnsley, D. Carugo, J. Owen, C. C. Coussios, and E. Stride, "Sonothrombolysis with Magnetically Targeted Microbubbles," *Ultrasound Med. Biol.*, vol. 45, no. 5, pp. 1151–1163, 2019.
[122] S. Monteith *et al.*, "Potential intracranial applications of magnetic resonance-guided focused ultrasound surgery ; A review," *J. Neurosurg.*, vol. 118, no. 2, pp. 215–221, 2013.
[123] A. Zafar *et al.*, "MRI-Guided High-Intensity Focused Ultrasound as an Emerging Therapy

for Stroke: A Review," *J. Neuroimaging*, vol. 29, no. 1, pp. 5–13, 2019.
[124] X. Zhang, G. E. Owens, C. A. Cain, H. S. Gurm, J. Macoskey, and Z. Xu, "Histotripsy Thrombolysis on Retracted Clots," *Ultrasound Med. Biol.*, vol. 42, no. 8, pp. 1903–1918, 2016.
[125] K. B. Bader, E. Vlaisavljevich, and A. D. Maxwell, "For Whom the Bubble Grows: Physical Principles of Bubble Nucleation and Dynamics in Histotripsy Ultrasound Therapy," *Ultrasound Med. Biol.*, vol. 45, no. 5, pp. 1056–1080, 2019.
[126] M. J. Garcia, "Endovascular Management of Acute Pulmonary Embolism Using the Ultrasound-Enhanced EkoSonic System," *Semin. Intervent. Radiol.*, vol. 32, no. 4, pp. 384–387, 2015.
[127] H. L. Weiss *et al.*, "Mechanical clot damage from cavitation during sonothrombolysis," *J. Acoust. Soc. Am.*, vol. 133, no. 5, pp. 3159–3175, 2013.
[128] E. C. Everbach and C. W. Francis, "Cavitational mechanisms in ultrasound-accelerated thrombolysis at 1 MHz," *Ultrasound Med. Biol.*, vol. 26, no. 7, pp. 1153–1160, 2000.
[129] R. A. Roy, S. Madanshetty, and R. E. Apfel, "An acoustic backscattering technique for the detection of transient cavitation produced by microsecond pulses of ultrasound," *J. Acoust. Soc. Am.*, vol. 87, no. 6, pp. 2451–2458, 1990.
[130] S. Madanshetty, R. A. Roy, and R. E. Apfel, "Acoustic microcavitation: Its active and passive acoustic detection," *J. Acoust. Soc. Am.*, vol. 90, no. 3, pp. 1515–1526, 1991.
[131] V. A. Salgaonkar, S. Datta, C. K. Holland, and T. D. Mast, "Passive cavitation imaging with ultrasound arrays," *J. Acoust. Soc. Am.*, vol. 126, no. 6, pp. 3071–3083, 2009.
[132] M. Gyöngy and C. C. Coussios, "Passive cavitation mapping for localization and tracking of bubble dynamics.," *J. Acoust. Soc. Am.*, vol. 128, no. 4, 2010.
[133] K. J. Haworth, K. B. Bader, K. T. Rich, C. K. Holland, and T. D. Mast, "Quantitative frequency-domain passive cavitation imaging," *IEEE Trans. Ultrason. Ferroelectr. Freq. Control*, vol. 64, no. 1, pp. 177–191, 2017.
[134] F. Vignon *et al.*, "Microbubble cavitation imaging," *IEEE Trans. Ultrason. Ferroelectr. Freq. Control*, vol. 60, no. 4, pp. 661–670, 2013.
[135] A. N. Pouliopoulos and J. J. Choi, "Superharmonic microbubble Doppler effect in ultrasound therapy," *Phys. Med. Biol.*, vol. 61, no. 16, pp. 6154–6171, 2016.
[136] C. D. Arvanitis, M. S. Livingstone, and N. McDannold, "Combined Ultrasound and MR Imaging to Guide Focused Ultrasound Therapies in the Brain," *Phys. Med. Biol.*, vol. 58, no. 14, pp. 4749–4761, 2013.
[137] C. D. Arvanitis and N. McDannold, "Integrated ultrasound and magnetic resonance imaging for simultaneous temperature and cavitation monitoring during focused ultrasound therapies," *Med. Phys.*, vol. 40, no. 11, pp. 1–14, 2013.
[138] C. Arvanitis and N. McDannold, "Transcranial spatial and temporal assessment of microbubble dynamics for brain therapies," *Proc. Meet. Acoust.*, vol. 19, 2013.
[139] C. N. Acconcia, R. M. Jones, D. E. Goertz, M. A. O'Reilly, and K. Hynynen, "Megahertz rate, volumetric imaging of bubble clouds in sonothrombolysis using a sparse hemispherical receiver array," *Phys. Med. Biol.*, vol. 62, no. 18, pp. L31–L40, 2017.
[140] S. M. Flight, P. P. Masci, M. F. Lavin, and P. J. Gaffney, "Resistance of porcine blood clots to lysis relates to poor activation of porcine plasminogen by tissue plasminogen activator," *Blood Coagul. Fibrinolysis*, vol. 17, pp. 417–420, 2006.
[141] S. Huang, H. Shekhar, and C. K. Holland, "Comparative lytic efficacy of rt-PA and ultrasound in porcine versus human clots," *PLoS One*, vol. 12, no. 5, pp. 1–20, 2017.

[142] L. Auboire *et al.*, “Microbubbles combined with ultrasound therapy in ischemic stroke: A systematic review of in-vivo preclinical studies,” *PLoS One*, vol. 13, no. 2, pp. 1–19, 2018.
[143] A. J. Dixon, J. Li, J. M. R. Rickel, A. L. Klibanov, Z. Zuo, and J. A. Hossack, “Efficacy of Sonothrombolysis Using Microbubbles Produced by a Catheter-Based Microfluidic Device in a Rat Model of Ischemic Stroke,” *Ann. Biomed. Eng.*, vol. 47, no. 4, pp. 1012–1022, 2019.
[144] A. V. Alexandrov *et al.*, “Safety and efficacy of sonothrombolysis for acute ischaemic stroke: a multicentre, double-blind, phase 3, randomised controlled trial,” *Lancet Neurol.*, vol. 18, no. 4, pp. 338–347, 2019.
[145] J. Eggers, G. Seidel, B. Koch, and I. R. Konig, “Sonothrombolysis in acute ischemic stroke for patients ineligible for rt-PA,” *Neurology*, vol. 64, no. 6, pp. 1052–1054, 2005.
[146] A. Nacu *et al.*, “NOR-SASS (Norwegian Sonothrombolysis in Acute Stroke Study): Randomized Controlled Contrast-Enhanced Sonothrombolysis in an Unselected Acute Ischemic Stroke Population,” *Stroke*, vol. 48, no. 2, pp. 335–341, 2017.
[147] B. C. V. Campbell *et al.*, “Tenecteplase versus alteplase before thrombectomy for ischemic stroke,” *N. Engl. J. Med.*, vol. 378, no. 17, pp. 1573–1582, 2018.
[148] M. Gauberti, “Reperfusion in acute ischaemic stroke by sonothrombolysis,” *Lancet Neurol.*, vol. 18, no. 4, pp. 320–321, 2019.
[149] A. J. Schissler, R. J. Gylnn, P. S. Sobieszczyk, and A. B. Waxman, “Ultrasound-assisted catheter-directed thrombolysis compared with anticoagulation alone for treatment of intermediate-risk pulmonary embolism,” *Pulm. Circ.*, vol. 8, no. 4, 2018.
[150] K. Landskroner, N. Olson, and G. Jesmok, “Cross-species pharmacologic evaluation of plasmin as a direct-acting thrombolytic agent: Ex vivo evaluation for large animal model development,” *J. Vasc. Interv. Radiol.*, vol. 16, no. 3, pp. 369–377, 2005.
[151] D. S. Liebeskind *et al.*, “CT and MRI early vessel signs reflect clot composition in acute stroke,” *Stroke*, vol. 42, no. 5, pp. 1237–1243, 2011.
[152] N. Simons, P. Mitchell, R. Dowling, M. Gonzales, and B. Yan, “Thrombus composition in acute ischemic stroke: A histopathological study of thrombus extracted by endovascular retrieval,” *J. Neuroradiol.*, vol. 42, no. 2, pp. 86–92, 2015.
[153] P. B. Sporns *et al.*, “Ischemic Stroke: What Does the Histological Composition Tell Us about the Origin of the Thrombus?,” *Stroke*, vol. 48, no. 8, pp. 2206–2210, 2017.
[154] C. A. Molina, “Imaging the clot: Does clot appearance predict the efficacy of thrombolysis?,” *Stroke*, vol. 36, no. 11, pp. 2333–2334, 2005.
[155] K. H. Cho, J. S. Kim, S. U. Kwon, A. H. Cho, and D. W. Kang, “Significance of susceptibility vessel sign on T2*-weighted gradient echo imaging for identification of stroke subtypes,” *Stroke*, vol. 36, no. 11, pp. 2379–2383, 2005.
[156] G. J. Shaw, N. Bavani, A. Dhamija, and C. J. Lindsell, “Effect of mild hypothermia on the thrombolytic efficacy of 120 kHz ultrasound enhanced thrombolysis in an in-vitro human clot model,” *Thromb. Res.*, vol. 117, no. 5, pp. 603–608, 2006.
[157] K. P. Mercado-Shekhar *et al.*, “Effect of clot stiffness on recombinant tissue plasminogen activator lytic susceptibility in vitro,” *Ultrasound Med. Biol.*, vol. 44, no. 12, pp. 2710–2727, 2018.
[158] V. J. Marder *et al.*, “Analysis of thrombi retrieved from cerebral arteries of patients with acute ischemic stroke,” *Stroke*, vol. 37, no. 8, pp. 2086–2093, 2006.
[159] A. V. Alexandrov *et al.*, “End-Diastolic Velocity Increase Predicts Recanalization and

Neurological Improvement in Patients With Ischemic Stroke With Proximal Arterial Occlusions Receiving Reperfusion Therapies," *Stroke*, vol. 41, no. 5, pp. 948–952, 2010.
[160] B. Devcic-Kuhar, S. Pfaffenberger, M. Groschl, C. Kollmann, E. Benes, and M. Gottsauner-Wolf, "In Vitro Thrombolysis Enhanced By Standing and Travelling Ultrasound Wave Fields," *Ultrasound Med. Biol.*, vol. 28, no. 9, pp. 1181–1187, 2002.
[161] V. Frenkel *et al.*, "Pulsed High-Intensity Focused Ultrasound Enhances Thrombolysis in an in Vitro Model," *Radiology*, vol. 239, no. 1, pp. 86–93, 2006.
[162] S. Pfaffenberger *et al.*, "Can a Commercial Diagnostic Ultrasound Device Accelerate Thrombolysis?," *Stroke*, vol. 36, no. 1, pp. 124–128, 2005.
[163] S. Xu, X. Li, Y. Liu, C. Xu, and M. Wan, "Cavitation enhanced ultrasound thrombolysis," in *IEEE Ultrasonics Symposium*, 2008, no. 1, pp. 2052–2055.
[164] M. A. Yenari, J. T. Palmer, P. M. Bracci, and G. K. Steinberg, "Thrombolysis with tissue plasminogen activator (tPA) is temperature dependent," *Thromb. Res.*, vol. 77, no. 5, pp. 475–481, 1995.
[165] P. M. Farrehi, Y. Zhu, and W. P. Fay, "An analysis of mechanisms underlying the antifibrinolytic properties of radiographic contrast agents," *J. Thromb. Thrombolysis*, vol. 12, no. 3, pp. 273–281, 2001.
[166] M. Pieters, R. T. Hekkenberg, M. Barrett-Bergshoeff, and D. C. Rijken, "The effect of 40 kHz ultrasound on tissue plasminogen activator-induced clot lysis in three in vitro models," *Ultrasound Med. Biol.*, vol. 30, no. 11, pp. 1545–1552, 2004.
[167] F. Bajd, J. Vidmar, A. Blinc, and I. Serša, "Microscopic clot fragment evidence of biochemo-mechanical degradation effects in thrombolysis," *Thromb. Res.*, vol. 126, no. 2, pp. 137–143, 2010.
[168] M. A. Kandadai, J. M. Meunier, K. Hart, C. K. Holland, and G. J. Shaw, "Plasmin-Loaded Echogenic Liposomes for Ultrasound-Mediated Thrombolysis," *Transl. Stroke Res.*, vol. 6, no. 1, pp. 78–87, 2014.
[169] W. T. Shi *et al.*, "Investigation of Effectiveness of Microbubble Stable Cavitation in Thrombolysis," in *2010 IEEE International Ultrasonics Symposium*, 2010, pp. 330–333.
[170] J. Wu *et al.*, "Improved sonothrombolysis from a modified diagnostic transducer delivering impulses containing a longer pulse duration," *Ultrasound Med. Biol.*, vol. 40, no. 7, pp. 1545–1553, 2014.
[171] O. O. Zaidat *et al.*, "Recommendations on Angiographic Revascularization Grading Standards for Acute Ischemic Stroke: A Consensus Statement and for the Cerebral Angiographic Revascularization, Grading (CARG) Collaborators, STIR Revascularization working group, and STIR Thrombol," *Stroke*, vol. 44, no. 9, pp. 2630–2663, 2013.
[172] S. Pfaffenberger *et al.*, "2 MHz ultrasound enhances t-PA-mediated thrombolysis: comparison of continuous versus pulsed ultrasound and standing versus travelling acoustic waves," *Thromb. Haemost.*, vol. 89, no. 3, pp. 583–589, 2003.
[173] M. Kimura, S. Iijima, K. Kobayashi, and H. Furuhata, "Evaluation of the thrombolytic effect of tissuetype plasminogen activator with ultrasonic irradiation: in vitro experiment involving assay of the fibrin degradation products from the clot," *Biol. Pharm. Bull.*, vol. 17, no. 1, pp. 126–130, 1994.
[174] A. Elnager *et al.*, "In vitro whole blood clot lysis for fibrinolytic activity study using D-dimer and confocal microscopy," *Adv. Hematol.*, vol. 2014, 2014.
[175] B. M. Härdig, J. Carlson, and A. Roijer, "Changes in clot lysis levels of reteplase and streptokinase following continuous wave ultrasound exposure, at ultrasound intensities

following attenuation from the skull bone," *BMC Cardiovasc. Disord.*, vol. 8, no. 19, 2008.
[176] B. Petit *et al.*, "Fibrin degradation during sonothrombolysis - Effect of ultrasound, microbubbles and tissue plasminogen activator," *J. Drug Deliv. Sci. Technol.*, vol. 25, no. 2015, pp. 29–35, 2015.
[177] N. Kucher *et al.*, "Randomized, controlled trial of ultrasound-assisted catheter-directed thrombolysis for acute intermediate-risk pulmonary embolism," *Circulation*, vol. 129, no. 4, pp. 479–486, 2014.
[178] W. C. Culp, T. R. Porter, J. Lowery, F. Xie, P. K. Roberson, and L. Marky, "Intracranial clot lysis with intravenous microbubbles and transcranial ultrasound in swine," *Stroke*, vol. 35, no. 10, pp. 2407–2411, 2004.
[179] Y. Birnbaum *et al.*, "Noninvasive in vivo clot dissolution without a thrombolytic drug: Recanalization of thrombosed iliofemoral arteries by transcutaneous ultrasound combined with intravenous infusion of microbubbles," *Circulation*, vol. 97, no. 2, pp. 130–134, 1998.
[180] A. Alonso *et al.*, "In vivo clot lysis of human thrombus with intravenous abciximab immunobubbles and ultrasound," *Thromb. Res.*, vol. 124, no. 1, pp. 70–74, 2009.
[181] F. Fluri, M. K. Schuhmann, and C. Kleinschnitz, "Animal models of ischemic stroke and their application in clinical research," *Drug Des. Devel. Ther.*, vol. 9, pp. 3445–3454, 2015.
[182] J. B. Casals *et al.*, "The use of animal models for stroke research: A review," *Comp. Med.*, vol. 61, no. 4, pp. 305–313, 2011.
[183] Y. Yamori, R. Horie, H. Handa, M. Sato, and M. Fukase, "Spontaneously Hypertensive Rats and Humans," *Stroke*, vol. 7, no. 1, pp. 46–53, 1976.
[184] J. O. Ström, E. Ingberg, A. Theodorsson, and E. Theodorsson, "Method parameters' impact on mortality and variability in mouse stroke experiments: A meta-analysis," *BMC NE*, vol. 14, no. 41, 2013.
[185] H. K. Gold *et al.*, "Animal models for arterial thrombolysis and prevention of reocclusion. Erythrocyte-rich versus platelet-rich thrombus.," *Circulation*, vol. 83, no. 6, pp. 26–40, 1991.
[186] P. Jagadeeswaran, B. C. Cooley, P. L. Gross, and N. Mackman, "Animal Models of Thrombosis from Zebrafish to Nonhuman Primates: Use in the Elucidation of New Pathologic Pathways and the Development of Antithrombotic Drugs," *Circ. Res.*, vol. 118, no. 9, pp. 1363–1379, 2016.
[187] A. M. Herrmann *et al.*, "Large animals in neurointerventional research: A systematic review on models, techniques and their application in endovascular procedures for stroke, aneurysms and vascular malformations," *J. Cereb. Blood Flow Metab.*, vol. 39, no. 3, pp. 375–394, 2019.
[188] S. Huang, "The effect of low - frequency ultrasound on thrombolytic efficacy in porcine thromboembolism models," University of Cincinnati, 2017.
[189] A. Y. Ammi *et al.*, "Characterization of Ultrasound Propagation Through Ex-vivo Human Temporal Bone," *Ultrasound Med. Biol.*, vol. 34, no. 10, pp. 1578–1589, 2008.
[190] J. Kollár *et al.*, "Image quality of the temporal bone window examined by transcranial doppler sonography and correlation with postmortem computed tomography measurements," *Cerebrovasc. Dis.*, vol. 17, no. 1, pp. 61–65, 2004.
[191] G. Bouchoux, R. Shivashankar, T. A. Abruzzo, and C. K. Holland, "In silico study of low-

frequency transcranial ultrasound fields in acute ischemic stroke patients," *Ultrasound Med. Biol.*, vol. 40, no. 6, pp. 1154–1166, 2014.
[192] G. Bouchoux *et al.*, "Experimental validation of a finite-difference model for the prediction of transcranial ultrasound fields based on CT images," *Phys. Med. Biol.*, vol. 57, pp. 8005–22, 2012.
[193] M. Daffertshofer *et al.*, "Transcranial low-frequency ultrasound-mediated thrombolysis in brain ischemia: Increased risk of hemorrhage with combined ultrasound and tissue plasminogen activator - Results of a phase II clinical trial," *Stroke*, vol. 36, no. 7, pp. 1441–1446, 2005.
[194] C. Baron, J. F. Aubry, M. Tanter, S. Meairs, and M. Fink, "Simulation of Intracranial Acoustic Fields in Clinical Trials of Sonothrombolysis," *Ultrasound Med. Biol.*, vol. 35, no. 7, pp. 1148–1158, 2009.
[195] G. Tsivgoulis *et al.*, "Safety and efficacy of ultrasound-enhanced thrombolysis: A comprehensive review and meta-analysis of randomized and nonrandomized studies," *Stroke*, vol. 41, no. 2, pp. 280–287, 2010.
[196] T. Azuma *et al.*, "Bubble Generation by Standing Wave in Water Surrounded by Cranium with Transcranial Ultrasonic Beam," *Jpn. J. Appl. Phys.*, vol. 44, no. 6B, pp. 4625–4630, 2005.
[197] K. Kooiman *et al.*, "Ultrasound-Responsive Cavitation Nuclei for Therapy and Drug Delivery," *Ultrasound Med. Biol.*, vol. 46, no. 6, pp. 1296–1325, 2020.
[198] M. Saqqur *et al.*, "The role of sonolysis and sonothrombolysis in acute ischemic stroke: A systematic review and meta-analysis of randomized controlled trials and case-control studies," *J. Neuroimaging*, vol. 24, no. 3, pp. 209–220, 2014.
[199] S. Gao *et al.*, "Improvements in cerebral blood flow and recanalization rates with transcranial diagnostic ultrasound and intravenous microbubbles after acute cerebral Emboli," *Invest. Radiol.*, vol. 49, no. 9, pp. 593–600, 2014.
[200] W. C. Culp, E. Erdem, P. K. Roberson, and M. M. Husain, "Microbubble Potentiated Ultrasound as a Method of Stroke Therapy in a Pig Model: Preliminary Findings," *J. Vasc. Interv. Radiol.*, vol. 14, no. 11, pp. 1433–1436, 2003.
[201] W. T. Shi *et al.*, "Investigation of image-guided sonothrombolysis in a porcine acute ischemic stroke model," *IEEE Int. Ultrason. Symp. IUS*, vol. 2, pp. 5–8, 2011.
[202] S. Yan, Q. Chen, M. Xu, J. Sun, D. S. Liebeskind, and M. Lou, "Thrombus Length Estimation on Delayed Gadolinium-Enhanced T1," *Stroke*, vol. 47, no. 3, pp. 756–761, 2016.
[203] J. L. Raymond *et al.*, "Broadband attenuation measurements of phospholipid-shelled ultrasound contrast agents," *Ultrasound Med. Biol.*, vol. 40, no. 2, pp. 410–421, 2014.
[204] S. Datta, C. C. Coussios, A. Y. Ammi, T. D. Mast, G. M. de Courten-Myers, and C. K. Holland, "Ultrasound-Enhanced Thrombolysis Using Definity as a Cavitation Nucleation Agent," *Ultrasound Med. Biol.*, vol. 34, no. 9, pp. 1421–1433, 2008.
[205] G. J. Shaw, M. Sperling, and J. M. Meunier, "Long-term stability of recombinant tissue plasminogen activator at -80 C," *BMC Res. Notes*, vol. 2, pp. 1–3, 2009.
[206] J. H. Verheijen, Y. F. de Jong, and G. T. G. Chang, "Quantitative Analysis of the Composition of Mixtures of One-chain and Two-chain Tissue-type Plasminogen Activator with a Spectrophotometric Method," *Thromb. Res.*, vol. 39, pp. 281–288, 1985.
[207] P. M. Daniel, J. D. K. Dawes, and M. L. Prichard, Marjorie, "Studies of the carotid rete and its associated arteries," *Philos. Trans. R. Soc. London Biol. Sci.*, vol. 237, no. 645, pp.

173–208, 1953.
[208] J. K. Eliyas, M. Niekrasz, C. Wardrip, and S. K. Lee, “Focused post mortem dissection technique for harvest of rete mirabile in domestic swine (Sus scrofa),” *J. Neurointerv. Surg.*, vol. 8, no. 9, pp. 973–976, 2016.
[209] M. M. Swindle and A. C. Smith, *Swine in the Laboratory: Surgery, Anesthesia, Imaging, and Experimental Techniques*, 3rd Ed., vol. 19, no. 1988. Boca Raton, FL: CRC Press, 2016.
[210] N. Badjatia *et al.*, “Preliminary Experience with Intra-Arterial Nicardipine as a Treatment for Cerebral Vasospasm,” *Am. J. Neuroradiol.*, vol. 25, no. May, pp. 819–826, 2004.
[211] S. Seldinger, “Catheter replacement of the needle in percutaneous arteriography; a new technique.,” *Acta radiol.*, vol. 39, no. 5, pp. 368–376, 1953.
[212] J. Cohen, *Statistical Power Analysis for the Behavioral Sciences*, 2nd editio. Hillsdale, NJ: Larence Erlbaum Associates, 1988.
[213] E. Demidenko, “Sample Size and Optimal Design for Logistic Regression with Binary Interaction,” *Stat. Med.*, vol. 27, no. 1, pp. 36–46, 2008.
[214] E. Demidenko, “Sample size determination for logistic regression revisited.,” *Stat. Med.*, vol. 26, no. 18, pp. 3385–3397, 2007.
[215] N. F. Kassell, G. Helm, N. Simmons, C. D. Phillips, and W. S. Cail, “Treatment of cerebral vasospasm with intra-arterial papaverine,” *J. Neurosurg.*, vol. 77, pp. 848–852, 1992.
[216] X. Chen, J. Wang, J. Pacella, and F. S. Villanueva, “The dynamic behavior of microbubbles during long ultrasound tone-burst excitation: mechanistic insights into ultrasound- microbubble mediated therapeutics using high-speed imaging and cavitation detection,” *Ultrasound Med. Biol.*, vol. 150, no. 2, pp. 137–143, 2016.
[217] E. S. Flamm *et al.*, “Dose-escalation study of intravenous nicardipine in patients with aneurysmal subarachnoid hemorrhage,” *J. Neurosurg.*, vol. 68, no. 3, pp. 393–400, 2009.
[218] P. Khatri, T. Abruzzo, S. D. Yeatts, C. Nichols, J. P. Broderick, and T. A. Tomsick, “Good clinical outcome after ischemic stroke with successful revascularization is time-dependent,” *Neurology*, vol. 73, no. 13, pp. 1066–1072, 2009.
[219] W. G. Pond and H. J. Mersmann, *Biology of the Domestic Pig*, 2nd ed. Ithaca, NY: Comstock Publishing Associates, 2001.
[220] K. R. Wagner *et al.*, “Lobar Intracerebral Hemorrhage Model in Pigs,” *Stroke*, vol. 27, no. 3, pp. 490–497, 1996.
[221] K. R. Wagner *et al.*, “Ultra-early clot aspiration after lysis with tissue plasminogen activator in a porcine model of intracerebral hemorrhage: edema reduction and blood-brain barrier protection,” *J. Neurosurg.*, vol. 90, pp. 491–498, 1999.
[222] A. Y. Ammi *et al.*, “120 kilohertz ultrasound-enhanced thrombolysis in a porcine intracerebral hemorrhage model,” *J. Acoust. Soc. Am.*, vol. 125, p. 2713, 2009.
[223] K. Kandara, P. A. Drinker, S. J. Singer, and D. Caramore, “Forceful pulsatile local infusion of enzyme accelerates thrombolysis: in vivo evaluation of a new delivery system,” *Radiology*, vol. 168, no. 3, pp. 739–744, 1988.
[224] K. B. Bader, G. Bouchoux, T. Peng, M. E. Klegerman, D. D. Mcpherson, and C. K. Holland, “Thrombolytic efficacy and enzymatic activity of rt-PA-loaded echogenic liposomes,” *J. Thromb. Thrombolysis*, vol. 40, pp. 144–155, 2015.
[225] G. M. De Courten Myers, M. Kleinholz, K. R. Wagner, and R. E. Myers, “Stroke assessment: Morphometric infarct size versus neurologic deficit,” *J. Neurosci. Methods*,

vol. 83, no. 2, pp. 151–157, 1998.
[226] S. L. Seldinger, “A new technique: catheter replacement of the needle in percutaneous arteriography,” *Acta radiol.*, vol. 39, no. 5, pp. 368–376, 1953.
[227] K. E. Hitchcock, “Ultrasound-assisted thrombolysis for stroke therapy: Better thrombus break-up with bubbles,” *Stroke*, vol. 41, no. 10, pp. S50–S53, 2010.
[228] J. W. Pickering and J. A. Hewitt, “The Syneresis of Blood Clots,” *Q. J. Exp. Physiol.*, vol. 13, no. 3, pp. 199–207, 1923.
[229] J. P. Hannon, C. A. Bossone, and C. E. Wade, “Normal physiological values for conscious pigs used in biomedical research,” *Lab. Anim. Sci.*, vol. 40, no. 3, pp. 293–298, 1990.
[230] K. A. Hossmann and S. Takagi, “Osmolality of brain in cerebral ischemia,” *Exp. Neurol.*, vol. 51, no. 1, pp. 124–131, 1976.
[231] Y. Matsuoka, S. Nishimura, and K. A. Hossmann, “Changes in Osmolarity of Brain, Cerebrospinal Fluid and Plasam in Acute Cytotoxic Edema in Cats,” in *Intracranial Pressure V*, 1983, pp. 389–393.
[232] M. J. Gruber, K. B. Bader, and C. K. Holland, “Cavitation thresholds of contrast agents in an in vitro human clot model exposed to 120-kHz ultrasound,” *J. Acoust. Soc. Am.*, vol. 135, no. 2009, pp. 646–653, 2014.
[233] Y. Lin *et al.*, “Effect of acoustic parameters on the cavitation behavior of SonoVue microbubbles induced by pulsed ultrasound,” *Ultrason. Sonochem.*, vol. 35, pp. 176–184, 2017.
[234] F. Xie *et al.*, “Effects of Attenuation and Thrombus Age on the Success of Ultrasound and Microbubble-mediated Thrombus Dissolution,” *Ultrasound Med. Biol.*, vol. 37, no. 2, pp. 280–288, 2011.
[235] C. M. Muth and E. S. Shank, “Gas embolism,” *N. Engl. J. Med.*, vol. 342, no. 7, pp. 476–82, 2000.
[236] Z. Fan, D. Chen, and C. X. Deng, “Characterization of the dynamic activities of a population of microbubbles driven by pulsed ultrasound exposures in sonoporation,” *Ultrasound Med. Biol.*, vol. 40, no. 6, pp. 1260–1272, 2014.
[237] L. A. Crum, “Rectified diffusion,” *Ultrasonics*, vol. 22, no. 5, pp. 215–223, 1984.
[238] M. Postema, P. Marmottant, C. T. Lancée, S. Hilgenfeldt, and N. De Jong, “Ultrasound-induced microbubble coalescence,” *Ultrasound Med. Biol.*, vol. 30, no. 10, pp. 1337–1344, 2004.
[239] M. Minnaert, “On musical air-bubbles and the sounds of running water,” *London, Edinburgh, Dublin Philos. Mag. J. Sci.*, vol. 16, no. 104, pp. 235–248, 1933.
[240] J. M. Parker *et al.*, “Safety of ultrasound contrast agents in patients with known or suspected cardiac shunts,” *Am. J. Cardiol.*, vol. 112, no. 7, pp. 1039–1045, 2013.
[241] M. A. (University of T. O’Reilly, Y. Huang, and H. (University of T. Kullervo, “The impact of standing wave effects on transcranial focused ultrasound disruption of the blood-brain barrier in a rat model,” *Phys. Med. Biol.*, vol. 55, no. 18, pp. 5251–5267, 2010.
[242] N. McDannold, M. S. Livingstone, C. B. Top, J. T. Sutton, N. Todd, and N. Vykhodtseva, “Preclinical evaluation of a low-frequency transcranial MRIguided focused ultrasound system in a primate model,” *Phys. Med. Biol.*, vol. 61, no. 21, pp. 7664–7687, 2016.
[243] A. N. Pouliopoulos, C. Li, M. Tinguely, and V. Garbin, “Rapid short-pulse sequences enhance the spatiotemporal uniformity of acoustically driven microbubble activity during flow conditions,” *J. Acoust. Soc. Am.*, vol. 140, no. October, pp. 2469–2480, 2016.

[244] H. H. Pennes, “Analysis of tissue and arterial blood temperatures in the resting human forearm,” *J. Appl. Physiol.*, vol. 1, no. 2, pp. 93–122, 1948.
[245] A. D. Pierce, *Acoustics: An Introduction to Its Physical Principles and Applications, 2nd ed.*, 2nd ed. New York: Acoustical Society of America, 1989.
[246] F. A. Duck, *Physical Properties of Tissue. A Comprehensive Reference Book*. San Diego: Academic Press, 1990.
[247] Y. Zhang, “Generalized dual-phase lag bioheat equations based on nonequilibrium heat transfer in living biological tissues,” *Int. J. Heat Mass Transf.*, vol. 52, no. 21–22, pp. 4829–4834, 2009.
[248] S. A. Sapareto and W. C. Dewey, “Thermal dose determination in cancer therapy,” *Int. J. Radiat. Oncol. Biol. Phys.*, vol. 10, no. 6, pp. 787–800, 1984.
[249] E. Seifried, P. Tanswell, D. Ellbruck, W. Haerer, and A. Schmidt, “Pharmacokinetics and haemostatic status during consecutive infusions of recombinant tissue-type plasminogen activator in patients with acute myocardial infarction,” *Thromb. Haemost.*, vol. 61, pp. 497–501, 1989.
[250] P. Tanswell, E. Seifried, E. Stang, and J. Krause, “Pharmacokinetics and hepatic catabolism of tissue-type plasminogen activator.,” *Arzneimittelforschung.*, vol. 41, pp. 1310–9, 1991.
[251] J. Y. Cheng, G. J. Shaw, and C. K. Holland, “In vitro microscopic imaging of enhanced thrombolysis with 120-kHz ultrasound in a human clot model,” *Acoust. Res. Lett. Online*, vol. 6, no. 1, pp. 25–29, 2005.
[252] J. M. Meunier, C. K. Holland, C. J. Lindsell, and G. J. Shaw, “Duty Cycle Dependence of Ultrasound Enhanced,” *Ulrasound Med. Biol.*, vol. 33, no. 4, pp. 576–583, 2007.
[253] M. Santin, S. L. Bridal, A. Haak, and W. D. O’Brien, “Spectral and temporal signal modifications occuring between stable and transient inertial cavitation,” in *Proceedings - IEEE Ultrasonics Symposium*, 2008, pp. 989–992.
[254] K. Radhakrishnan *et al.*, “Relationship between cavitation and loss of echogenicity from ultrasound contrast agents,” *Phys. Med. Biol.*, vol. 58, no. 18, pp. 6541–6563, 2013.
[255] J. T. Sutton, K. J. Haworth, G. Pyne-Geithman, and C. K. Holland, “Ultrasound-mediated drug delivery for cardiovascular disease.,” *Expert Opin. Drug Deliv.*, vol. 10, no. 5, pp. 573–92, 2013.
[256] C. F. Caskey, S. Qin, P. A. Dayton, and K. W. Ferrara, “Microbubble tunneling in gel phantoms,” *J. Acoust. Soc. Am.*, vol. 125, no. 5, p. EL183, 2009.
[257] C. Acconcia, B. Y. C. Leung, K. Hynynen, and D. E. Goertz, “Interactions between ultrasound stimulated microbubbles and fibrin clots,” *Appl. Phys. Lett.*, vol. 103, no. 5, pp. 053701 (1–4), 2013.
[258] V. Ciaravino, H. Flynn, and M. Miller, “Pulsed Enhancement of acoustic cavitation: a postulated model.,” *Ultrasound Med. Biol.*, vol. 7, no. 2, pp. 159–66, 1981.
[259] B. A. Blinc, C. W. Francis, J. L. Trudnowski, and E. L. Carstensen, “Characterization of Ultrasound-Potentiated Fibrinolysis In Vitro,” *Blood*, vol. 81, no. 10, pp. 2636–2643, 1993.
[260] S. Pichardo, V. W. Sin, and K. Hynynen, “Multi-frequency characterization of the speed of sound and attenuation coefficient for longitudinal transmission of freshly excised human skulls,” *Phys. Med. Biol.*, vol. 56, no. 1, pp. 219–250, 2011.
[261] D. Faille, J. Labreuche, E. Meseguer, M. G. Huisse, N. Ajzenberg, and M. Mazighi, “Endothelial markers are associated with thrombolysis resistance in acute stroke patients,”

Eur. J. Neurol., vol. 21, no. 4, pp. 643–7, 2014.
[262] M. A. O'Reilly, R. M. Jones, and K. Hynynen, "Three-dimensional transcranial ultrasound imaging of microbubble clouds using a sparse hemispherical array," *IEEE Trans. Biomed. Eng.*, vol. 61, no. 4, pp. 1285–1294, 2014.
[263] C. D. Arvanitis, G. T. Clement, and N. McDannold, "Transcranial assessment and visualization of acoustic cavitation: Modeling and experimental validation," *IEEE Trans. Med. Imaging*, vol. 34, no. 6, pp. 1270–1281, 2015.
[264] T. D. . Mast and F. Yu, "Simplified expansions for radiation from a baffled circular piston," *J. Acoust. Soc. Am.*, vol. 118, no. 6, pp. 3457–3464, 2005.
[265] K. R. Wagner, G. Xi, Y. Hua, M. Kleinholz, G. M. De Courten-Myers, and R. E. Myers, "Early metabolic alterations in edematous perihematomal brain regions following experimental intracerebral hemorrhage," *J. Neurosurg.*, vol. 88, no. 6, pp. 1058–1065, 1998.
[266] G. L. Britton *et al.*, "In vivo therapeutic gas delivery for neuroprotection with echogenic liposomes," *Circulation*, vol. 122, no. 16, pp. 1578–1587, 2010.